EDGE CURRENT AND ANGULAR MOMENTUM IN ELECTRON SYSTEMS AT EQUILIBRIUM

HONOURS PROJECT IN PHYSICS

National University of Singapore
Department of Physics

Ren Yuhua
Supervisor: Prof. Wang Jian-Sheng

April 14, 2022

Edge current and angular momentum in electron systems at equilibrium

Abstract

We study non-interacting electrons on discrete lattices, with a particular focus on their energy spectra, persistence current, and electromagnetic radiation. The persistent current and thermal radiation were computed with the energy levels and energy eigenstates found numerically using MATLAB. Several high-temperature limit results for square lattices were obtained analytically using combinatorial arguments. We discovered that the persistent current goes to the boundary and vanishes as T^{-3} for square lattices. Invoking spontaneous emission, the radiation power saturates at high temperatures. At zero-field, the radiation power scales as the perimeter of the system, while the effect of the magnetic field is an additional sinusoidal contribution proportional to the area of the system. The radiation torque vanishes at high temperature as T^{-2}, and it is also a sinusoidal function of B, a linear function of μ, and scales with the area of the system.

Acknowledgements

I want to thank Prof. Wang for giving me the opportunity to work on this interesting project in his group for my FYP. I am especially grateful for his patience and the invaluable guidance provided. Many thanks to the other members in the group for the frequent sharings and insightful discussions. To my family and friends, thank you for being around and supporting me throughout this challenging period!

Contents

Chapter 1

Introduction

Over the years, there has been considerable interest in the quantum Hall effect (QHE). Two important findings since the pioneering works on QHE are the use of the quantum hall conductivity as a resistance standard [1] and the recent experimental realization of anyon statistics [2, 3]. QHE is usually studied with electrons confined in 2D systems and subjected to a magnetic field, and this will also be the set-up for the thesis.

Classically, in the presence of a uniform magnetic field, charged particles exhibit uniform circular motion when confined to a plane perpendicular to the magnetic field. The motion of these charged particles gives rise to an electrical current distribution. In the case of an isolated small 1D conducting ring, quantum mechanics predicts a persistent current that does not dissipate even for non-superconducting materials. Several authors have studied the properties of such current both theoretically [4, 5] and experimentally [6–9].

One method of analysis is the continuum model, where the position is a continuous variable. However, in this work, the discrete lattice model approach is used, where we will examine finite 2D rectangular systems. The electrons are assumed to be spinless fermions, and they only interact through the Pauli exclusion. We mainly use a square lattice, where the electrons are allowed to hop from one site to the sites that are its nearest neighbors. In essence, the calculations are carried out using a tight-binding model. Magnetic field will be added via the Peierls substitution. Numerical diagonalization is implemented using MATLAB to solve for the energy spectra and eigenstates in the 1-particle theory. Subsequently, the average current distribution and the resulting electromagnetic radiation at finite temperature are investigated.

Chapter 2

Background

2.1 Second quantization

Consider atoms arranged on a square lattice, with electrons moving between them. Each lattice site is labeled by an index j and its location is $\boldsymbol{r}_j$. The fermionic creation operator $c_j^\dagger$ creates an electron at site j, while the annihilation operator c_j removes an electron from the site j. The electron wavefunctions at different sites are assumed to have minimal overlap, such that the corresponding position eigenstates are orthogonal. All these can be summarized in terms of anti-commutation relations. The notation for the anti-commutator of two operators is $\{A, B\} \equiv AB + BA$.

$$\{c_i, c_j\} = \{c_i^\dagger, c_j^\dagger\} = 0, \qquad \{c_i, c_j^\dagger\} = \delta_{ij} \tag{2.1}$$

The reason for introducing second quantization is to deal with many-particle states more elegantly. Fermionic statistics will automatically be taken care of, and in particular, Pauli's exclusion principle is guaranteed by the statement $(c_j^\dagger)^2 = 0$. For a single-particle operator, the second-quantized generalization is simply given by

$$A = \sum_{jk} A_{jk} \left|j\right\rangle \left\langle k\right| \qquad \overset{\text{Second-quantized}}{\longrightarrow} \qquad \mathcal{A} = \sum_{jk} A_{jk} c_j^\dagger c_k$$

Dirac's bra-ket notation is used to describe pure states both before and after second quantization. The difference after second-quantization is the dimension of the Hilbert space, and the anti-commutation relations. It is also a convenient moment now to define the number operator in second quantization.

$$n_j \equiv c_j^\dagger c_j \tag{2.2}$$

We will verify that the key machinery of quantum mechanics (QM) is preserved in the second quantization formalism.

2.1.1 Eigenvectors and eigenvalues

The non-interacting Hamiltonian is second-quantized as follows.

$$H = \sum_{jk} H_{jk} |j\rangle \langle k| \qquad \overset{\text{Second-quantized}}{\longrightarrow} \qquad \mathcal{H} = \sum_{jk} H_{jk} c_j^\dagger c_k \tag{2.3}$$

Suppose we have the eigenstates $|\psi_n\rangle = \sum_l \alpha_{nl} |l\rangle$, i.e. $H|\psi_n\rangle = E_n |\psi_n\rangle$, with $n = 1, 2, \ldots, N$. In second quantization, such states are written as $|\psi_n\rangle = \sum_l \alpha_{nl} c_l^\dagger |0\rangle$. One can quickly verify that they indeed remain as energy eigenstates.

$$\begin{aligned}
\mathcal{H}|\psi_n\rangle &= \sum_{jk} H_{jk} c_j^\dagger c_k \sum_l \alpha_{nl} c_l^\dagger |0\rangle \\
&= \sum_{jkl} H_{jk} \alpha_{nl} c_j^\dagger (-c_l^\dagger c_k + \delta_{kl}) |0\rangle \\
&= \sum_{jk} H_{jk} \alpha_{nk} c_j^\dagger |0\rangle \\
&= \sum_j E_n \alpha_{nj} c_j^\dagger |0\rangle \\
&= E_n |\psi_n\rangle
\end{aligned} \tag{2.4}$$

To be more concise in notation, define a new orthonormal set of creation operators that creates particles in their energy eigenstates (or mode space).

$$d_n^\dagger \equiv \sum_l \alpha_{nl} c_l^\dagger \tag{2.5}$$

The usual fermionic anti-commutation relations are satisfied, which is a consequence of the fact that eigenvectors of the Hermitian operator H forms an orthonormal basis.

$$\{d_i, d_j\} = \{d_i^\dagger, d_j^\dagger\} = 0, \qquad \{d_i, d_j^\dagger\} = \delta_{ij}$$

The Eqn. 2.4 can then be generalized as an operation equation

$$\mathcal{H} d_n^\dagger = E_n d_n^\dagger + d_n^\dagger \mathcal{H} \tag{2.6}$$

Before second quantization, the Hermitian operator H has a complete set of N eigenvectors. After second quantization, the dimension of the Hilbert space is expected to be enlarged to 2^N for fermionic systems, such that $\mathcal{H}$ has 2^N linearly independent eigenvectors.

The vacuum state, $|0\rangle$, which is annihilated by any c_j, is trivially an eigenstate of $\mathcal{H}$ with eigenvalue 0. This is also called the zero-particle state. The above analysis verifies that the one-particle states, $d_j^\dagger |0\rangle$, remain as eigenstates of $\mathcal{H}$.

There are also two-particle eigenstates of $\mathcal{H}$, $d_j^\dagger d_k^\dagger |0\rangle$. It is fairly straightforward to use Eqn. 2.6 to show that the corresponding eigenvalue is $E_j + E_k$. Since the Pauli exclusion principle requires $j \neq k$, and the swap $j \leftrightarrow k$ merely introduces a minus sign, there are $\binom{N}{2}$ linearly independent 2-particle eigenstates.

The process works analogously for three-particle eigenstates, four-particle eigenstates, all the way up till the unique N-particle eigenstate. The binomial identity implies that the set of eigenstates is complete.

$$2^N = (1+1)^N = \binom{N}{0} + \binom{N}{1} + \ldots + \binom{N}{N}$$

Now, define the total number operator $\mathcal{N}$ as.

$$\mathcal{N} \equiv \sum_j n_j = \sum_j c_j^\dagger c_j = \sum_j d_j^\dagger d_j \tag{2.7}$$

The last equality holds again because eigenstates of the Hermitian operator H are orthogonal to one another. Below are a few useful commutation relation involving $\mathcal{N}$. The notation for the commutator is $[A, B] \equiv AB - BA$.

$$\begin{aligned} [\mathcal{N}, c_j^\dagger] &= c_j^\dagger \\ [\mathcal{N}, c_j] &= -c_j \\ [\mathcal{N}, c_j^\dagger c_k] &= 0 \end{aligned} \tag{2.8}$$

For the non-interacting Hamiltonian (Eqn. 2.3), the commutation relation $[\mathcal{H}, \mathcal{N}] = 0$ says that the total particle number is conserved. This can be immediately deduced from Eqn. 2.8. A consequence is that $\mathcal{H}$ and $\mathcal{N}$ share a common set of eigenvectors. Furthermore, the 2^N eigenstates furnished above are also eigenstates of $\mathcal{N}$. (There is no need to take linear combinations.)

To verify the above claim of the eigenstates of $\mathcal{N}$, consider the two-particle eigenstate, $d_j^\dagger d_k^\dagger |0\rangle$, as an example. First, note that

$$[\mathcal{N}, d_j^\dagger d_k^\dagger] = 2 d_j^\dagger d_k^\dagger \tag{2.9}$$

Thus, the eigenvalue of $\mathcal{N}$ in the two-particle state is 2.

$$\begin{aligned} \mathcal{N} d_j^\dagger d_k^\dagger |0\rangle &= d_j^\dagger d_k^\dagger (\mathcal{N} + 2) |0\rangle \\ &= 2 d_j^\dagger d_k^\dagger |0\rangle \end{aligned}$$

As the example shows, $\mathcal{N}$ counts the number of particles in a given state by its eigenvalue. The generalization of the key step (Eqn. 2.9) to higher number states is straightforward and can be shown rigorously using induction. The takeaway is that we can get away with diagonalizing H (dimension N) instead of $\mathcal{H}$ (dimension 2^N). The multi-particle spectrum is obtained by simply filling the single-particle energy states while obeying the Pauli exclusion principle. Under such a "reversed second quantization" (restriction onto the one-particle subspace), $\mathcal{N}$ becomes the identity operator.

2.1.2 Heisenberg equation of motion

In the Heisenberg picture, operators evolve according to the Heisenberg equation,

$$\frac{\mathrm{d}}{\mathrm{d}t} A = \frac{1}{i\hbar} [A, H]$$

$$= \frac{1}{i\hbar}\left[\sum_{mn} A_{mn} |m\rangle \langle n|, \sum_{\alpha\beta} H_{\alpha\beta} |\alpha\rangle \langle \beta|\right]$$
$$= \frac{1}{i\hbar}\sum_{mn\alpha\beta} A_{mn}H_{\alpha\beta}\left[|m\rangle \langle n|, |\alpha\rangle \langle \beta|\right]$$

It is imperative to check that this relation is still true after second quantization. It is sufficient to evaluate the commutator above.

$$\left[|m\rangle \langle n|, |\alpha\rangle \langle \beta|\right] = \delta_{n\alpha} |m\rangle \langle \beta| - \delta_{m\beta} |\alpha\rangle \langle n|$$

By repeated usage of the anti-commutation relations, a similar result can be established for the fermionic creation and annihilation operators.

$$\left[c_m^\dagger c_n, c_\alpha^\dagger c_\beta\right] = \delta_{n\alpha} c_m^\dagger c_\beta - \delta_{m\beta} c_\alpha^\dagger c_n$$

Incidentally, this relation holds for the bosonic operators too. Therefore, commutators between two second-quantized operators is the same as performing second quantization after computing the commutator. The latter is more useful for our computations as it is simply a matrix multiplication.

2.2 Lattice models

In this project, we will be describing our system with the spinless and non-interacting tight-binding Hamiltonian.

$$\mathcal{H} = -t\sum_{\langle j,k\rangle} c_j^\dagger c_k \tag{2.10}$$

It only contains a kinetic energy term. The Hamiltonian will be modified when there is magnetic field present. When considering only nearest-neighbor hopping, the Hamiltonian is identical to the adjacency matrix of the corresponding graph. The study of the eigenvalues of adjacency matrices is part of the well-established field of spectral graph theory.

2.2.1 Boundary conditions

In the tight-binding Hamiltonian, open boundary conditions (BC) are adopted. This means that sites located along the boundary will have few neighbors compared to sites in the bulk. However, for efficient computation, periodic BC is preferable. The presence of translational symmetry allows the Bloch theorem to provide a basis in which the Hamiltonian is block-diagonal. This can be implemented using a discrete Fourier transform (DFT), and the dimension of the problem will be reduced from 2D to 1D or 0D. Diagonalizing the blocks individually saves a lot of computation resources for large systems than if we were to diagonalize the original Hamiltonian as the time complexity scales as $\mathcal{O}(N^3)$, where $N = N_x N_y$ is the total number of sites.

2.2.2 Exact energy spectrum and eigenstates

Some of the simplest tight-binding Hamiltonians can be solved exactly. [10] Consider the 1D tight-binding chain of N sites with periodic BC. The Hamiltonian can be written in the position basis as

$$H = -\begin{pmatrix} 0 & t & & & t \\ t & 0 & t & & \\ & & \ddots & & \\ & & t & 0 & t \\ t & & & t & 0 \end{pmatrix}$$

The above matrix is diagonalized using DFT and the eigenstates are

$$\psi_j = \frac{1}{\sqrt{N}} \begin{pmatrix} 1 \\ \zeta^j \\ \zeta^{2j} \\ \vdots \\ \zeta^{(N-1)j} \end{pmatrix}$$

where $\zeta \equiv \exp\left(i\frac{2\pi}{N}\right)$ is the N^{th} root of unity, and $j = 1, 2, \cdots, N$. The corresponding eigenvalues are

$$\begin{aligned} E_j &= -2t \cos \frac{2\pi j}{N} \\ &= -2t \cos ka \end{aligned}$$

where a is the lattice constant and $k = \frac{2\pi j}{Na}$ is the wave vector. In the limit $a \to 0$, the small angle approximation $\cos ka = 1 - \frac{k^2a^2}{2}$ holds. Coincidentally, the dispersion relation of a free particle is $E = \frac{p^2}{2m} = \frac{\hbar^2 k^2}{2m}$. By matching the curvature of the dispersion relation at $k = 0$, the continuum limit is recovered with the following relation

$$t = \frac{\hbar^2}{2ma^2} \tag{2.11}$$

In this case, m is the effective mass of the electron and may differ significantly from its true mass. For the case of 1D chain with open BC, the spectrum is [11]

$$E_j = -2t \cos \frac{\pi j}{N+1}$$

In higher dimension, the Hamiltonian is more complicated. But in the case of a square lattice, the Hamiltonian can fortunately be written as a sum of mutually commuting matrices

$$H = H_x \otimes I_y + I_x \otimes H_y$$

where H_x and H_y are the familiar 1D Hamiltonians. The fact that they commute means that they share a common set of eigenvectors. As such, the energy spectrum is (for periodic BC in both directions) [10]

$$E_{k_x,k_y} = -2t(\cos k_x a + \cos k_y a) \tag{2.12}$$

This result will be used in the derivation of the Peirels substitution later when an external magnetic field is switched on. The Hamiltonian is modified and the old trick of simultaneous diagonalization cannot be used anymore. As such, we will resort to numerical diagonalization instead.

Chapter 3

Imposing Magnetic Field

3.1 Minimal coupling Hamiltonian

In the continuum case, the magnetic field enters the Hamiltonian through the vector potential, $\nabla \times \boldsymbol{A} = \boldsymbol{B}$.

$$H = \frac{1}{2m}(\boldsymbol{p} - q\boldsymbol{A})^2 + q\phi \tag{3.1}$$

For our problem, there is no scalar potential ϕ. The canonical momentum $\boldsymbol{p}$ is not gauge invariant but the kinetic momentum $\boldsymbol{\Pi} \equiv \boldsymbol{p} - q\boldsymbol{A}$ is gauge invariant. Since the magnetic field is uniform and out-of-plane, $\boldsymbol{B} = B\hat{\boldsymbol{z}}$, a suitable (but not unique) choice for the vector potential is the Landau gauge, $\boldsymbol{A} = -yB\hat{\boldsymbol{x}}$, such that $\nabla \times \boldsymbol{A} = B\hat{\boldsymbol{z}}$.. The Hamiltonian then is

$$H = \frac{1}{2m}[(p_x + qyB)^2 + p_y^2]$$

Solving this Hamiltonian will give us the Landau levels [12].

$$E_n = \hbar\omega_B \left(n + \frac{1}{2}\right) \tag{3.2}$$

where $\omega_B = \frac{qB}{m}$ is the cyclotron frequency.

3.2 Peierls substitution

For the discrete case, the magnetic field is incorporated into the tight-binding model via the Peierls substitution [13]. Following [14], we substitute the k's in the eigenvalue expression (Eqn. 2.12) into quantum operators. The heuristic is that a linear operator is completely determined by its action on a basis.

$$\hbar k_x \to p_x - qA_x$$

$$= -i\hbar\partial_x - qA_x$$
$$\hbar k_y \to -i\hbar\partial_y - qA_y$$

The substituted Hamiltonian is as follows.

$$H = -2t\left(\cos a\left(i\partial_x + \frac{q}{\hbar}A_x\right) + \cos a\left(i\partial_y + \frac{q}{\hbar}A_y\right)\right)$$

(The negative sign disappeared as cosine is an even function.) The cosine function of an operator has to be interpreted as a power series. In the limit of $a \to 0$, the continuum limit is again recovered with the same result as Eqn. 2.11. To proceed, the same Landau gauge, $\boldsymbol{A} = -yB\hat{\boldsymbol{x}}$, is chosen. The Hamiltonian then simplifies to

$$H = -2t\left(\cos a\left(i\partial_x - \frac{qB}{\hbar}y\right) + \cos a\,(i\partial_y)\right)$$

The cosines can be expressed in terms of complex exponentials, using the identity $\cos\theta = \frac{1}{2}(e^{i\theta} + e^{-i\theta})$. The complex exponential can then be evaluated using the Baker–Campbell–Hausdorff formula. The higher-order commutators do not occur as

$$\left[i\partial_x, \frac{qB}{\hbar}y\right] = 0$$

The Hamiltonian can then be written as

$$H = -t\left(e^{a\partial_x}e^{i\frac{qBa}{\hbar}y} + e^{-a\partial_x}e^{-i\frac{qBa}{\hbar}y} + e^{a\partial_y} + e^{-a\partial_y}\right) \tag{3.3}$$

For a differentiable function $\psi(x, y)$, translations can be written as

$$e^{a\partial_y}\psi\big|_{(x,y)} = \psi(x, y + a)$$

In the above example, the function $\psi(x, y)$ was translated in the negative y-direction by an amount a. If we choose a generic position eigenstate, $|x, y\rangle$, then the effect of H in Eqn. 3.3 is

$$H\,|x, y\rangle = -t\left(e^{i\frac{qBa}{\hbar}y}\,|x - a, y\rangle + e^{-i\frac{qBa}{\hbar}y}\,|x + a, y\rangle + |x, y - a\rangle + |x, y + a\rangle\right)$$

By focusing on a particular matrix element of H, say

$$\langle x + a, y|\,H\,|x, y\rangle = (-t)e^{-i\frac{qBa}{\hbar}y}$$

the hopping element is observed to be modified by a complex phase, which is also called the Peirels phase. Separately, consider the line integral of the vector potential along the straight line extending from the site (x, y) to the site $(x + a, y)$.

$$\int_{(x,y)}^{(x+a,y)} \boldsymbol{A}\cdot\mathrm{d}\boldsymbol{r} = -yBa$$

This motivates the definition of the Peirels phase as

$$\theta_{(x,y)\to(x+a,y)} = \frac{qBa}{\hbar}y = \frac{q}{\hbar}\int_{(x,y)}^{(x+a,y)} \boldsymbol{A}\cdot\mathrm{d}\boldsymbol{r}$$

Henceforth, the Peirels substitution is carried out in position basis by multiplying each hopping element with the Peierls phase. At this moment, it is not very clear why the vector potential should be written as such a line integral. Nevertheless, we choose a straight-line path for the line integral as it is the simplest and most intuitive kind of path that produces the correct phase. Work has been done to justify the line integral and the straight-line path choice based on a gauge invariance arguments [15–19]. Although this derivation is based on a square lattice, we generalize this procedure for any tight-binding Hamilitonian with only nearest-neighbours interaction. The MATLAB code implementing the Peierls substitution is provided in Appendix G.

3.2.1 Gauge invariance

Here we will demonstrate that gauge invariance is still maintained in the Peierls substitution. The Peierls substitution is implemented in practice using one particular choice of gauge. But physical observations should not be changed upon a gauge transformation. In electromagnetism, a gauge transformation is achieved by a (scalar) gauge function χ, such that the potentials change as

$$\boldsymbol{A} \to \boldsymbol{A}' = \boldsymbol{A} + \nabla\chi$$
$$\phi \to \phi' = \phi - \frac{\partial\chi}{\partial t}$$

but the electric and magnetic field remain unchanged. In Peierls substitution, the gauge transformation is realized in the form of a line integral. However, the additional term in the line integral only depends on the values of χ on the endpoints.

$$\exp\left(i\frac{q}{\hbar}\int_{\boldsymbol{r}_k}^{\boldsymbol{r}_j}(\boldsymbol{A}+\nabla\chi)\cdot\mathrm{d}\boldsymbol{r}\right) = e^{-i\frac{q}{\hbar}\chi(\boldsymbol{r}_k)}\exp\left(i\frac{q}{\hbar}\int_{\boldsymbol{r}_k}^{\boldsymbol{r}_j}\boldsymbol{A}\cdot\mathrm{d}\boldsymbol{r}\right)e^{i\frac{q}{\hbar}\chi(\boldsymbol{r}_j)}$$

This amounts to a similarity transformation by a diagonal and unitary matrix, U.

$$H \xrightarrow{\chi} U^\dagger H U \tag{3.4}$$

The matrix elements of U are

$$U_{jk} = \delta_{jk}e^{i\frac{q}{\hbar}\chi(\boldsymbol{r}_j)}$$

As similar operators represent the same linear operator with respect to (possibly) different bases, the important physical observables, such as the spectrum, will not be affected. In the continuum QM model, a gauge change will also cause a unitary transformation in the wavefunction. Eqn 3.4 is simply the discrete version on a lattice. An important identity in electromagnetism is the following application of Stoke's theorem

$$\oint \boldsymbol{A}\cdot\mathrm{d}\boldsymbol{r} = \iint \boldsymbol{B}\cdot\mathrm{d}\boldsymbol{S}$$

In the context of Peierls substitution, if we travel around edges to form a closed loop, the accumulated (sum of) Peierls phases is proportional to the magnetic flux,

which is also known as the Aharonov-Bohm effect. Crucially, it does not depend on the choice of the gauge.

Periodic BC is unfortunately not compatible with gauge invariance. Firstly, the choice of the gauge should be such that the vector potential is periodic. (Discontinuous vector potential at the boundary will give rise to an infinite magnetic field.) This is not possible if periodic BC is enforced in both directions. ($\boldsymbol{A}$ has to be linear.) We then relax our condition and only require periodic BC in the x-direction. In that case, the Landau gauge $\boldsymbol{A} = -(y - y_0)B\hat{x}$ is good. y_0 can be any number and can be understood as gauge freedom. Physically, this corresponds to translating the system in the y-direction. For the closed loop with lattice coordinates $(1,1) \to (2,1) \to \ldots \to (N_x,1) \to (1,1)$, the Peierls phase along all the edges are the same but depends linearly on y_0. This contradicts our earlier statement that the total Peierls phase around a closed loop should be gauge independent.

3.3 Hofstadter's butterfly

In the limit of an infinitely large system (regarding the number of sites, not the physical length), the beautiful Hofstadter's butterfly emerges if the energy spectrum is plotted as a function of the magnetic field. The nature of the energy eigenvalues depend critically on the ratio of the magnetic flux per plaquette $\Phi = Ba^2$ to the magnetic flux quantum $\Phi_0 = 2\pi\hbar/e$.

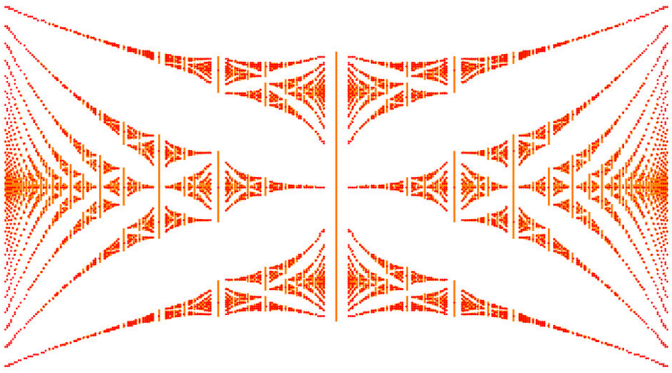

Figure 3.1: Fractal spectrum, also known as Hofstadter's butterfly [20]. The vertical axis is energy while the horizontal axis is magnetic field. When the ratio Φ/Φ_0 is a rational number p/q, the energy levels form exactly q bands (vertical lines). On the other hand, when the ratio is irrational, the energies form a Cantor set [12].

For the first output of this thesis, we check that our code implements the Peirels substitution correctly. The Hamiltonian is a periodic function of B, and the unit Peierls phase is

$$\theta_0 = \frac{qBa^2}{\hbar} \tag{3.5}$$

Only one period of the spectrum, $-\frac{\pi\hbar}{qa^2} \leq B \leq \frac{\pi\hbar}{qa^2}$, needs to be plotted. But nevertheless, it is customary to only plot for the positive fields, as a negative magnetic

field gives an identical spectrum. ($B \to -B \implies H \to H^* = H^T$, which has the same eigenvalues.) In physical terms, one half-period is $\frac{\pi}{qa^2}$. Fig. 3.2 shows for the butterfly spectrum for a few finite systems. These plots were obtained by diagonalizing the Hamiltonian numerically at different magnetic fields.

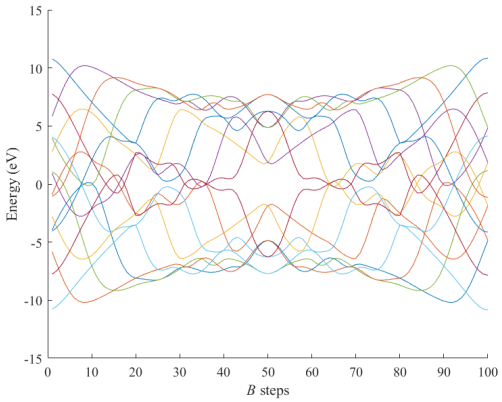

(a) 4×4 square lattice

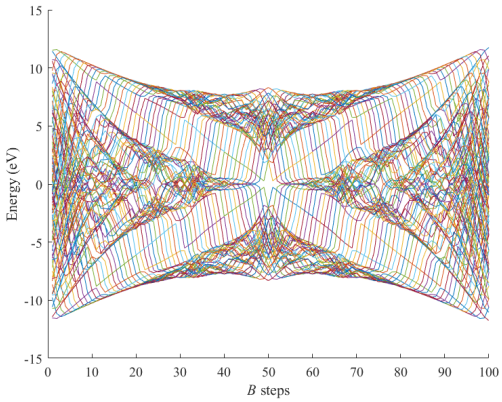

(b) 10×10 square lattice

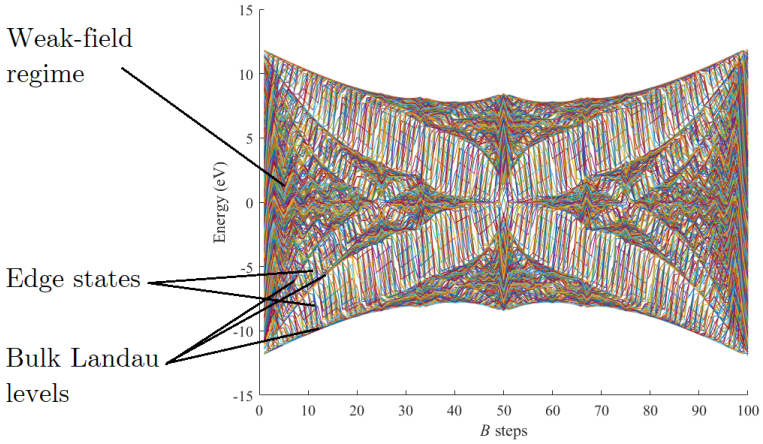

(c) 25×25 square lattice

Figure 3.2: Energy spectrum for a few finite systems. Hopping constant of $t = 3$eV was used to generate the plots.

Lines are colored in the MATLAB plots, which show the adiabatic movement of the energy levels as the magnetic field is varied. The number of energy levels is always equal to the number of lattice sites, $N \equiv N_x N_y$. For small systems, closed-form expressions for energy as a function can be found (Appendix F). However, as the number of energy gets larger, the energy levels move in an increasingly complicated manner. There are dense stripes analogous to Landau levels, and states move occasionally from one stripe to another. In each stripe, there is an enormous number of energy eigenstates, just like how Landau levels are highly degenerate. The region in between stripes in the original Hofstadter's butterfly (the "wings" of the butterfly) does not contain any energy levels. Due to our use of finite systems, some energy levels (edge states) now creep into this forbidden region. As the number of sites is increased (and so correspondingly the number of eigenstates), the relative density of edge states is reduced.

Gauge invariance is tested numerically by using both the Landau gauge and the symmetric gauge to perform the same calculations. Note that the energy levels are between $-4t$ and $4t$, which is in agreement with the special case of Eqn. 2.12. The choice of the chemical potential μ to use in our calculations later is guided by this fact.

One feature of the spectra of square lattices is that if E is an eigenvalue of the Hamiltonian, then $-E$ will also be an eigenvalue (Fig. 3.2). This happens if and only if the characteristic polynomial has only even powers. However, the triangular lattice does not have this property (Fig. 3.3). The implementation of the Peirels substitution is given in Appendix B. One magnetic period for the triangular lattice is $\frac{8\pi}{\sqrt{3}}\frac{1}{qa^2}$.

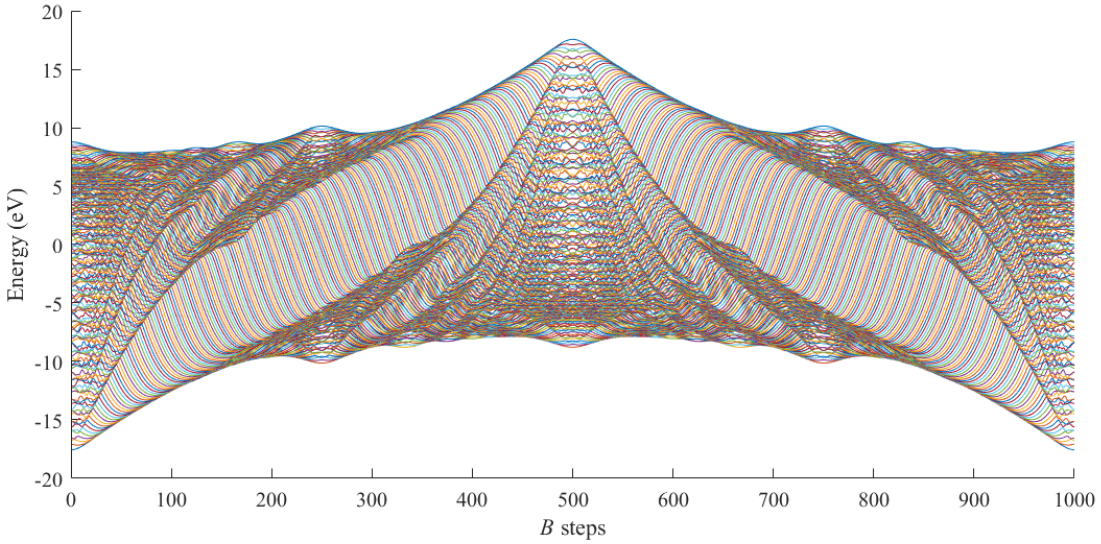

Figure 3.3: Spectrum of a tight-binding model on a 15×15 triangular lattice. Peierls substitution is used to implement the effect of a magnetic field via a phase in the hopping elements. There is no longer a mirror symmetry in the vertical direction.

On a similar note, we can also implement a tight-binding model on a hexagonal lattice. This can be used to model the 2D material graphene. The spectrum for the hexagonal lattice is shown below. One magnetic period for the hexagonal lattice is $\frac{4\pi}{3\sqrt{3}}\frac{1}{qa^2}$. Again, the details of the implementation of the Peierls substitution is given in Appendix B. The result agrees visually with the previous work done by Tradunsky and Cohen [21].

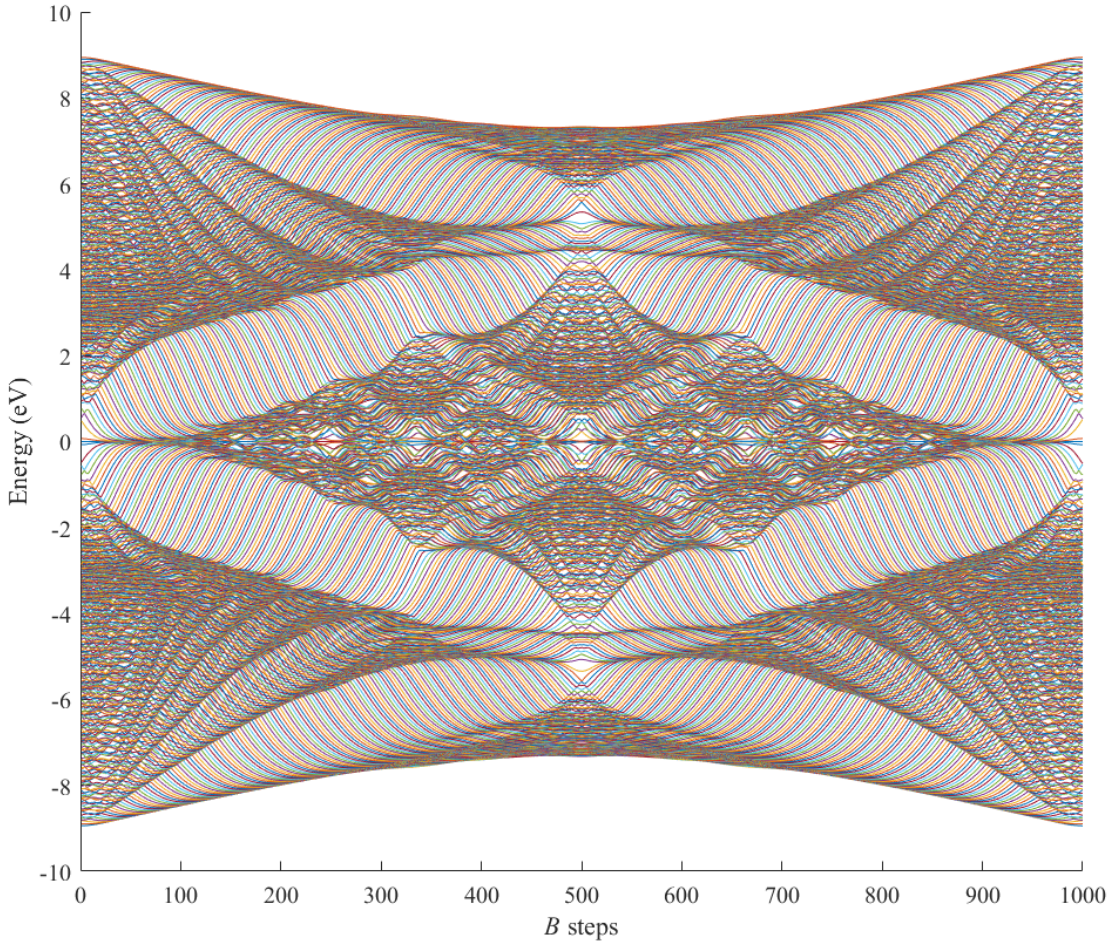

Figure 3.4: Spectrum of a tight-binding model on a 25×25 hexagonal lattice. Mirror symmetry in the vertical direction is present again.

Before we end the chapter, a few general remarks are in order. The role of the hopping constant t is just to set an energy scale. Changing the hopping constant amounts to stretching the butterfly spectrum vertically, which is an overall scaling to the energy levels. Thus, it does not give rise to any interesting physical phenomenon.

Another observation is that the lattice constant always appears together in an expression with the magnetic field (Ba^2). This expression reflects the flux per plaquette in the square lattice, which is relevant in the context of the Aharonov-Bohm effect. Since they do not appear independently, increasing the magnetic field strength is physically equivalent to increasing the lattice constant for energy calculations.

Chapter 4

Persistent Currents

4.1 Current operators

Schrödinger first interpreted his wavefunction for an electron as a charge density. [22] Define the charge operator that measures the total charge at a site l as simply the number operator multiplied by an electron's charge, $q = -e$.

$$Q_l = q c_l^\dagger c_l \tag{4.1}$$

One can then ask, how does the charge operator change with time? In the Heisenberg picture, the derivative of an operator is given by the Heisenberg equation

$$\begin{aligned}
\frac{\mathrm{d}}{\mathrm{d}t} Q_l &= \frac{1}{i\hbar}[Q_l, \mathcal{H}] \\
&= \frac{1}{i\hbar}\left[q c_l^\dagger c_l, \sum_{jk} H_{jk} c_j^\dagger c_k\right] \\
&= \frac{q}{i\hbar}\sum_{jk} H_{jk}\left[c_l^\dagger c_l, c_j^\dagger c_k\right] \\
&= \frac{q}{i\hbar}\sum_{j,k} H_{jk}\left(\delta_{lj} c_l^\dagger c_k - \delta_{lk} c_j^\dagger c_l\right) \\
&= \frac{q}{i\hbar}\sum_{j}\left(H_{lj} c_l^\dagger c_j - H_{jl} c_j^\dagger c_l\right)
\end{aligned}$$

This is a statement on the conservation of charge, or the continuity equation. Considering the form of Kirchhoff current law, the last step can be written as

$$\frac{\mathrm{d}}{\mathrm{d}t} Q_l = \sum_j \frac{q}{i\hbar}\left(H_{lj} c_l^\dagger c_j - H_{jl} c_j^\dagger c_l\right) = \sum_j \hat{I}_{j\to l}$$

and we can identify the current operator as [23]

$$I_{j\to l} = \frac{q}{i\hbar}\left(H_{lj} c_l^\dagger c_j - H_{jl} c_j^\dagger c_l\right) \tag{4.2}$$

Intuitively, Eqn. 4.2 also has the meaning of transport, given the use of annihilation and creation operators. The second term describes an electron destroyed at l and created at j contributing a negative current. In the position basis, the current operator is very sparse and only contains two non-zero elements. In the one particle representation, the current matrix looks like Eqn. 4.20. We will take advantage of this fact by defining our current matrix to be of type 'sparse' in MATLAB.

4.1.1 Relation to momentum operators

Since electrons have mass, and electrons move to produce current, there is a linear relation between the momentum and current, even for the quantum operators. The momentum operator in QM can again be obtained using the Heisenberg equation

$$mV^\mu = \frac{m}{i\hbar}[X^\mu, H] \tag{4.3}$$

These are the kinetic momenta (as opposed to canonical momenta) and they are gauge invariant. If the mass were not multiplied, they would simply be called the velocity matrices. Supposing a wire carries current I, and consider a segment of length a running in the x-direction. The total x-momentum of the wire is

$$\frac{ma}{q} I^x$$

It can be checked that summing all the current operators in the μ-direction indeed gives the total μ-direction velocity operator multiplied by the charge, qV^μ.

$$\begin{aligned} I^\mu &= \frac{1}{2}\sum_{jl} I_{j\to l}(x_l^\mu - x_j^\mu) \\ &= \frac{1}{2}\sum_{jl} \frac{q}{i\hbar}(H_{lj}c_l^\dagger c_j - H_{lj}c_j^\dagger c_l)(x_l^\mu - x_j^\mu) \\ &= \frac{q}{i\hbar}\sum_{jl} H_{lj}(x_l^\mu - x_j^\mu)c_l^\dagger c_j \\ &= \frac{q}{i\hbar}(X^\mu H - HX^\mu) \\ &= qV^\mu \end{aligned} \tag{4.4}$$

4.2 Grand canonical ensemble

In statistical mechanics, the grand canonical ensemble is used to describe systems in thermal and chemical equilibrium with a reservoir. The system is free to exchange energy and particles with the reservoir, so we instead work with Lagrange multipliers, the temperature T and chemical potential μ, instead. To describe a microstate, one specifies the particles are in each energy level (at most 1 for fermions). These microstates happen to be characterized by the eigenstates of the number operator $\mathcal{N}$ (Eqn. 2.7). An example of a microstate is given below.

$$|\phi\rangle = |1, 0, 1, \ldots, 1\rangle \equiv d_1^\dagger d_3^\dagger \ldots d_N^\dagger |0\rangle$$

The order of creation operators is important for fermionic systems.

4.2.1 Density operator in equilibrium

To each microstate, $|\phi\rangle$, the grand canonical ensemble assigns a probability

$$P(\phi) = \frac{1}{\mathcal{Z}} e^{-\beta(E(\phi)-\mu N(\phi))}$$

In our convention, $E - \mu N$ is an eigenvalue of $(\mathcal{H} - \mu\mathcal{N})$. $\mathcal{Z}$ is the grand partition function, and its role is to normalize the probabilities across all the microstates.

$$\begin{aligned}\mathcal{Z} &= \sum_{\{|\phi\rangle\}} e^{-\beta(E(\phi)-\mu N(\phi))} \\ &= \mathrm{Tr}(e^{-\beta(\mathcal{H}-\mu\mathcal{N})})\end{aligned}$$

The grand partition function can also be factorized. Suppose the microstate is written as $|\phi\rangle = |n_1, \ldots, n_N\rangle$ (these are labels, which take either 0 or 1. They are not to be confused with the number operators), and ϵ_j is the jth energy level.

$$\begin{aligned}\mathcal{Z} &= \sum_{\{|\phi\rangle\}} e^{-\beta\sum_{j=1}^{N} n_j(\epsilon_j-\mu)} \\ &= (1 + e^{-\beta(\epsilon_1-\mu)}) \sum e^{-\beta\sum_{j=2}^{N} n_j(\epsilon_j-\mu)} \\ &= \prod_{j=1}^{N} (1 + e^{-\beta(\epsilon_j-\mu)})\end{aligned}$$

In semi-classical physics, it is sufficient to know the probability distribution of the microstates. However, in QM, the phase relationship between different states is also required. If the phase relaxation length is short, the off diagonal elements in the density matrix becomes negligible. [24] In the basis of the microstates, the density operator is at thermal equilibrium is [25]

$$\begin{aligned}\rho &= \sum_{\{|\phi\rangle\}} P(\phi) \, |\phi\rangle \langle\phi| \\ &= \frac{1}{\mathcal{Z}} \sum_{\{|\phi\rangle\}} e^{-\beta(E(\phi)-\mu N(\phi))} \, |\phi\rangle \langle\phi| \\ &= \frac{1}{\mathcal{Z}} \sum_{\{|\phi\rangle\}} e^{-\beta\mathcal{H}} \, |\phi\rangle \langle\phi| \\ &= \frac{1}{\mathcal{Z}} e^{-\beta(\mathcal{H}-\mu\mathcal{N})}\end{aligned}$$

The density matrix does not evolve in time, which can be seen using the Liouville-von Neumann equation

$$i\hbar \frac{\partial \rho}{\partial t} = [\mathcal{H}, \rho] = 0$$

4.2.2 Expectation of operator

For a pure state $|\psi\rangle$ (in Fock space), the expectation of an operator $\mathcal{A}$ is given by

$$\langle \mathcal{A} \rangle = \langle \psi | \, \mathcal{A} \, | \psi \rangle$$

For a mixed state described by the density operator ρ, the expectation value is generalized to

$$\langle \mathcal{A} \rangle = \mathrm{Tr}(\rho \mathcal{A})$$

This formula can be checked to agree with the special case when $\rho = |\psi\rangle \langle \psi|$.

4.2.3 Computation in 1-particle Hilbert space

As much as possible, we would prefer to carry out computations in the one-particle Hilbert space and not in the entire Fock space. We will show here how this is done. Take a one-particle operator which has been second quantized.

$$\mathcal{A} = \sum_{jk} \alpha_{jk} d_j^\dagger d_k$$

where $d_j^\dagger$ is defined in Eqn. 2.5 to create a particle in the jth energy eigenstate. We shall see that to compute the thermal expectation, only the diagonal elements, α_{jj}, matter. Again, the microstate is written as either sides of $|\phi\rangle = |n_1, \ldots, n_N\rangle$, depending on the clarity needed. The expectation value is given by the following trace.

$$\mathrm{Tr}(\rho \mathcal{A}) = \frac{1}{\mathcal{Z}} \sum_{\{|\phi\rangle\}} e^{-\beta \langle \phi | \mathcal{H} | \phi \rangle} \, \langle \phi | \, \mathcal{A} \, | \phi \rangle$$

The summand depends only on the diagonal elements of $\mathcal{A}$.

$$\langle n_1, \ldots, n_N | \, \mathcal{A} \, | n_1, \ldots, n_N \rangle = \sum_{j=1}^{N} \alpha_{jj} n_j \tag{4.5}$$

This can be understood by considering the simpler expression

$$\langle n_1, \ldots, n_N | \, d_j^\dagger d_k \, | n_1, \ldots, n_N \rangle = \delta_{jk} n_j$$

Plugging in the expression from Eqn. 4.5,

$$\begin{aligned} \mathrm{Tr}(\rho \mathcal{A}) &= \frac{1}{\mathcal{Z}} \sum_{\{|\phi\rangle\}} e^{-\beta \langle \phi | (\mathcal{H} - \mu \mathcal{N}) | \phi \rangle} \sum_{j=1}^{N} \alpha_{jj} n_j \\ &= \sum_{j=1}^{N} \alpha_{jj} \sum_{\{|\phi\rangle\}} \frac{e^{-\beta \langle \phi | (\mathcal{H} - \mu \mathcal{N}) | \phi \rangle}}{\mathcal{Z}} n_j \end{aligned}$$

$$= \sum_{j=1}^{N} \alpha_{jj} \frac{1}{1 + e^{\beta(\epsilon_j - \mu)}}$$
$$= \sum_{j=1}^{N} \alpha_{jj} f(\epsilon_j) \tag{4.6}$$

The last expression is the expectation value in a single-particle eigenstate ($\alpha_{jj} = \langle 0| d_j \mathcal{A} d_j^\dagger |0\rangle$) multiplied by the average number of particle in the j energy eigenstate, which is given by the Fermi-Dirac distribution

$$f(E) = \left(1 + e^{\beta(E-\mu)}\right)^{-1} \tag{4.7}$$

In practice, we work with the one-particle Hamiltonian H, which can always be unitarily diagonalized as

$$H = PDP^\dagger$$

P is a matrix that stores the normalized eigenvectors of H in its columns. The operator A (no longer second-quantized) can also be represented as a matrix, $A = P(\sum_{jk} \alpha_{jk} |E_j\rangle \langle E_k|)P^\dagger$. It is written in this form because the current operator is usually defined in the position basis, not the energy basis. Thus, P is used to convert it via a similarity transform. It is then the diagonal of the matrix $P^\dagger AP$ that stores the relevant matrix elements for our calculation of the thermal average.

Now that D is a diagonal matrix storing the energy levels, we can instead convert it to store the Fermi factors. This can be accomplished in MATLAB using the matrix exponential.

$$F = (I + e^{-\beta\mu} e^{\beta H})^{-1}$$

However, the exponential function in MATLAB or Python does not differentiate between a diagonal matrix and a non-diagonal one. To speed up, the diagonal matrix is first converted into a 1D vector and element-wise exponential is used instead. It would be inefficient and potentially incorrect to use the element-wise exponential on the original matrix, as we do not want the exponentials of the off-diagonal elements.

The diagonal elements of $P^\dagger AP$ need to be weighted by the Fermi factors, before being summed up. It happens that multiplying a matrix by another diagonal one on the right has the effect of scaling the left matrix's columns, which achieves our objective. The sum of the diagonal element is accomplished by taking the trace. In terms of code, we just have to compute

$$\langle A \rangle = \mathrm{Tr}(P^\dagger APF)$$
$$= \mathrm{Tr}(APFP^\dagger) \tag{4.8}$$

Again, there is a chance to speed up calculations here. In our code, $P^\dagger AP$ is computed, where A is specifically the current operator. The product AP can be very quickly calculated as the current operator is sparse. The next step to realize is that since F is diagonal, it is sufficient to just calculate the diagonal elements of $P^\dagger(AP)$. In code, F is stored as a 1D vector, so if the diagonal elements of $P^\dagger(AP)$ can be

extracted as a vector, the trace can be calculated by an inner product. One way to accomplish this is using the element-wise multiplication in MATLAB (.*).

In the next section, the matrix $PFP^\dagger$ is interpreted as a Green function. This concept is needed as the Green functions will be used in our radiation calculations later. We will therefore take the chance now and introduce their definitions in the next section. But at this point, one can already point out that the Green function can be simultaneously diagonalized with the Hamiltonian.

4.3 Green functions

We now temporarily retreat from the Schrödinger picture and enter the Heisenberg picture. In the Heisenberg picture, operators acquire the time dependence. The definitions of the various Green functions are given below. As usual, the Roman indices represent lattice sites. At equilibrium, the Green function is only a function of 1 time variable [26].

$$G^<_{jk}(t) \equiv \frac{i}{\hbar}\langle c^\dagger_k(0)c_j(t)\rangle \tag{4.9}$$

$$G^>_{jk}(t) \equiv -\frac{i}{\hbar}\langle c_j(t)c^\dagger_k(0)\rangle \tag{4.10}$$

$$\begin{aligned} G^r_{jk}(t) &\equiv -\frac{i}{\hbar}\theta(t)\langle\{c_j(t), c^\dagger_k(0)\}\rangle \\ &= \theta(t)(G^>_{jk}(t) - G^<_{jk}(t)) \end{aligned} \tag{4.11}$$

$$\begin{aligned} G^a_{jk}(t) &\equiv \frac{i}{\hbar}\theta(-t)\langle\{c_j(t), c^\dagger_k(0)\}\rangle \\ &= -\theta(-t)(G^>_{jk}(t) - G^<_{jk}(t)) \end{aligned} \tag{4.12}$$

By definition, the four Green functions are linearly dependent.

$$G^r_{jk}(t) - G^a_{jk}(t) = G^>_{jk}(t) - G^<_{jk}(t) \tag{4.13}$$

These Green functions can be viewed as the matrix elements of $G^<(t)$, $G^>(t)$, $G^r(t)$, $G^a(t)$. They are functions of time, and so they can be Fourier-transformed into energy domain, which we define with the following convention

$$G(E) = \int_{-\infty}^{\infty} G(t)e^{iEt/\hbar}\mathrm{d}t$$

The same symbol is used for the Fourier transformed quantity, so the argument (whether it is time or energy/frequency) is used to distinguish the two functions. Our convention is that the factor of 2π goes with the inverse Fourier transform

$$G(t) = \frac{1}{2\pi\hbar}\int_{-\infty}^{\infty} G(E)e^{-iEt/\hbar}\mathrm{d}E$$

4.3.1 Fluctuation-dissipation theorem

In equilibrium, there is a fluctuation-dissipation theorem that gives a relation between $G^<$ and $G^>$ in energy domain. Suppose we have the complete set of energy

eigenstates, i.e. $\{|E_l\rangle\}_l$ such that $H|E_l\rangle = E_l|E_l\rangle$. It appears that $G^<(E)$ and $G^>(E)$ are diagonal are this basis, with the diagonal elements being proportional to the Fermi factors. Their exact expressions are provided below, and the detailed derivation can be found in Appendix A.

$$\begin{aligned} G^<(E) &= -f(E)[G^r(E) - G^a(E)] \\ &= (2\pi i) f(E) \sum_l \delta(E - E_l) |E_l\rangle \langle E_l| \end{aligned} \tag{4.14}$$

$$\begin{aligned} G^>(E) &= [1 - f(E)][G^r(E) - G^a(E)] \\ &= -(2\pi i)[1 - f(E)] \sum_l \delta(E - E_l) |E_l\rangle \langle E_l| \end{aligned} \tag{4.15}$$

With this, $G^<(t = 0)$ can be calculated by taking the inverse Fourier transform.

$$\begin{aligned} G^<(t = 0) &= \frac{1}{2\pi\hbar} \int_{-\infty}^{\infty} G^<(E) \mathrm{d}E \\ &= \frac{i}{\hbar} \sum_l f(E_l) |E_l\rangle \langle E_l| \end{aligned} \tag{4.16}$$

We then see that $-i\hbar G^<(t = 0)$ is exactly the same as the matrix $PFP^\dagger$ in Eqn. 4.8.

4.4 Current distribution plots

In this section, we will show some plots of the current distribution in finite systems. Similar work was done in [27]. Our parameters were carefully chosen to mimic real materials. In the following plots, the calculations were performed using a hopping of t =3 eV, lattice constant a =2.76 Å, magnetic field strength B =1 T. In our code, we adopt a special set of units that are almost identical to the Hartree atomic units, except that the unit of length is defined implicitly by measuring energy in eV. A complete list of the various units for different quantities can be found in Appendix H.

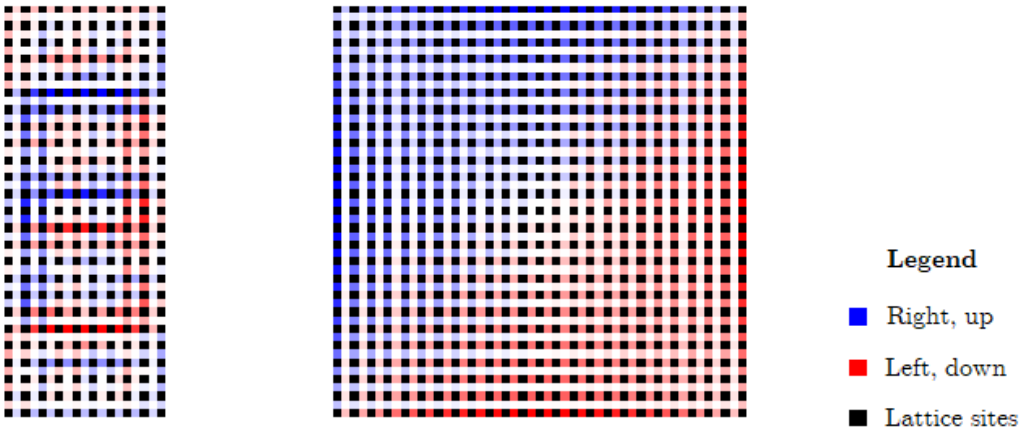

N_x: 10, N_y: 25
T: 290.07K
B: 1T
μ: -9.0000eV
I normalization: 2.577e-08A

(a)

N_x: 25, N_y: 25
T: 290.07K
B: 1T
μ: 0.0000eV
I normalization: 3.146e-06A

(b)

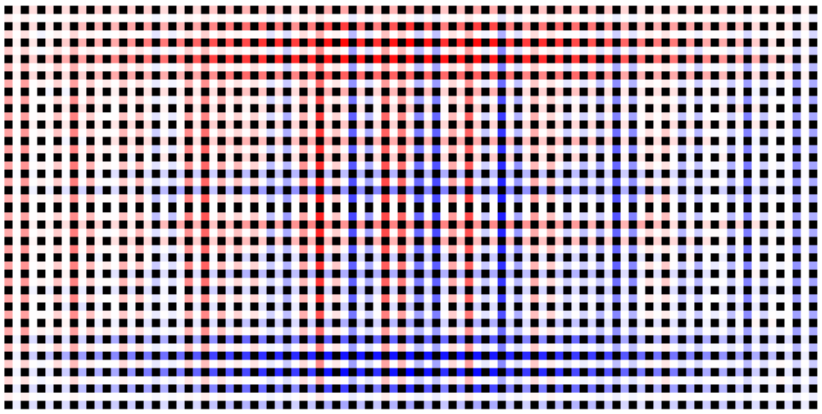

N_x: 50, N_y: 25
T: 290.07K
B: 1T
μ: -9.0000eV
I normalization: 6.476e-08A

(c)

Figure 4.1: Current distribution for a few systems of various sizes at low temperature and negative chemical potential. Lattice sites are labelled by black tiles. Colors of tiles between lattice sites shows the amount of current flowing between two nearest neighbours. Blue color represents current flowing in the positive x and y directions, while red color represents current flowing in the negative x and y directions. A paler color signifies that less current is flowing.

Although the resulting patterns are difficult to decipher, a few important and general observations can be made. Firstly, conservation of charge is obeyed. The

total current entering a lattice site is always equal to the total current leaving the same site. Alternatively, this means that the current flow can be represented as a superposition of current loops. The original motivation of this project was to study the current loops that arise due to the Lorentz force acting on the electrons. In classical electromagnetism, the electrons move in a circular motion. But as the above calculation shows, the constraint to move on a lattice causes the motion here to be far more complicated. The classical theory predicts that the charged particles will circulate in only one direction (clockwise or counter-clockwise). However, here the current is observed to flow in both directions.

Next, we discuss some symmetry present in the current distributions. The current flow has a π-rotation symmetry in the xy-plane, which is consistent with the fact that the underlying physics is invariant under the transformation $x \to -x$, $y \to -y$. A consequence of this fact is that if the system has an odd length, then there cannot be current flowing through the sites in the middle row/column.

Another symmetry that is present (but not shown) is related to time-reversal symmetry. When $B \to -B$, the current flows in the opposite direction, $I \to -I$. This is due to $H \to H^*$ when the magnetic field is reversed. If $|E\rangle$ is an eigenstate of H, then $|E\rangle^*$ is an eigenstate of H^* with the same eigenvalue. The current operator is also modified as $I \to -I^*$. Then the sum in Eqn. 4.6 becomes

$$\sum_j f(E_j)(\langle E_j|)^*(-I^*)(|E_j\rangle)^* = -\sum_j f(E_j)(\langle E_j| \, I \, |E_j\rangle)^*$$

Lastly, regarding particle-hole symmetry, $\mu \to -\mu$ gives the same current distribution, which is mainly due to the symmetry in the expectation values of the current operator.

$$\langle -E_l| \, I \, |-E_l\rangle = -\langle E_l| \, I \, |E_l\rangle$$

This allows the terms in the summation (Eqn. 4.6) to pair up.

$$f(E)\langle E| \, I \, |E\rangle + f(-E)\langle -E| \, I \, |-E\rangle = (f(E) - f(-E))\langle E| \, I \, |E\rangle \tag{4.17}$$

Changing $\mu \to -\mu$ has no effect due to the following identity.

$$f(E) - f(-E) = \frac{1}{1+e^{\beta(E-\mu)}} - \frac{1}{1+e^{\beta(-E-\mu)}} = \frac{1}{1+e^{\beta(E+\mu)}} - \frac{1}{1+e^{\beta(-E+\mu)}}$$

4.4.1 Angular momentum and magnetic moment

Classically, a current-carrying loop has a magnetic moment that is equal to its current times the area, $\boldsymbol{\mu} = I\boldsymbol{A}$. The magnetic moment is induced by the external magnetic field and can be classified as either paramagnetic or diamagnetic according to its sign. Since electrons have mass, there is also an angular momentum associated with the circulation of the charge carriers. The ratio between the magnetic moment and the angular momentum is a constant known as the gyromagnetic ratio, γ.

In classical mechanics, the angular momentum is well-defined (i.e. does not depend on the choice of origin) when the total linear momentum of the system is

zero. This result remains true in quantum mechanics. In Fig. 4.1, the current distribution can be decomposed into many smaller simple current loops, and for each current loop, the choice of origin does not affect the angular momentum. We will formulate an expression for the total angular momentum for our system and obtain its value numerically.

Consider the current operator $I_{j\to l}$, as given in Eqn. 4.2. This operator lives on an edge on the lattice and its associated x-momentum is

$$\begin{aligned} v^x_{j\to l} &= \frac{1}{q} I_{j\to l}(x_l - x_j) \\ &= \frac{1}{i\hbar}\Big(H_{lj}c^\dagger_l c_j - H_{jl}c^\dagger_j c_l\Big)(x_l - x_j) \end{aligned}$$

A similar definition hold for the linear momentum in the y-direction. The angular momentum of the current flowing in the edge $j \to l$ is then

$$\begin{aligned} l^z_{j\to l} &= m\frac{x_j + x_l}{2} v^y_{j\to l} - m\frac{y_j + y_l}{2} v^x_{j\to l} \\ &= \frac{m}{i\hbar}\Big(H_{lj}c^\dagger_l c_j - H_{jl}c^\dagger_j c_l\Big)(x_j y_l - y_j x_l) \end{aligned}$$

The midpoint is used as the current is uniform across the length of the edge. The angular momentum is non-zero only when j, k are nearest-neighbours. The total angular momentum, L_z, is then obtained by summing across contributions from all edges. The factor of half accounts for the double-counting due to $l^z_{j\to l} = l^z_{l\to j}$.

$$\begin{aligned} L^z &= \frac{1}{2}\sum_{j,l} l^z_{j\to l} \\ &= \frac{1}{2}\frac{m}{i\hbar}\sum_{j,l}\Big(H_{lj}c^\dagger_l c_j - H_{jl}c^\dagger_j c_l\Big)(x_j y_l - y_j x_l) \\ &= \frac{m}{i\hbar}\sum_{j,l} H_{lj}(x_j y_l - y_j x_l)c^\dagger_l c_j \end{aligned}$$

This means that the matrix elements of L_z in the position basis are

$$\begin{aligned} \langle l|\, L^z\, |j\rangle &= \frac{m}{i\hbar} H_{lj}(x_j y_l - y_j x_l) \\ &= \frac{m}{i\hbar}\langle l|\, YHX - XHY\, |j\rangle \end{aligned}$$

Therefore,

$$\begin{aligned} L^z &= \frac{m}{i\hbar}(YHX - XHY) \\ &= \frac{m}{i\hbar}(YHX - YXH + YXH - XYH + XYH - XHY) \\ &= \frac{m}{i\hbar}(-Y[X,H] + \underbrace{[Y,X]}_{=0} H + X[Y,H]) \\ &= X\frac{m}{i\hbar}[Y,H] - Y\frac{m}{i\hbar}[X,H] \end{aligned}$$

$$= m(XV^y - YV^x)$$

This simple result agrees with the classical definition of total angular momentum. To find the thermal average using the single-particle representation, the lesser Green function is used (Eqn. 4.16).

$$\begin{aligned}\langle L^z \rangle &= -i\hbar \mathrm{Tr}(G^<(t=0)L^z) \\ &= \sum_{E_l} \langle E_l | L^z | E_l \rangle f(E_l)\end{aligned}$$

The thermal average of the angular momentum is independent of the choice of origin. It is ultimately due to the following.

$$\begin{aligned}\langle \Pi^x \rangle &= -i\hbar m \mathrm{Tr}(G^<(t=0)V^x) = 0 \\ \langle \Pi^y \rangle &= -i\hbar m \mathrm{Tr}(G^<(t=0)V^y) = 0\end{aligned}$$

This is an analogous statement in QM that the total linear momentum is conserved. A few plots of the average angular momentum against an applied magnetic field at different chemical potential are shown below.

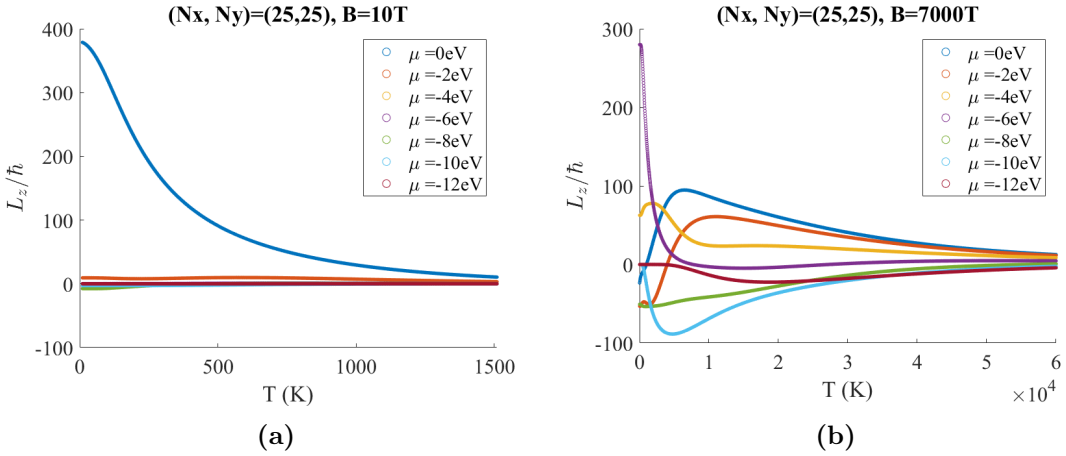

Figure 4.2: Total angular momentum at different temperatures, magnetic field strength and chemical potentials. They all decay to zero at high temperature.

Due to the symmetry $\langle -E_l | L_z | -E_l \rangle = -\langle E_l | L_z | E_l \rangle$, the angular momentum is the same when $\mu \to -\mu$. Therefore, only the plots for $\mu < 0$ are shown. In the presence of weak magnetic field, the total angular momentum vanishes more quickly as seen in Fig. 4.2. The precise way in which the current vanishes will be the topic for the next section.

4.4.2 High-temperature limit

In the high-temperature limit, the current flow vanishes. We found that for edges along the boundary of our system, the current decays as T^{-3}, whereas for edges in the interior of the system, the current decays as T^{-5} or faster. Therefore, it would appear as if the current becomes localized at the boundary.

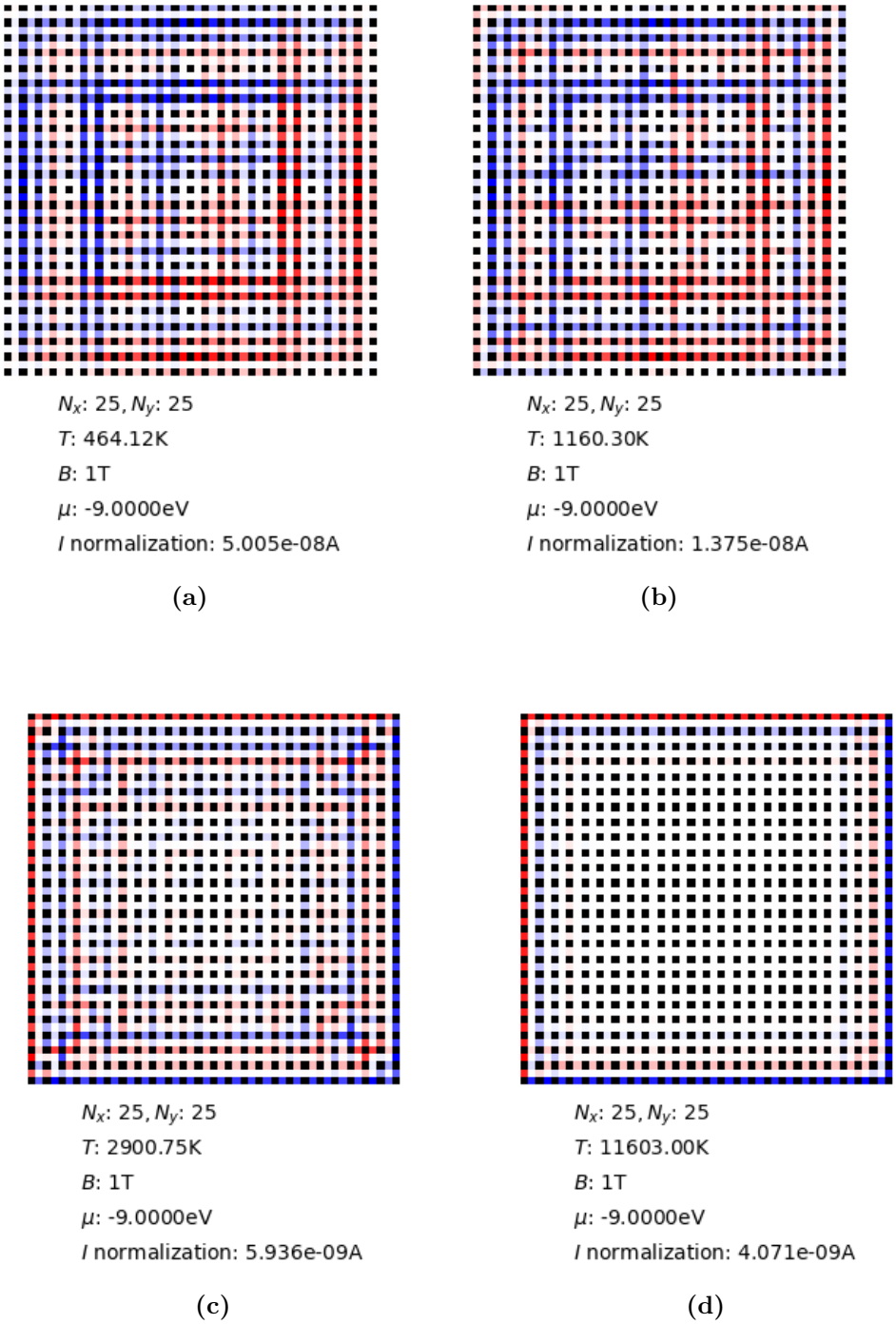

Figure 4.3: Persistent current plots at different temperatures. The ratio of current in the interior to the current boundary approaches zero at high temperatures. This result appears to be independent of the value of the chemical potential.

4.4.3 Taylor expansion of Fermi-distribution

We will give an analysis of the results shown above. Firstly, the high-energy Taylor expansion for the Fermi-Dirac distribution is given by

$$f(E) = \frac{1}{1+e^{\beta(E-\mu)}} = \frac{1}{2} - \frac{(E-\mu)}{4}\beta + \frac{(E-\mu)^3}{48}\beta^3 + \dots \tag{4.18}$$

If the one-particle energy eigenstate basis is written as $\{|E\rangle\}$, then, from Eqn. 4.6, the following sum needs to be computed

$$\langle I \rangle = \sum_{|E\rangle} f(E) \langle E| I |E\rangle$$

Previously, the symmetry allows the eigenstates to be paired up, as in Eqn. 4.17. We can do a little trick by double-counting and then taking half of the result.

$$\langle I \rangle = \frac{1}{2} \sum_{|E\rangle} [f(E) - f(-E)] \langle E| I |E\rangle$$

Now, it is clear that the reason the current goes to zero at high temperature is due to $f(E) - f(-E) \to 0$ as $\beta \to 0^+$. We can even go further and investigate at what rate the current decays. Use the above Taylor expansion (Eqn. 4.18) to write

$$f(E) - f(-E) = -\frac{E}{2}\beta + \frac{E^3 - 3\mu^2 E}{24}\beta^3 + \dots$$

The current expectation can then be written as an infinite series.

$$\begin{aligned} \langle I \rangle &= \frac{1}{2} \sum_{|E\rangle} \left[-\frac{E}{2}\beta + \frac{E^3 - 3\mu^2 E}{24}\beta^3 + \dots \right] \langle E| I |E\rangle \\ &= -\frac{\beta}{4} \sum_{|E\rangle} E \langle E| I |E\rangle + \frac{\beta^3}{48} \sum_{|E\rangle} (E^3 - 3\mu^2 E) \langle E| I |E\rangle + \dots \end{aligned} \tag{4.19}$$

From the above expansion, one would naively expect the current to decay as β, since the first term is the dominant term. However, we shall see that this is not the case.

4.4.4 First-order trace

In the first term of Eqn. 4.19, the coefficient involves computing $\sum E \langle E| I |E\rangle$. This can be expressed as a trace.

$$\begin{aligned} \sum_{|E\rangle} E \langle E| I |E\rangle &= \sum_{|E\rangle} E \mathrm{Tr}(|E\rangle \langle E| I) \\ &= \mathrm{Tr}\left(\left[\sum_{|E\rangle} E |E\rangle \langle E| \right] I \right) \\ &= \mathrm{Tr}(HI) \end{aligned}$$

This trace vanishes for the current operators of all edges. From Eqn. 4.2, an example of a current operator expressed as a matrix is

$$I_{j \to l} = \frac{q}{i\hbar} \begin{pmatrix} & & \\ & & H_{lj} \\ & & \\ & -H_{jl} & \end{pmatrix} \tag{4.20}$$

$$= \frac{q}{i\hbar}(E_l H E_j - E_j H E_l)$$

where E_l is the matrix with zero everywhere except the (l, l) element, which is one. Then, the trace is seen to be zero using the cyclic property

$$\begin{aligned}\mathrm{Tr}(HI_{j\to l}) &= \mathrm{Tr}\left(H\frac{q}{i\hbar}(E_l H E_j - E_j H E_l)\right) \\ &= \frac{q}{i\hbar}[\mathrm{Tr}(HE_l H E_j) - \mathrm{Tr}(HE_j H E_l)] \\ &= 0\end{aligned}$$

Note that none of the geometrical features of the square lattice was used to achieve this result. The zero-order coefficient vanishes as long as $\mathrm{Tr}(I) = 0$, which is true in general. This means that the same argument can be repeated for lattices of other geometry, such as the triangular lattice and hexagonal lattice. Hence, in those lattices, the high-temperature limit current also does not decay as β.

4.4.5 Third-order trace

The next dominant term is third order in β. However, from the calculations above, we conclude immediately that the term with $-3\mu^2 E$ is zero. Therefore, we focus on the remaining terms.

$$\sum_{|E\rangle} E^3 \langle E| I |E\rangle = \mathrm{Tr}(H^3 I)$$

For geometrical reasons, this quantity vanishes whenever the current operator is associated to an edge in the interior. For edges along the boundary, the trace has the same non-zero value (up to sign). A detailed explanation of this phenomenon is provided in Appendix C. Therefore, using this result, the exact value of the trace can be computed using the simplest system, the 2×2 square lattice. We get the following

$$\mathrm{Tr}(H^3 I_{\mathrm{boundary}}) = \pm\frac{2qt^4}{\hbar}\sin\left(\frac{qBa^2}{\hbar}\right)$$

In the weak-field regime, the expression for the average current simplifies to

$$\begin{aligned}\langle I\rangle &= \frac{qt^4\beta^3}{24\hbar}\sin\left(\frac{qBa^2}{\hbar}\right) \\ &\approx \frac{q^2 t^4 \beta^3 B a^2}{24\hbar^2}\end{aligned}$$

A log-log plot of the maximum current versus the inverse temperature is shown below, which confirms that the current indeed decays as β^3. The theoretical curve is a straight line with a slope of 3. Indeed, the behavior of systems of various sizes all tends towards this straight line when β is small.

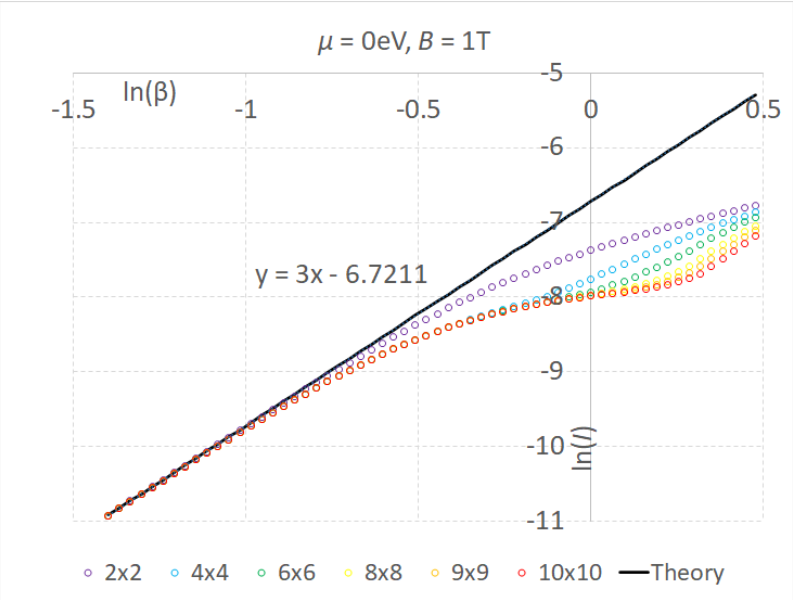

Figure 4.4: Plot of $\ln I$ vs $\ln \beta$ for systems of various sizes. The asymptotic behaviour all agrees with the theoretical curve, which decays as β^3. We then proceed to use the 2x2 system to calculate the analytic expression for the boundary current in the high-temperature limit.

Some related macroscopic quantities are more easily measured in the laboratory. Since the current is at the boundary, the system can be modeled as a current loop with area of

$$A = (N_x - 1)(N_y - 1)a^2$$

Therefore, the magnetic moment of the system is

$$\begin{aligned} \mu_z &= \frac{qt^4\beta^3}{24\hbar} \sin\left(\frac{qBa^2}{\hbar}\right)(N_x - 1)(N_y - 1)a^2 \\ &\approx \frac{q^2t^4\beta^3 Ba^4}{24\hbar^2} N_x N_y \end{aligned}$$

The issue with the model above is that to observe a significant proportion of the current accumulating at the edges, one needs to go to unrealistically high temperatures.

4.4.6 Triangular lattice

A similar analysis can be extended to systems with a different kind of lattice structure. After modifying the Hamiltonian to reflect the triangular lattice, we re-ran the algorithm to compute the persistent currents. From the simulations, the boundary current was found to vanish again as β^3. A log-log plot for the current versus the inverse temperature is given below.

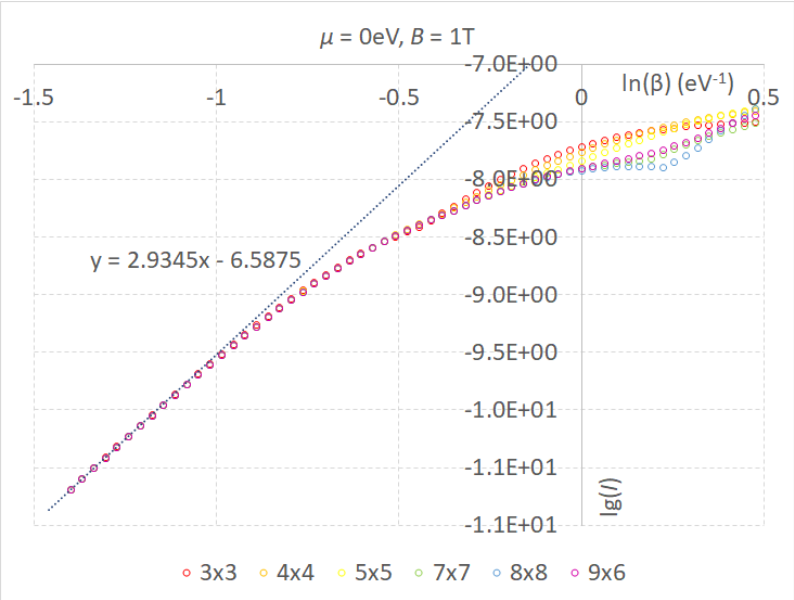

Figure 4.5: Plot of $\ln I$ vs $\ln B$ for triangular lattice. The high-temperature limit for the triangular lattice seems to be identical to the high-temperature limit for the square lattice. In the triangular lattice, there are two routes for the boundary current to flow. Primarily, the current flows along the true boundary, while there is also a secondary current flowing in a zig-zag manner that is grazing the boundary.

4.4.7 Hexagonal lattice

Similar to the square and triangular lattice, we also investigate the high-temperature behaviour of the boundary current for the hexagonal lattice. This time, the boundary current was found to vanish as β^5. A log-log plot for the current versus the inverse temperature is given below.

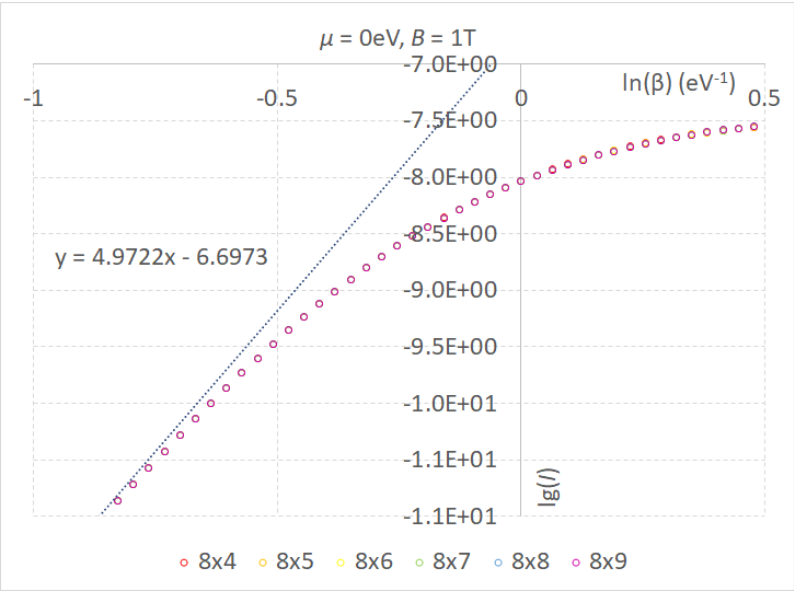

Figure 4.6: Plot of $\ln I$ vs $\ln B$ for hexagonal lattice. The coefficient is almost 5, which agrees with the reasoning given in Appendix C.

Chapter 5

Electromagnetic Radiation

The transition of electrons among different energy eigenstates will produce spontaneous emission of photons. These photons carry energy, momentum and angular momentum away from the system. In the following sections, we will derive the expression for the power and torque exerted by the radiation.

5.1 Current-current correlation function

We start with the current-current correlation functions, as given in [28]. μ, ν are the spatial indices and can be either x, y, z.

$$\Pi^{<}_{\mu\nu}(t,t') = \frac{1}{i\hbar}\langle I^{\nu}(t')I^{\mu}(t)\rangle$$

This correlation function can be written in terms of the electron Green functions (Eqn. 4.9 and Eqn. 4.10), and the velocity matrices (Eqn. 4.3). See Appendix D for the full derivation.

$$\Pi^{<}_{\mu\nu}(t,t') = -i\hbar q^2 \mathrm{Tr}[V^{\mu}G^{<}(t,t')V^{\nu}G^{>}(t',t)]$$

In equilibrium, the Green functions are only a function of one variable, the time difference $t - t'$ [26]. Thus, we can set $t' = 0$ for convenience and write

$$\Pi^{<}_{\mu\nu}(t) = -i\hbar q^2 \mathrm{Tr}[V^{\mu}G^{<}(t)V^{\nu}G^{>}(-t)] \tag{5.1}$$

A Fourier transform into frequency domain, with the usage of the convolution theorem, yields

$$\begin{aligned}\Pi^{<}_{\mu\nu}(\omega) &\equiv \int_{-\infty}^{\infty} \Pi^{<}_{\mu\nu}(t)e^{i\omega t}\mathrm{d}t \\ &= -\frac{iq^2}{2\pi}\int_{-\infty}^{\infty} \mathrm{Tr}[V^{\mu}G^{<}(E)V^{\nu}G^{>}(E-\hbar\omega)]\mathrm{d}E \end{aligned} \tag{5.2}$$

5.2 Total radiation power

The total power emitted (received at infinity) is given by the following expression [28]. The derivation is reproduced in Appendix E.

$$P_\infty = -\frac{\hbar}{6\pi^2\epsilon_0 c^3}\int_0^\infty \omega^2 \Im \mathrm{Tr}\Pi^<(\omega)\mathrm{d}\omega \tag{5.3}$$

The trace here means $\mathrm{Tr}\Pi^< = \Pi^<_{xx} + \Pi^<_{yy} + \Pi^<_{zz}$. First, express the terms inside the integral in terms of the energy eigenstates using Eqn. 4.14.

$$\begin{aligned} V^\mu G^<(E)V^\nu G^>(E-\hbar\omega) &= -(2\pi i)^2 f(E)[1-f(E-\hbar\omega)]\sum_{jk} \\ &\quad \delta(E-E_j)\delta(E-\hbar\omega-E_k)V^\mu\left|E_j\right\rangle\left\langle E_j\right|V^\nu\left|E_k\right\rangle\left\langle E_k\right| \\ \mathrm{Tr}[V^\mu G^<(E)V^\nu G^>(E-\hbar\omega)] &= (2\pi)^2 f(E)[1-f(E-\hbar\omega)]\sum_{jk} \\ &\quad \delta(E-E_j)\delta(E-\hbar\omega-E_k)\left\langle E_k\right|V^\mu\left|E_j\right\rangle\left\langle E_j\right|V^\nu\left|E_k\right\rangle \end{aligned}$$

When integrated over E, one of the delta disappears.

$$\begin{aligned} \Pi^<_{\mu\nu}(\omega) &= -\frac{iq^2}{2\pi}\int_{-\infty}^{\infty}\mathrm{Tr}[V^\mu G^<(E)V^\nu G^>(E-\hbar\omega)]\mathrm{d}E \\ &= -iq^2(2\pi)\int_{-\infty}^{\infty} f(E)[1-f(E-\hbar\omega)]\sum_{jk} \\ &\quad \delta(E-E_j)\delta(E-\hbar\omega-E_k)\left\langle E_k\right|V^\mu\left|E_j\right\rangle\left\langle E_j\right|V^\nu\left|E_k\right\rangle\mathrm{d}E \\ &= -iq^2(2\pi)\sum_{jk} f(E_j)[1-f(E_j-\hbar\omega)]\delta(E_j-\hbar\omega-E_k)\left\langle E_k\right|V^\mu\left|E_j\right\rangle\left\langle E_j\right|V^\nu\left|E_k\right\rangle \end{aligned}$$

When integrated over ω, the other delta is captured only when $E_j - E_k = \hbar\omega > 0$.

$$\begin{aligned} \int_0^\infty \omega^2\Im\Pi^<_{\mu\nu}(\omega)\mathrm{d}\omega &= -q^2(2\pi)\sum_{jk}\int_0^\infty \omega^2 f(E_j)[1-f(E_j-\hbar\omega)] \\ &\quad \delta(E_j-\hbar\omega-E_k)\Re\left\langle E_k\right|V^\mu\left|E_j\right\rangle\left\langle E_j\right|V^\nu\left|E_k\right\rangle\mathrm{d}\omega \\ &= -\frac{q^2(2\pi)}{\hbar}\sum_{jk}\theta(E_j-E_k)\left(\frac{E_j-E_k}{\hbar}\right)^2 \\ &\quad f(E_j)[1-f(E_k)]\Re\left\langle E_k\right|V^\mu\left|E_j\right\rangle\left\langle E_j\right|V^\nu\left|E_k\right\rangle \end{aligned}$$

In particular, for $\mu = x$ and $\nu = x$,

$$\begin{aligned} \int_0^\infty \omega^2\Im\Pi^<_{xx}(\omega)\mathrm{d}\omega &= -\frac{q^2(2\pi)}{\hbar^3}\sum_{jk}\theta(E_j-E_k)(E_j-E_k)^2 \\ &\quad f(E_j)[1-f(E_k)]|\left\langle E_j\right|V^x\left|E_k\right\rangle|^2 \end{aligned}$$

In the end, we need to compute the trace. At this point, it is handy to introduce the acceleration matrix, defined by the Heisenberg equation.

$$A^\mu \equiv \frac{1}{i\hbar}[V^\mu, H]$$

It is straightforward to check from the definition that the matrix elements in energy representation are

$$\begin{aligned}\langle E_j|\, A^\mu\, |E_k\rangle &= \frac{1}{i\hbar}(E_k - E_j)\,\langle E_j|\, V^\mu\, |E_k\rangle \\ &= -\frac{1}{\hbar^2}(E_k - E_j)^2\,\langle E_j|\, X^\mu\, |E_k\rangle\end{aligned}$$

Next, define the following vector.

$$\boldsymbol{a}_{jk} \equiv \langle E_j|\, A^x\, |E_k\rangle\,\hat{x} + \langle E_j|\, A^y\, |E_k\rangle\,\hat{y} + \langle E_j|\, A^z\, |E_k\rangle\,\hat{z} \tag{5.4}$$

This definition can be understood as the matrix elements of a real symmetric matrix in the basis of energy eigenstates. In terms of implementation, this is just the sum of the element-wise absolute-square of the 3 acceleration matrices in the energy basis. The trace over x, y, z is then

$$\int_0^\infty \omega^2 \Im\mathrm{Tr}\Pi^<(\omega)\mathrm{d}\omega = -\frac{q^2(2\pi)}{\hbar}\sum_{jk}\theta(E_j - E_k)f(E_j)[1 - f(E_k)]|\boldsymbol{a}_{jk}|^2$$

Thus, the total power emitted is

$$\begin{aligned}P_\infty &= \frac{\hbar}{6\pi^2\epsilon_0 c^3}\int_0^\infty \omega^2 \Im\mathrm{Tr}\Pi^<(\omega)\mathrm{d}\omega \\ &= \frac{q^2}{3\pi\epsilon_0 c^3}\sum_{jk}\theta(E_j - E_k)f(E_j)[1 - f(E_k)]|\boldsymbol{a}_{jk}|^2 \\ &= \frac{4}{3}\frac{\alpha\hbar}{c^2}\sum_{jk}\theta(E_j - E_k)f(E_j)[1 - f(E_k)]|\boldsymbol{a}_{jk}|^2\end{aligned} \tag{5.5}$$

where $\alpha = \frac{1}{4\pi\epsilon_0}\frac{e^2}{\hbar c}$ is the fine structure constant. A few plots of the total radiation power for a square lattice at different temperature and chemical potential is shown below.

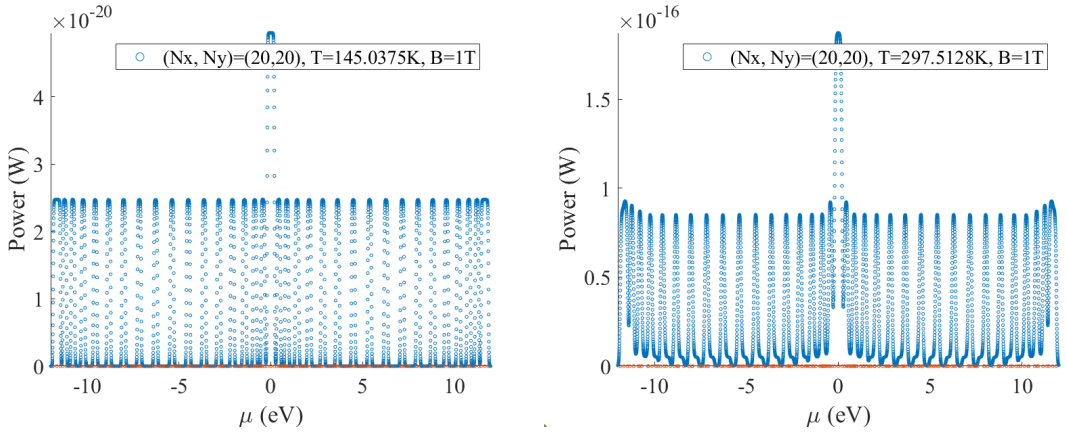

(a) **(b)**

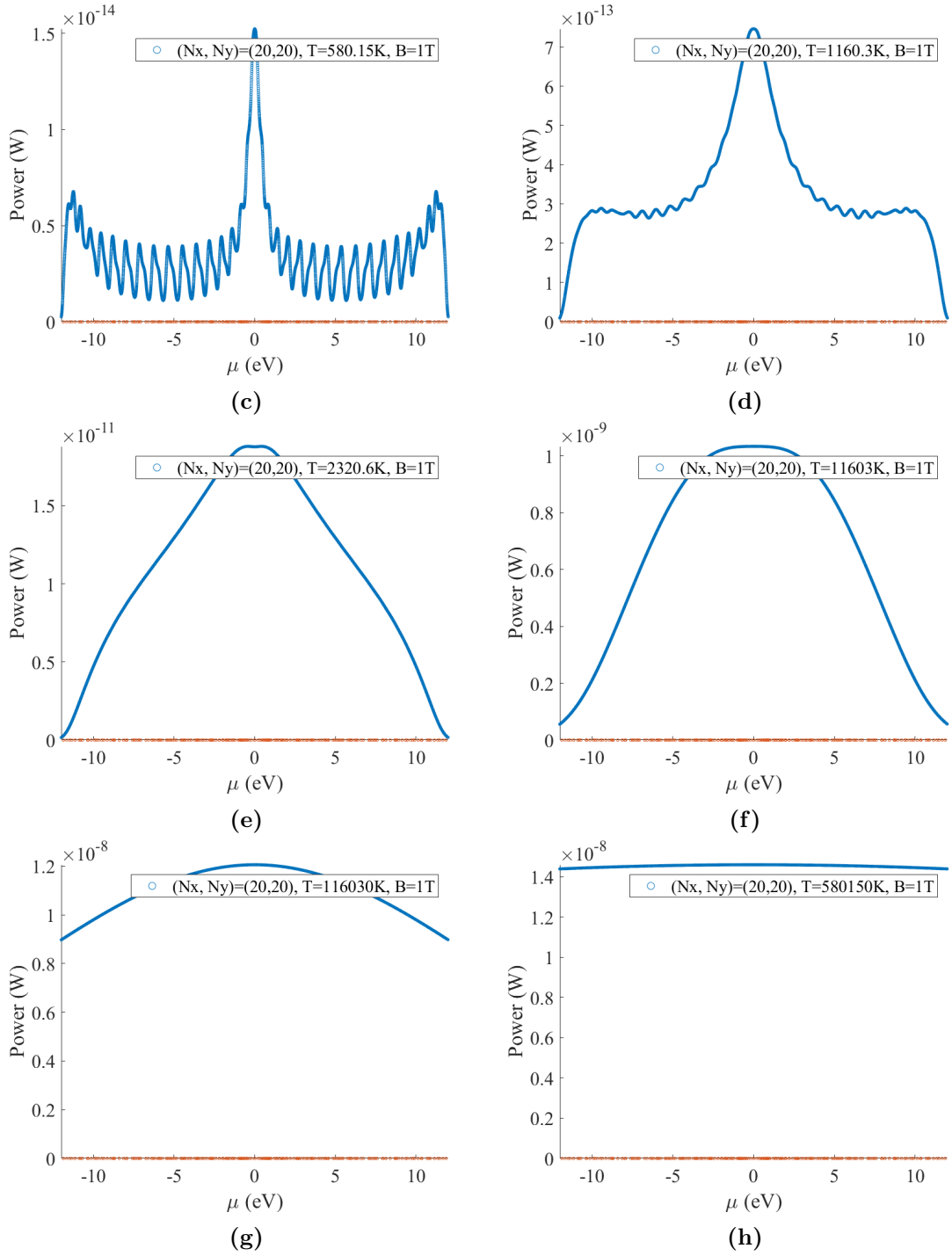

Figure 5.1: Plots of total radiation power against chemical potential at various temperature. A 20x20 system is used to generate these plots. Orange points marks the energy levels of the Hamiltonian as reference. The physical parameters for the systems are: a =276 pm, t =3 eV, B =1 T. At high temperatures, the radiation power approaches a constant value.

We can also look at it from literally another angle by plotting the power against the temperature.

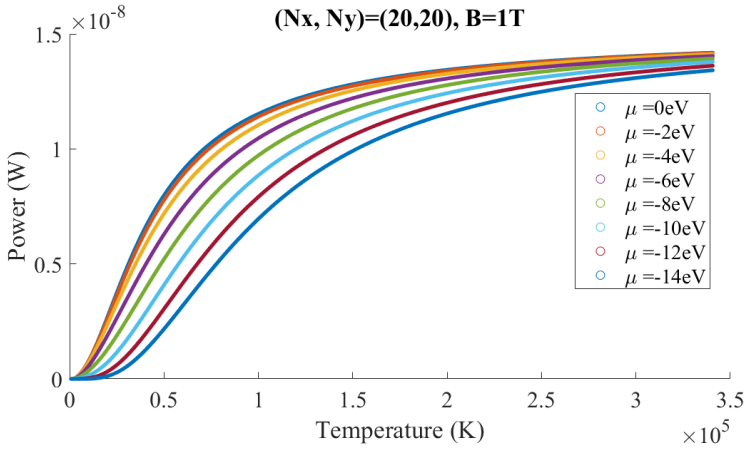

Figure 5.2: Plots of total radiation power against chemical potential at various temperature, using the same set of physical parameters as Fig. 5.1.

5.3 Low-temperature limit for radiation power

In the low-temperature limit, $\beta \to \infty$. The Fermi distribution then becomes essentially a step function. The only non-zero terms are when $E_j < \mu$ and $\mu < E_k$. However, the step function enforces $E_j > E_k$. More precisely,

$$\begin{aligned} f(E_j)[1 - f(E_k)] &= \frac{1}{1 + e^{\beta(E_j - \mu)}} \frac{1}{1 + e^{-\beta(E_k - \mu)}} \\ &= e^{-\beta(E_j - E_k)} \frac{1}{e^{-\beta E_j} + e^{-\beta\mu}} \frac{1}{e^{\beta E_k} + e^{\beta\mu}} \end{aligned}$$

The first term decays exponentially with β. The product of the remaining two terms is a rectangle function in the limit $\beta \to \infty$.

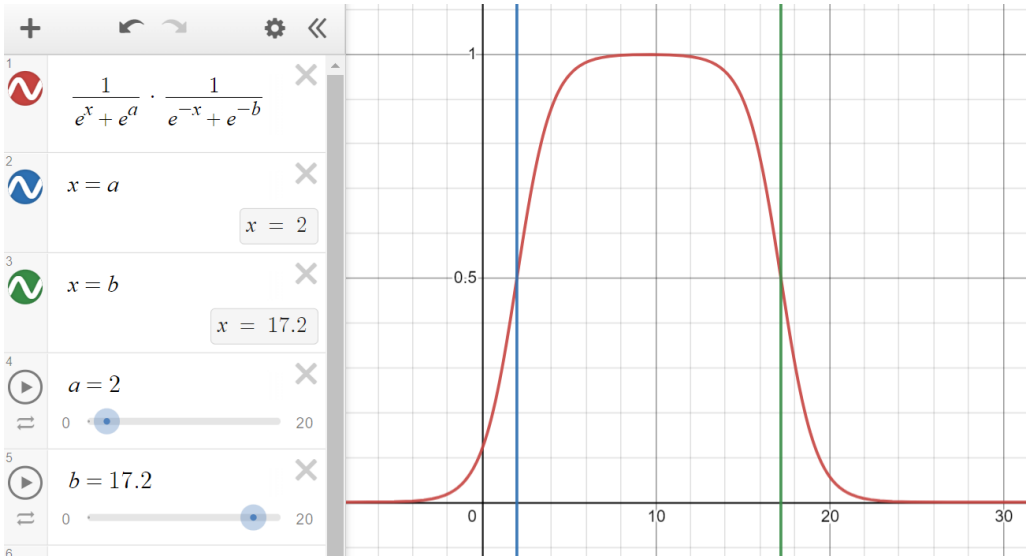

Figure 5.3: Plot of the product of the last two terms, with $E_j = b$ and $E_k = a$. Maximum is achieved at $\mu = \frac{E_j + E_k}{2}$. This can be verified by the first derivative.

It is straightforward to see that the function is bounded above by 1.

$$\frac{1}{e^{-\beta E_j}+e^{-\beta\mu}}\frac{1}{e^{\beta E_k}+e^{\beta\mu}} = \frac{1}{e^{-\beta(E_j-E_k)}+e^{-\beta(\mu-E_k)}+e^{-\beta(E_j-\mu)}+1} < 1$$

This means that, overall, the term decays as

$$f(E_j)[1-f(E_k)] < e^{-\beta(E_j-E_k)}$$

and there is significant contribution only when $E_k < \mu < E_j$. The most significant term in the sum (Eqn. 5.5) is when $(E_j - E_k)$ is small. This explains the strong peaks at certain values of μ in Fig. 5.1. The criterion for "low temperature" is therefore $k_b T \ll (E_j - E_k)$, which depends mainly on the hopping constant.

From our earlier plot of the butterfly spectrum (Fig. 3.2), each "Landau level" is highly degenerate, with many energy levels close together. Unfortunately, the chosen magnetic field of B =1 T was too weak to produce the energy bands. In the next plot, the calculations were repeated with an artificially high field of B =14 000 T.

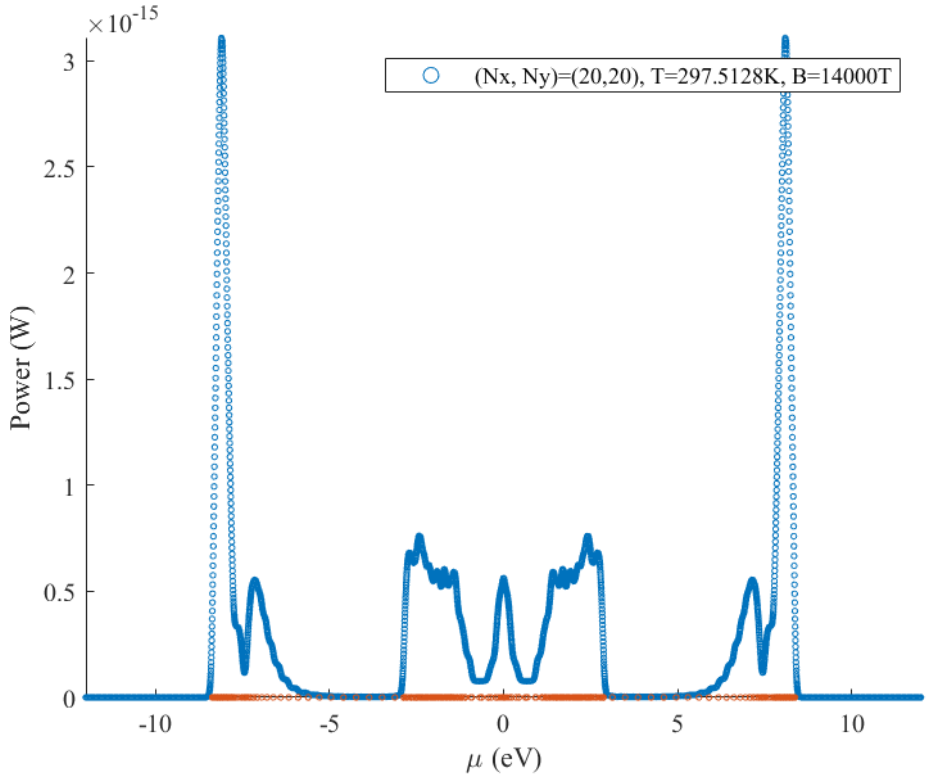

Figure 5.4: Plot of power emitted vs chemical potential. a =276 pm, t =3 eV, B =14 000 T. Compared to the low-field case (Fig. 5.1), the peaks are more prominent.

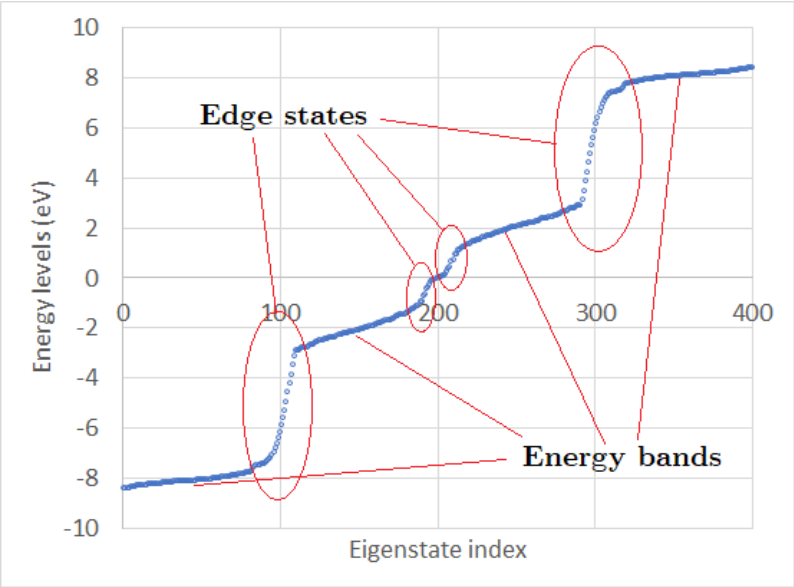

Figure 5.5: Distribution of the $20 \times 20 = 400$ energy level for B =14 000 T. States in the same band contribute more to the radiation in the low-temperature limit.

One can also study how the radiation power depends on the magnetic field at low temperatures. Below, we present the numerical results for the radiation power versus the magnetic field for a small system of 5×9 at different chemical potentials.

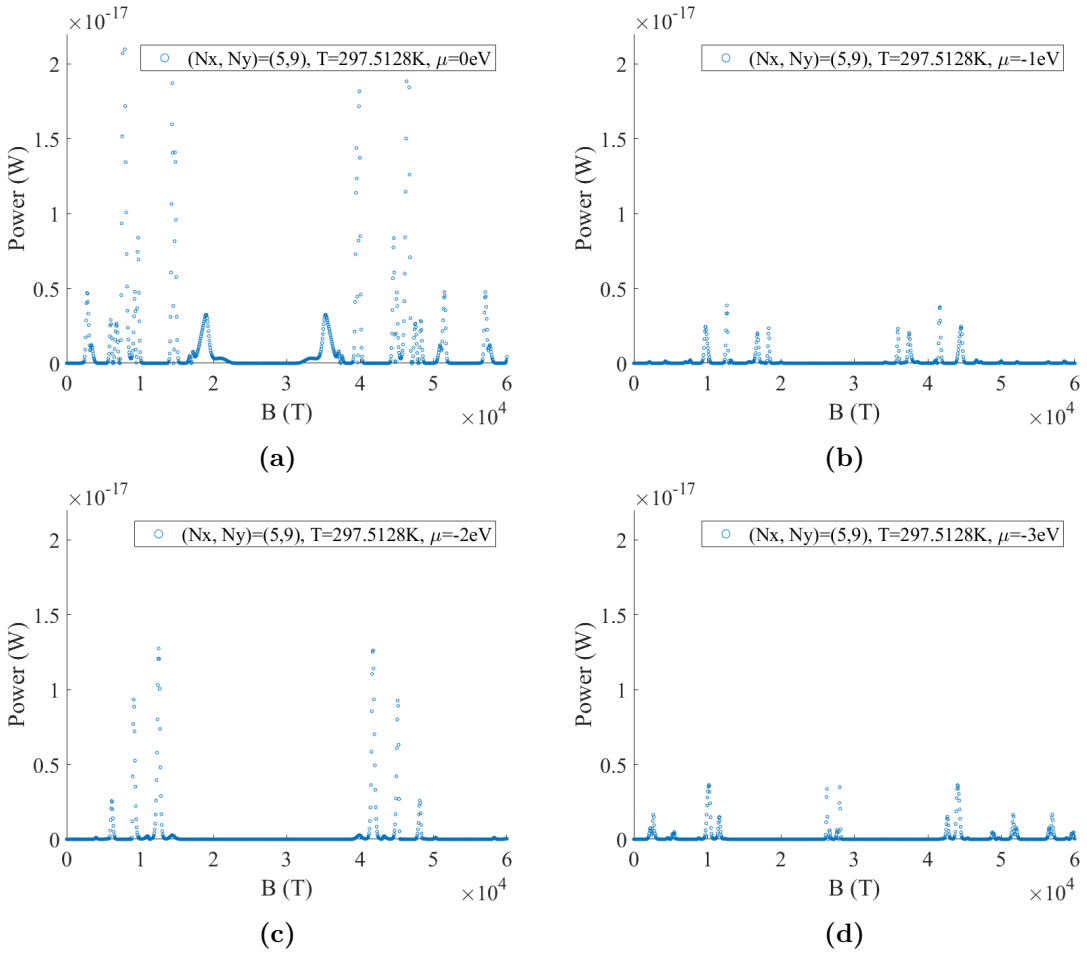

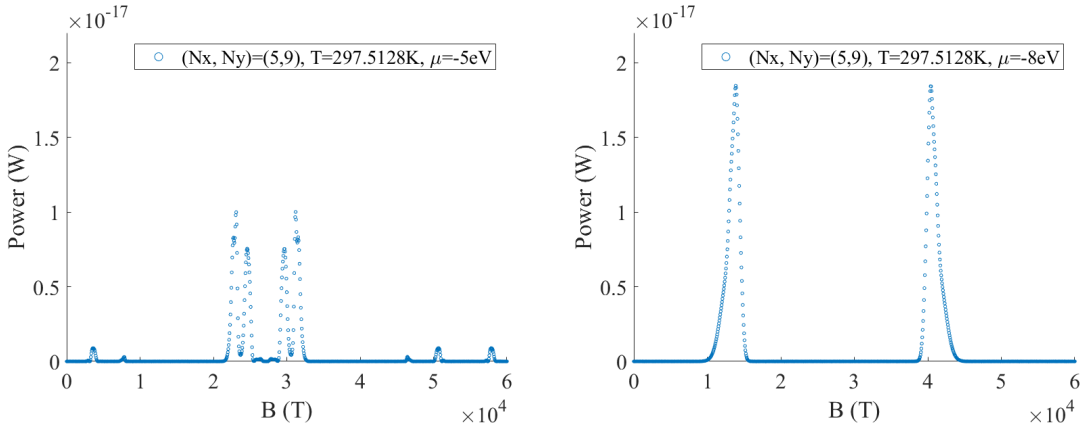

Figure 5.6: Plots of total radiation power versus the magnetic field for a 5×9 system at different chemical potentials. The location and strength of the peaks are sensitive to the chemical potential. For easy visual comparison, the y-axis is the same for all 6 figures.

To have significant radiation, it was previously established that the chemical potential needs to fall in between two energy levels. In the case of low chemical potential, this can only happen at certain fields (take a horizontal slice in Fig. 3.2).

5.4 High-temperature limit for radiation power

In the high-temperature limit, $\beta \to 0^+$ and $f(E_j) \to \frac{1}{2}$. This removes any dependency on the chemical potential. The expression for the total power (Eqn. 5.5) simplifies to

$$\begin{aligned}
P_\infty &= \frac{q^2}{12\pi\epsilon_0 c^3} \sum_{jk} \theta(E_j - E_k) |\boldsymbol{a}_{jk}|^2 \\
&= \frac{q^2}{24\pi\epsilon_0 c^3} \sum_{jk} |\boldsymbol{a}_{jk}|^2 \\
&= \frac{q^2}{24\pi\epsilon_0 c^3} \sum_{jk} (|\langle E_j| A^x |E_k\rangle|^2 + |\langle E_j| A^y |E_k\rangle|^2) \\
&= \frac{q^2}{24\pi\epsilon_0 c^3} \sum_{jk} (\langle E_j| A^x |E_k\rangle \langle E_k| A^x |E_j\rangle + \langle E_j| A^y |E_k\rangle \langle E_k| A^y |E_j\rangle) \\
&= \frac{q^2}{24\pi\epsilon_0 c^3} \mathrm{Tr} \sum_{jk} (A^x |E_k\rangle \langle E_k| A^x |E_j\rangle \langle E_j| + A^y |E_k\rangle \langle E_k| A^y |E_j\rangle \langle E_j|) \\
&= \frac{q^2}{24\pi\epsilon_0 c^3} \mathrm{Tr}((A^x)^2 + (A^y)^2)
\end{aligned} \tag{5.6}$$

Eqn 5.6 is almost the same as the famous Larmor formula, $P_\infty = \frac{(-e)^2}{6\pi\epsilon_0 c^3} a^2$, which describes the radiation due to an accelerating non-relativistic point charge. The factor of 1/4 can be thought of as arising from the fermi factors due to all the

sites being half-occupied in the high-temperature limit. For the system used in Fig. 4.3, the high-temperature limit of the power is calculated (using Eqn. 5.6) to be 1.51×10^{-8} W, which agrees well with the simulation results.

Next, we are interested in the high-temperature radiation power limit as a function of the magnetic field. We first show some numerical results.

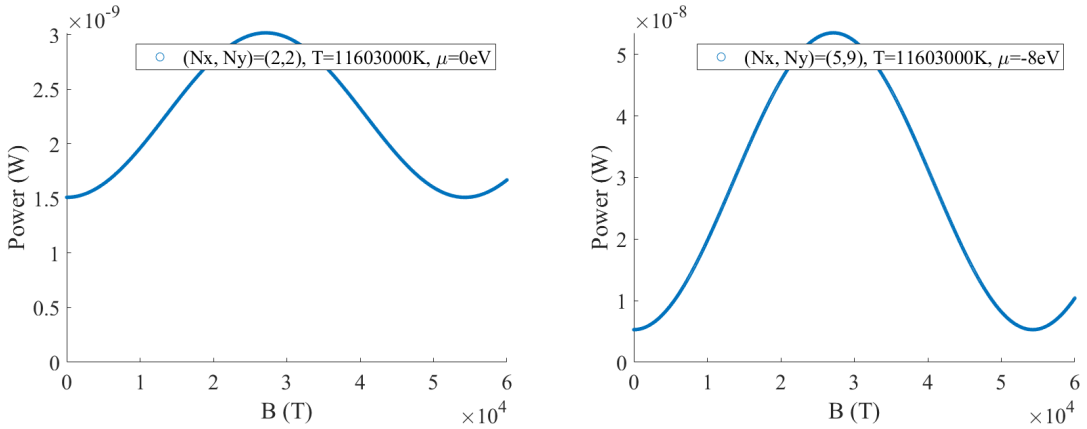

Figure 5.7: Plots of radiation power in the high-temperature limit against magnetic field.

The power appears to be a sinusoidal function of the magnetic field, with the same period of $\frac{2\pi\hbar}{qa^2}$ as the Hamiltonian. At zero field, the radiation is the same for all systems with the same perimeter. The variance/amplitude of the radiation power (as a function of magnetic field) is instead the same for all systems with the same area. The exact expression is given later in Eqn. 5.12. The proof of this statement is as follows.

The matrix elements of A^x in the position basis (where X is diagonal) are of interest. Here, there is possible confusion as to whether the matrix elements are in the position or energy basis. The context and the accompanying explanations aim to make this clear. First, evaluate the matrix elements of the velocity matrix in the position basis.

$$\begin{aligned} V^x_{jk} &= \frac{1}{i\hbar} \langle j | (XH - HX) | k \rangle \\ &= \frac{1}{i\hbar}(x_j - x_k)H_{jk} \end{aligned}$$

For the acceleration, a similar computation is performed. But this time, the completeness relation $\sum_l |l\rangle \langle l| = 1$ is inserted.

$$\begin{aligned} A^x_{jk} &= \frac{1}{i\hbar} \langle j | (V^x H - HV^x) | k \rangle \\ &= \frac{1}{i\hbar} \sum_l (\langle j | V^x | l \rangle \langle l | H | k \rangle - \langle j | H | l \rangle \langle l | V^x | k \rangle) \\ &= \frac{1}{i\hbar} \sum_l \left(\frac{1}{i\hbar}(x_j - x_l)H_{jl}H_{lk} - H_{jl}\frac{1}{i\hbar}(x_l - x_k)H_{lk} \right) \end{aligned}$$

$$= -\frac{1}{\hbar^2}\sum_l (x_j - 2x_l + x_k)H_{jl}H_{lk}$$

Therefore, the entire operator is written out as

$$\begin{aligned} A^x &= A^x_{jk}\,|j\rangle\,\langle k| \\ &= -\frac{1}{\hbar^2}\sum_l (x_j - 2x_l + x_k)H_{jl}H_{lk}\,|j\rangle\,\langle k| \end{aligned}$$

We still need to square it.

$$\begin{aligned} (A^x)^2 &= \sum_{jkl} A_{jk}A_{kl}\,|j\rangle\,\langle l| \\ &= \frac{1}{\hbar^4}\sum_{jkl\alpha\beta} (x_j - 2x_\alpha + x_k)(x_k - 2x_\beta + x_l)H_{j\alpha}H_{\alpha k}H_{k\beta}H_{\beta l}\,|j\rangle\,\langle l| \end{aligned}$$

Taking the trace simplifies the expression a little

$$\mathrm{Tr}((A^x)^2) = \frac{1}{\hbar^4}\sum_{jk\alpha\beta} (x_j - 2x_\alpha + x_k)(x_k - 2x_\beta + x_j)H_{j\alpha}H_{\alpha k}H_{k\beta}H_{\beta j}$$

Here we use the idea of adjacency matrix from graph theory again (see Appendix C). We are supposed to sum over all possible sites j, k, α, β, but $H_{j\alpha}H_{\alpha k}H_{k\beta}H_{\beta j}$ is non-zero if and only if $j \to \alpha \to k \to \beta \to j$ describes a closed walk of length 4. There are only a few ways this can be achieved. So, the summation can be reinterpreted as summing over all closed walks of length 4. But first, note that for those closed walks of length 4, the product of matrix elements is nothing but

$$H_{j\alpha}H_{\alpha k}H_{k\beta}H_{\beta j} = (-t)^4 e^{i(\theta_{j\to\alpha}+\theta_{\alpha\to k}+\theta_{k\to\beta}+\theta_{\beta\to j})}$$

The argument in the Peierls phase can only be zero (most cases) or $\pm\theta_0$ (Eqn. 3.5), if the closed walk surrounds a plaquette. Now, the problem reduces to counting the number of possible closed walks of length 4 in a graph. This is then to be weighted by the value of the coefficient $\zeta \equiv (x_j - 2x_\alpha + x_k)(x_k - 2x_\beta + x_j)$. We show a few representative closed walks below and their corresponding coefficients.

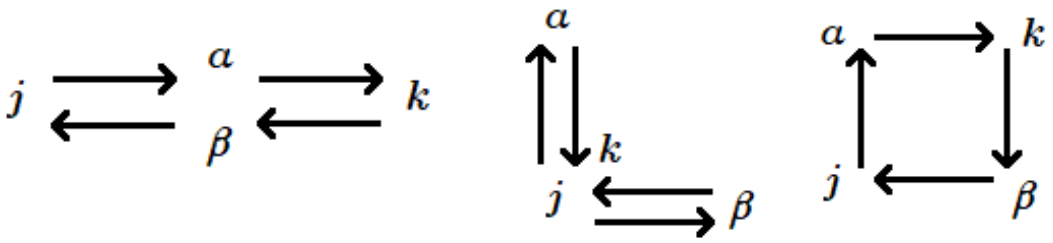

(a) $\zeta = 0$ **(b)** $\zeta = 0$ **(c)** $\zeta = -a^2$

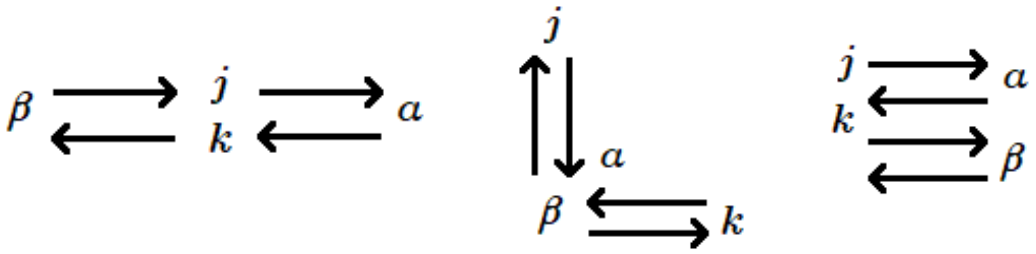

(d) $\zeta = -4a^2$ **(e)** $\zeta = a^2$ **(f)** $\zeta = 4a^2$

Figure 5.8: Some closed walks of length 4.

First, count the number of loops going clockwise (Fig. 5.8c). There are $(N_x - 1)(N_y - 1)$ of these loops. Since any of the vertices can be the starting vertex, there is a multiplicity of 4. So the contribution from summing over clockwise loops is (ignoring the common factor of $t^4/\hbar^4$)

$$-4a^2(N_x - 1)(N_y - 1)e^{-i\theta_0} \tag{5.7}$$

The number of loops going anti-clockwise is similarly

$$-4a^2(N_x - 1)(N_y - 1)e^{+i\theta_0} \tag{5.8}$$

Next, count the number of long horizontal walks (Fig. 5.8d). There are a total of $(N_x - 2)N_y$ ways to place them on the lattice. (j/k cannot start at the left or right boundaries.) There is a multiplicity of 2 since that $\alpha \leftrightarrow \beta$ is also valid (and with the same coefficient). Thus, the total contribution is

$$-8a^2(N_x - 2)N_y \tag{5.9}$$

Next, count the number of L-shaped walks with non-zero coefficients (Fig. 5.8e). There are a total of $(N_x - 1)(N_y - 1)$ ways to place them on the lattice. There are also 8 symmetry operations available. Thus, the total contribution is

$$8a^2(N_x - 1)N_y \tag{5.10}$$

Lastly, count the number of closed walks in the form of Fig. 5.8f. There are $(N_x - 1)N_y$ number of ways to accomplish this. A factor of two takes into account those going in the opposite direction. In total, they would contribute

$$8a^2(N_x - 1)(N_y - 1) \tag{5.11}$$

Adding up all the contributions from the four scenarios, the grand total is

$$8a^2[N_y + (N_x - 1)(N_y - 1)(1 - \cos\theta_0)]$$

For the trace of $(A^y)^2$, we can get the results for free by $x \leftrightarrow y$. The result is

$$8a^2[N_x + (N_x - 1)(N_y - 1)(1 - \cos\theta_0)]$$

Thereafter, we add them up to get the trace of $(A^x)^2 + (A^y)^2$.

$$8a^2[N_x + N_y + 2(N_x - 1)(N_y - 1)(1 - \cos\theta_0)]$$

Restoring the invisible factors of $t^4/\hbar^4$, we get

$$\mathrm{Tr}((A^x)^2 + (A^y)^2) = 8\frac{a^2t^4}{\hbar^4}\left[N_x + N_y + 2(N_x - 1)(N_y - 1)\left(1 - \cos\frac{qBa^2}{\hbar}\right)\right]$$

Hence, the high-temperature limit of the radiation power expression is

$$P_\infty = \frac{q^2}{3\pi\epsilon_0 c^3}\frac{a^2t^4}{\hbar^4}\left[N_x + N_y + 2(N_x - 1)(N_y - 1)\left(1 - \cos\frac{qBa^2}{\hbar}\right)\right] \tag{5.12}$$

The constant term scales as the perimeter of the system while the coefficient of the cos term (which contains the effect of the magnetic field) scales as the area.

5.5 Radiation torque

To calculate the torque, there is a similar formula that uses the current-current correlation function introduced in Eqn. 5.2. The total torque in the z-direction is given by the following [28, 29]

$$\begin{aligned} N_z &= \frac{-\hbar}{6\pi^2\epsilon_0 c^3}\sum_{\mu\nu}\epsilon_{z\mu\nu}\int_0^\infty \omega\Re\Pi^<_{\mu\nu}(\omega)\mathrm{d}\omega \\ &= \frac{-\hbar}{6\pi^2\epsilon_0 c^3}\int_0^\infty \omega\Re(\Pi^<_{xy}(\omega) - \Pi^<_{yx}(\omega))\mathrm{d}\omega \end{aligned}$$

First, we try to simplify the term $\Pi^<_{xy}(\omega) - \Pi^<_{yx}(\omega)$ in the integrand.

$$\begin{aligned} \Pi^<_{xy}(\omega) - \Pi^<_{yx}(\omega) &= -iq^2(2\pi)\sum_{jk} f(E_j)[1 - f(E_j - \hbar\omega)]\delta(E_j - \hbar\omega - E_k) \\ &\qquad (\langle E_k|\, V^x\, |E_j\rangle \langle E_j|\, V^y\, |E_k\rangle - \langle E_k|\, V^y\, |E_j\rangle \langle E_j|\, V^x\, |E_k\rangle) \\ &= 4\pi q^2\sum_{jk} f(E_j)[1 - f(E_j - \hbar\omega)]\delta(E_j - \hbar\omega - E_k)\Im(\langle E_k|\, V^x\, |E_j\rangle \langle E_j|\, V^y\, |E_k\rangle) \end{aligned}$$

We made use of the fact that the velocity operators are Hermitian to reach the last step. With the appearance of the Dirac-delta functions, we are now ready to integrate. When integrated over ω, the step function ensures that the delta is captured only when $E_j - E_k = \hbar\omega > 0$.

$$\begin{aligned} N_z &= \frac{(-\hbar)(4\pi q^2)}{6\pi^2\epsilon_0 c^3}\sum_{jk}\theta(E_j - E_k)\left(\frac{E_j - E_k}{\hbar}\right)\frac{1}{\hbar} \\ &\qquad f(E_j)[1 - f(E_k)]\Im(\langle E_k|\, V^x\, |E_j\rangle \langle E_j|\, V^y\, |E_k\rangle) \\ &= -\frac{8\alpha}{3c^2}\sum_{jk}\theta(E_j - E_k)(E_j - E_k)f(E_j)[1 - f(E_k)]\Im(\langle E_k|\, V^x\, |E_j\rangle \langle E_j|\, V^y\, |E_k\rangle) \end{aligned}$$

$$= -\frac{8\alpha\hbar}{3c^2}\sum_{jk}\theta(E_j - E_k)f(E_j)[1 - f(E_k)]\Re(\langle E_k|\, A^x\, |E_j\rangle\, \langle E_j|\, V^y\, |E_k\rangle) \tag{5.13}$$

MATLAB stores the eigenvalues in ascending order, i.e. $k < j \implies E_k < E_j$. We thus construct a lower triangular matrix to recast Eqn. 5.13 as a matrix multiplication. Some numerical results are shown below.

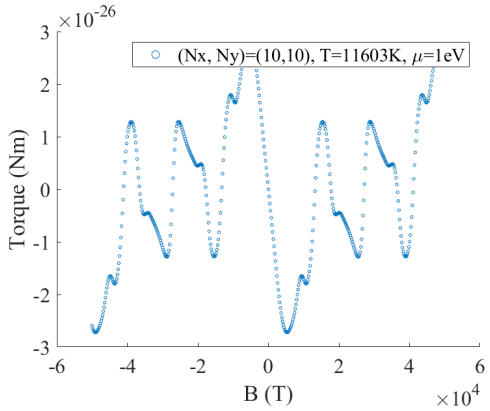

(a) Plot of torque against magnetic field at T =11 603 K and μ =1 eV.

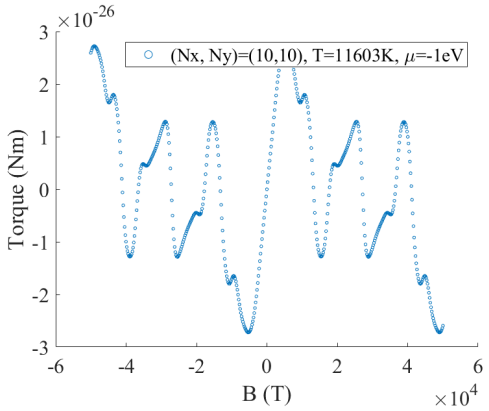

(b) Plot of torque against magnetic field at T =11 603 K and μ =−1 eV.

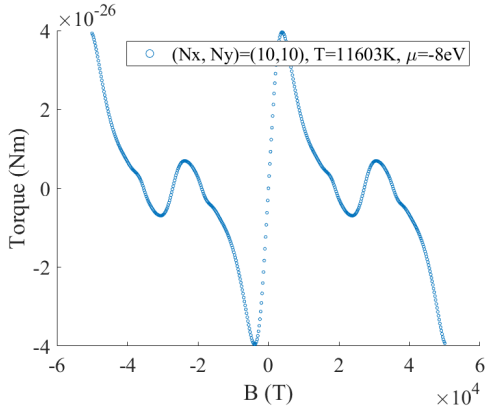

(c) Plot of torque against magnetic field at T =11 603 K and μ =−8 eV.

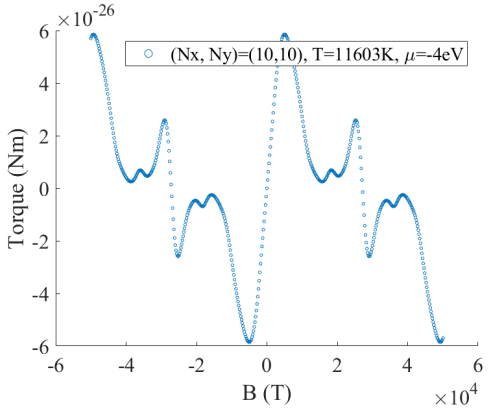

(d) Plot of torque against magnetic field at T =11 603 K and μ =−4 eV.

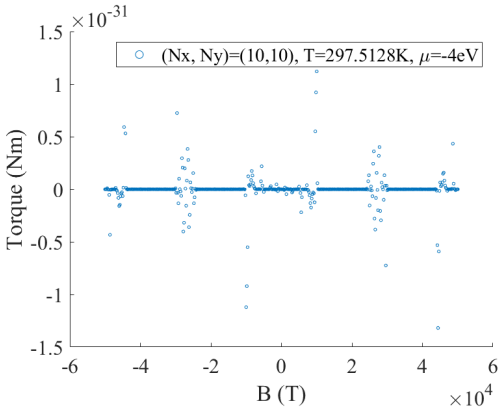

(e) Plot of torque against magnetic field at T =297 K and μ =−4 eV.

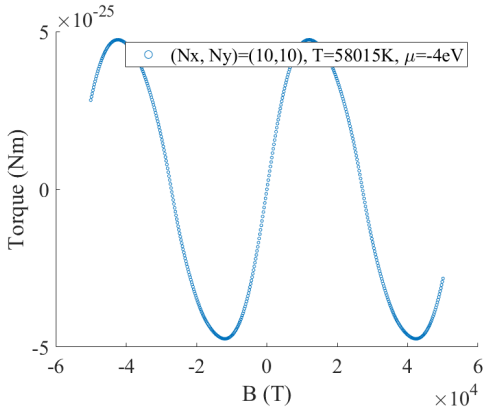

(f) Plot of torque against magnetic field at T =58 015 K and μ =−4 eV.

Figure 5.9: Plots of radiation torque against magnetic field at different temperatures and chemical potentials for a 10 × 10 system.

The torque radiated appears to vanish in the low-temperature limit, except at a few special values of the magnetic field. In the high-temperature limit, the radiation torque approaches a sinusoidal function of the magnetic field, similar to the 5.12.

5.6 Low-temperature limit for radiation torque

From the previous analysis on the low-temperature limit of the radiation power, we have understood that the exponential decay when $\beta \to 0^+$, due to the vanishing Fermi factors. The terms only contribute significantly when $E_k < \mu < E_j$. The reasoning here is the same, and the only difference is a different set of matrix elements. Two plots of the low-temperature radiation torque are presented below

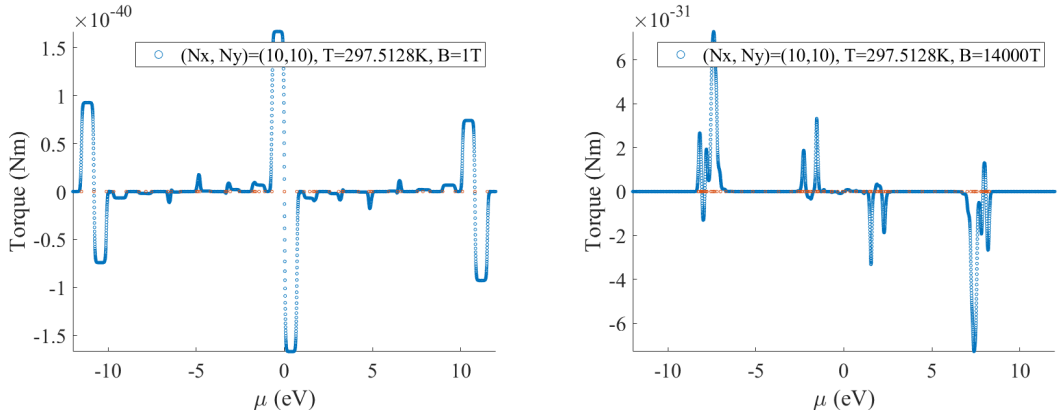

(a) Plot of torque against chemical potential for 10×10 system in the low-temperature and weak-field limit.

(b) Plot of torque against chemical potential for 10×10 system in the low-temperature limit and with significant magnetic field.

Figure 5.10: Plots of radiation torque in the low-temperature limit at two different magnetic field region. The torque radiated in the presence of a strong magnetic field is about 10^9 times larger than in a weak field. The largest peaks in Fig. 5.4 occur in the same positions as in Fig. 5.10b.

5.7 High-temperature limit for radiation torque

As seen previously, the Fermi distribution goes to half in the high-temperature limit, and supposedly removing any dependence on μ. However, our numerical simulations 5.11 suggests that the radiation torque is linearly proportional to μ (Fig. 5.11). In the high-temperature limit, Eqn 5.13 simplifies to

$$\begin{aligned} N_z &= -\frac{2\alpha\hbar}{3c^2}\sum_{jk}\theta(E_j - E_k)\Re(\langle E_k|\, A^x\, |E_j\rangle \langle E_j|\, V^y\, |E_k\rangle) \\ &= -\frac{\alpha\hbar}{3c^2}\Re\sum_{jk}\langle E_k|\, A^x\, |E_j\rangle \langle E_j|\, V^y\, |E_k\rangle \\ &= -\frac{\alpha\hbar}{3c^2}\Re\mathrm{Tr}(A^xV^y) = -\frac{\alpha\hbar}{3c^2}\mathrm{Tr}(A^xV^y) \end{aligned}$$

In the last step, A^x and V^x are both Hermitian, and thus the trace of their product is automatically real. However, it turns out that the trace is actually zero. Evaluating the trace in the position basis,

$$\mathrm{Tr}(A^x V^y) = -\frac{1}{i\hbar^3}\sum_{jkl}(x_j - 2x_l + x_k)(y_k - y_l)H_{jl}H_{lk}H_{kj}$$

We can borrow the previous idea of counting closed walks. However, there is no closed walk of length 3 on a square lattice. Thus, we conclude that $\mathrm{Tr}(A^x V^y) = 0$. Therefore, the radiation torque vanishes in the high-temperature limit.

However, to be more precise about how the torque vanishes, we should not be so hasty to take the limit of $f(E) \to \frac{1}{2}$. Instead, expand about $T = \infty$, or $\beta = 0$ (Eqn. 4.18). On hindsight, it is sufficient to expand to second order in β.

$$\begin{aligned} f(E_j)[1 - f(E_k)] &\approx \left[\frac{1}{2} - \frac{(E_j - \mu)}{4}\beta\right]\left[\frac{1}{2} + \frac{(E_k - \mu)}{4}\beta\right] \\ &= \frac{1}{4} + \frac{(E_k - E_j)}{8}\beta - \frac{(E_j - \mu)(E_k - \mu)}{16}\beta^2 \end{aligned}$$

We have already seen that the zeroth-order term vanishes. It turns out that the first-order term vanishes too.

$$\begin{aligned} \sum_{jk}(E_k - E_j)\langle E_k|A^x|E_j\rangle\langle E_j|V^y|E_k\rangle &= i\hbar\sum_{jk}\langle E_k|A^x|E_j\rangle\langle E_j|A^y|E_k\rangle \\ &= i\hbar\mathrm{Tr}(A^x A^y) \end{aligned}$$

But by considering all closed walks of length 4, it can be shown that the "destructive interference" between different walks causes the trace to be zero.

$$\mathrm{Tr}(A^x A^y) = \frac{1}{\hbar^4}\sum_{jk\alpha\beta}(x_j - 2x_\alpha + x_k)(y_k - 2y_\beta + y_j)H_{j\alpha}H_{\alpha k}H_{k\beta}H_{\beta j} = 0$$

For the second-order term, the numerator can be expanded

$$(E_j - \mu)(E_k - \mu) = E_j E_k - \mu E_j - \mu E_k + \mu^2$$

As seen already, the constant term μ^2 does not contribute. It also turns out that the $E_j E_k$ term does not contribute, as by a similar counting of closed walks with length 6,

$$\begin{aligned} &\sum_{jk} E_j E_k \langle E_k|A^x|E_j\rangle\langle E_j|A^y|E_k\rangle = \mathrm{Tr}(HA^xHA^y) \\ &= \frac{1}{\hbar^4}\sum_{\alpha\beta j\gamma\delta k}(x_\beta - 2x_j + x_\gamma)(y_\delta - 2y_k + y_\alpha)H_{\alpha\beta}H_{\beta j}H_{j\gamma}H_{\gamma\delta}H_{\delta k}H_{k\alpha} \\ &= 0 \end{aligned}$$

Therefore, the remaining surviving term is the dominant term.

$$N_z = -\frac{8\alpha\hbar}{3c^2}\Re\sum_{jk}\theta(E_j - E_k)f(E_j)[1 - f(E_k)]\langle E_k|A^x|E_j\rangle\langle E_j|V^y|E_k\rangle$$

$$
\begin{aligned}
&\approx -\frac{8\alpha\hbar}{3c^2}\Re\sum_{jk}\theta(E_j-E_k)\frac{\mu(E_j+E_k)}{16}\beta^2\left\langle E_k\right|A^x\left|E_j\right\rangle\left\langle E_j\right|V^y\left|E_k\right\rangle \\
&= -\frac{\alpha\hbar}{6c^2}\mu\beta^2\Re\sum_{jk}\theta(E_j-E_k)(E_j+E_k)\left\langle E_k\right|A^x\left|E_j\right\rangle\left\langle E_j\right|V^y\left|E_k\right\rangle \\
&= -\frac{\alpha\hbar}{12c^2}\mu\beta^2\Re\sum_{jk}(E_j+E_k)\left\langle E_k\right|A^x\left|E_j\right\rangle\left\langle E_j\right|V^y\left|E_k\right\rangle \\
&= -\frac{\alpha\hbar}{12c^2}\mu\beta^2\mathrm{Tr}(A^xHV^y+HA^xV^y) \\
&= -\frac{\alpha\hbar}{12c^2}\mu\beta^2\mathrm{Tr}(A^x(\underbrace{HV^y-V^yH}_{-i\hbar A^y}+2V^yH)) \\
&= -\frac{\alpha\hbar}{6c^2}\mu\beta^2\mathrm{Tr}(A^xV^yH) \qquad (5.14)
\end{aligned}
$$

In the second last step, we made use of $\mathrm{Tr}(A^xA^y)=0$. The radiation torque is proportional to μ and β^2 in the high-temperature limit. This is confirmed numerically in the following plots.

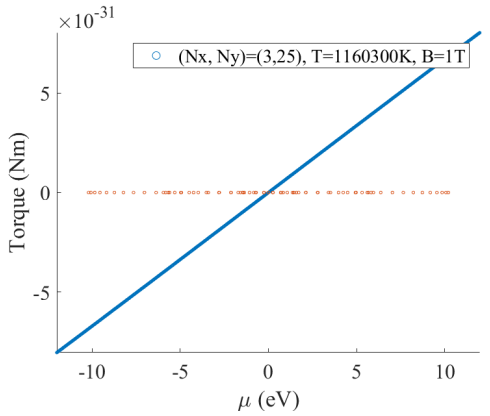

(a) Plot of torque against chemical potential for 3×25 system in the high-temperature limit.

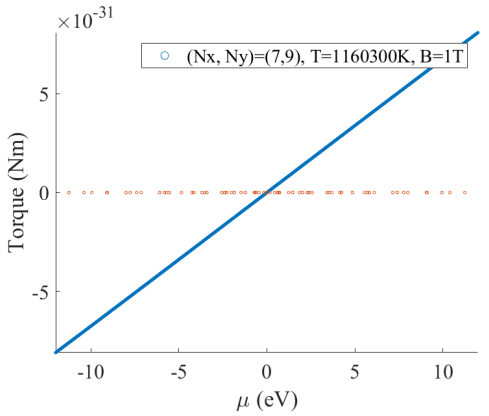

(b) Plot of torque against chemical potential for 7×9 system in the high-temperature limit.

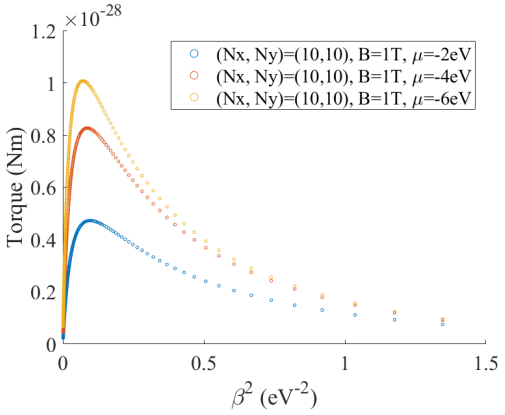

(c) Plot of torque against inverse temperature squared for 7×9 system.

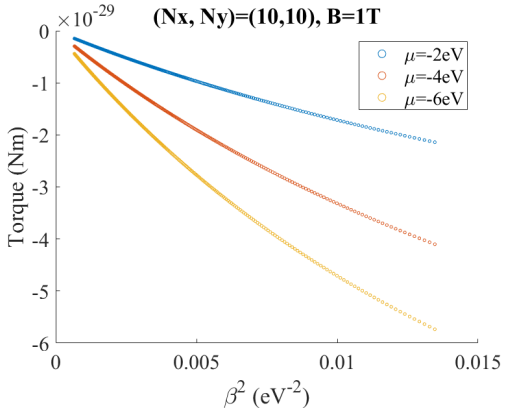

(d) Same plot as (c), but in the region of high temperatures.

Figure 5.11: Plots of radiation torque in the high-temperature limit. Figure (a) and (b) both shows the same torque radiated.

The first two plots confirm that the torque is proportional to μ, as derived in Eqn. 5.14. This also agrees with Eqn. 5.15, that in the high-temperature limit, the area is the only significant geometric quantity. The last plot shows that the radiation torque is linearly proportional to β^2 in the high-temperature limit. The remaining trace does not depend on μ or β and can be further evaluated.

$$\mathrm{Tr}(A^x V^y H) = -\frac{1}{i\hbar^3}\sum_{ijkl}(x_i - 2x_j + x_k)(y_k - y_l)H_{ij}H_{jk}H_{kl}H_{li}$$

If all the x are the same, or all the y are the same, there will be no contribution to the sum. Furthermore, a closed walks has to return to its starting site, so there are exactly two vertical edges and two horizontal edges for the non-zero terms. The 4 L-shape closed walks (Fig. 5.8b) of different orientations cancel exactly and only the 4 (out of 8) square loops (Fig. 5.8c) need to be considered. Again, there are $(N_x-1)(N_y-1)$ ways to place these square loops in the lattice. The full summation carried out is

$$\begin{aligned}\mathrm{Tr}(A^x V^y H) &= -\frac{t^4}{i\hbar^3}(N_x-1)(N_y-1)(-4ia^2\sin\theta_0)\\ &= \frac{4a^2t^4}{\hbar^3}(N_x-1)(N_y-1)\sin\theta_0\end{aligned}$$

This formula is checked numerically in MATLAB. Therefore, the high-temperature limit of the radiation torque expression is

$$N_z = -\frac{2a^2t^4\alpha}{3c^2\hbar^2}(N_x-1)(N_y-1)\mu\beta^2\sin\frac{qBa^2}{\hbar} \tag{5.15}$$

It is a sinusoidal function of the magnetic field and is also proportional to the area of the system. This result is verified numerically with the two plots below.

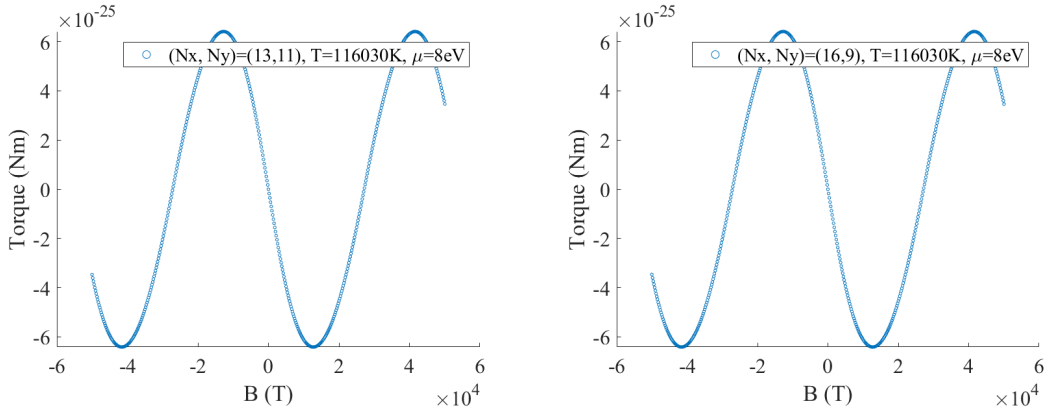

(a) Plot of torque against magnetic field for 13×11 system in the high-temperature limit.

(b) Plot of torque against magnetic field for 16×9 system in the high-temperature limit.

Figure 5.12: Plots of radiation torque in the high-temperature limit for two systems of different sizes but with the same area. The radiation torque plots have the same amplitude, as predicted by Eqn. 5.15.

Chapter 6

Conclusion

6.1 Main outcomes

We have investigated the physics of non-interacting electrons on discrete lattices, with a particular focus on their energy spectra, persistence current, and electromagnetic radiation. The effects of an external magnetic field were accounted for by the Peierls substitution. The eigenvalues and the eigenvectors of the Hamiltonian were found numerically using MATLAB.

Using the energy levels and energy eigenstates, we formed the Green functions. They can be used to compute the expectation values of the current operators and angular momentum at thermal equilibrium. The resulting current distributions are complicated, but basic symmetries were observed. In the high-temperature limit, the current decays to zero in an interesting way. The current vanishes faster in the interior and thus appears to be localized along the boundary. Through a Taylor expansion of the Fermi-Dirac distribution, we found that the current at the boundary of the square lattice vanishes as β^3. This power law is obeyed also for the triangle lattices, but not for the hexagonal lattice.

Using the energy levels and energy eigenstates, we also studied the electromagnetic radiation that arises from electron transitions. We used the electron Green function and velocity matrices to construct the current-current correlation function. Thecurrent-current correlation function allows us to find the total power and torque radiated using the energy eigenstates. The radiation was computed numerically and plotted while varying the parameters B, μ and T. Obtaining exact expressions was impractical due to the lack of exact expressions for the eigenstates, and further complicated by the summation involving the Fermi-Dirac distribution. But nevertheless, we managed to obtain simple analytic expressions in the high-temperature limit by Taylor expansion and considering closed walks of fixed lengths on the lattice. This led us to conclude that the radiation power scales with both the edge and the bulk of the system, whereas the radiation torque is a bulk effect at high temperatures. In the low temperature, the radiation is suppressed by an exponential factor, and will only radiate at specific values of μ and B.

6.2 Future works

For the next part of the project, we might want to consider systems with periodic boundary conditions. Despite having some physical inconsistencies, the eigenstates and eigenvectors are easily computed, and they might be good approximations when the system is large. We can also study the radiation phenomena in non-equilibrium, where the system is connected to heat baths. The non-equilibrium Green functions formalism will be most useful then.

Bibliography

[1] M. E. Cage, R. F. Dziuba, and B. F. Field, IEEE Transactions on Instrumentation and Measurement **IM-34**, 301 (1985).

[2] H. Bartolomei et al., Science **368**, 173 (2020).

[3] J. Nakamura, S. Liang, G. C. Gardner, and M. J. Manfra, Nature Physics **16**, 931 (2020).

[4] M. Büttiker, Phys. Rev. B **32**, 1846 (1985).

[5] H.-F. Cheung, Y. Gefen, E. K. Riedel, and W.-H. Shih, Phys. Rev. B **37**, 6050 (1988).

[6] R. A. Webb, S. Washburn, C. P. Umbach, and R. B. Laibowitz, Phys. Rev. Lett. **54**, 2696 (1985).

[7] L. P. Lévy, G. Dolan, J. Dunsmuir, and H. Bouchiat, Phys. Rev. Lett. **64**, 2074 (1990).

[8] V. Chandrasekhar et al., Phys. Rev. Lett. **67**, 3578 (1991).

[9] A. C. Bleszynski-Jayich et al., Science **326**, 272 (2009).

[10] N. W. Ashcroft and N. D. Mermin, *Solid state physics*, Cengage Learning, 1976.

[11] J. Jiang, An introduction to spectral graph theory, `http://math.uchicago.edu/~may/REU2012/REUPapers/JiangJ.pdf`.

[12] D. Tong, The quantum Hall effect, 2021, `http://www.damtp.cam.ac.uk/user/tong/qhe.html`.

[13] R. Peierls, Zeitschrift für Physik **80**, 763 (1933).

[14] D. R. Hofstadter, Phys. Rev. B **14**, 2239 (1976).

[15] W. Kohn, Phys. Rev. **115**, 1460 (1959).

[16] E. I. Blount, Phys. Rev. **126**, 1636 (1962).

[17] G. H. Wannier, Rev. Mod. Phys. **34**, 645 (1962).

[18] M. Graf and P. Vogl, Phys. Rev. B **51**, 4940 (1995).

[19] T. B. Boykin, R. C. Bowen, and G. Klimeck, Phys. Rev. B **63**, 245314 (2001).

[20] K. Ikeda, Journal of Mathematical Physics **59**, 061704 (2018).

[21] C. Tradunsky and O. Cohen, Hofstadter butterfly, 2006, `http://phelafel.technion.ac.il/~orcohen/butterfly.html`.

[22] S. Gao, Foundations of Science **23**, 145 (2018).

[23] G. D. Mahan, *Many-particle physics*, Springer (India), 2014.

[24] S. Datta, *Electronic transport in mesoscopic systems*, Cambridge University Press, 1999.

[25] M. Srednicki, Phys. Rev. E **50**, 888 (1994).

[26] J. Schmalian, Theory of condensed matter ii, 2018, `https://www.tkm.kit.edu/downloads/ss2018_tkm2/TKM2_revised.pdf`.

[27] R. Kotlyar, C. A. Stafford, and S. Das Sarma, Phys. Rev. B **58**, 3989 (1998).

[28] Y.-M. Zhang, T. Zhu, Z. Zhang, and J.-S. Wang, Microscopic theory of photon-induced energy, momentum, and angular momentum transport in nonequilibrium, 2021, `https://arxiv.org/abs/2108.07649`.

[29] Z.-Q. Zhang, J.-T. Lü, and J.-S. Wang, Phys. Rev. B **101**, 161406 (2020).

[30] Griffiths, *Introduction to electrodynamics*, Cambridge University Press, 2017.

[31] M. Janowicz, D. Reddig, and Holthaus, Physical Review A **68**, 043823 (2003).

[32] O. Keller, *Quantum theory of near-field electrodynamics*, Springer Berlin, 2013.

Appendix A

Fluctuation-dissipation theorem

Here we give a detailed derivation of the fluctuation-dissipation theorem. Recall that the electron Green functions/correlation functions are a function of a single real variable t. Extend the domain of the time argument into the complex numbers and observe the Kubo-Martin-Schwinger condition.

$$\begin{aligned}
\langle c_k^\dagger(0) c_j(t + i\hbar\beta)\rangle &= \frac{1}{\mathcal{Z}}\mathrm{Tr}(e^{-\beta(\mathcal{H}-\mu\mathcal{N})} c_k^\dagger e^{\frac{i}{\hbar}\mathcal{H}(t+i\beta\hbar)} c_j e^{-\frac{i}{\hbar}\mathcal{H}(t+i\beta\hbar)}) \\
&= \frac{1}{\mathcal{Z}}\mathrm{Tr}(e^{-\beta\mathcal{H}} e^{\beta\mu\mathcal{N}} c_k^\dagger e^{-\beta\mathcal{H}} e^{\frac{i}{\hbar}\mathcal{H}t} c_j e^{-\frac{i}{\hbar}\mathcal{H}t} e^{\beta\mathcal{H}}) \\
&= \frac{1}{\mathcal{Z}}\mathrm{Tr}(e^{\beta\mu\mathcal{N}} c_k^\dagger e^{-\beta\mathcal{H}} c_j(t)) \\
&= \frac{1}{\mathcal{Z}}\mathrm{Tr}(e^{-\beta\mathcal{H}} c_j(t) e^{\beta\mu\mathcal{N}} c_k^\dagger) \\
&= \frac{1}{\mathcal{Z}}\mathrm{Tr}(e^{-\beta\mathcal{H}} c_j(t) e^{\beta\mu n_k} e^{\beta\mu(\mathcal{N}-n_k)} c_k^\dagger) \\
&= \frac{1}{\mathcal{Z}}\mathrm{Tr}(e^{-\beta\mathcal{H}} c_j(t) e^{\beta\mu n_k} c_k^\dagger e^{\beta\mu(\mathcal{N}-n_k)}) \\
&= \mathrm{Tr}(e^{\beta\mu\mathcal{N}} e^{-\beta\mathcal{H}} c_j(t) e^{\beta\mu n_k} c_k^\dagger e^{-\beta\mu n_k}) \\
&= \frac{1}{\mathcal{Z}}\mathrm{Tr}(e^{-\beta(\mathcal{H}-\mu\mathcal{N})} c_j(t) e^{\beta\mu n_k} c_k^\dagger) \\
&= \frac{1}{\mathcal{Z}}\mathrm{Tr}(e^{-\beta(\mathcal{H}-\mu\mathcal{N})} c_j(t) e^{\beta\mu} c_k^\dagger) \\
&= e^{\beta\mu}\frac{1}{\mathcal{Z}}\mathrm{Tr}(e^{-\beta(\mathcal{H}-\mu\mathcal{N})} c_j(t) c_k^\dagger) \\
&= e^{\beta\mu}\langle c_j(t) c_k^\dagger(0)\rangle
\end{aligned}$$

The above relation applies to the Green functions directly from the defnitions.

$$-e^{\beta\mu} G_{jk}^{>}(t) = G_{jk}^{<}(t + i\hbar\beta)$$

Translation in time domain corresponds to multiplication by an exponential after Fourier transform, so intuitively

$$\begin{aligned}
e^{\beta\mu} G_{jk}^{>}(E) &= -e^{\beta E} G_{jk}^{<}(E) \\
G_{jk}^{>}(E) &= -e^{\beta(E-\mu)} G_{jk}^{<}(E)
\end{aligned}$$

Although the result is true, the reason is not as simple. The Green functions are not integrable because they do not decay as $t \to \infty$. Therefore, the Fourier transform has to be understood in the sense of distribution theory. One way to work this out is by using the Lehmann representation [26]. Eqn 4.13 can then be used to express $G^<_{jk}(E)$ and $G^>_{jk}(E)$ in terms of $G^r_{jk}(E)$ and $G^a_{jk}(E)$.

$$\begin{aligned} G^<_{jk}(E) &= -\frac{1}{e^{\beta(E-\mu)}+1}(G^r_{jk}(E) - G^a_{jk}(E)) \\ &= -f(E)(G^r_{jk}(E) - G^a_{jk}(E)) \\ G^>_{jk}(E) &= \frac{e^{\beta(E-\mu)}}{e^{\beta(E-\mu)}+1}(G^r_{jk}(E) - G^a_{jk}(E)) \\ &= [1-f(E)](G^r_{jk}(E) - G^a_{jk}(E)) \end{aligned}$$

In the energy domain, there is a nice formula for $G^r(E)$ and $G^a(E)$ [26]. Expanding in the energy basis and using the Sokhotsky-Plemelj formula,

$$\begin{aligned} G^r(E) &= (E + i0^+ - H)^{-1} \\ &= \sum_l \left[-i\pi\delta(E-E_l) + \mathcal{P}\left(\frac{1}{E-E_l}\right)\right] |E_l\rangle \langle E_l| \\ G^a(E) &= (E - i0^+ - H)^{-1} \\ &= \sum_l \left[i\pi\delta(E-E_l) + \mathcal{P}\left(\frac{1}{E-E_l}\right)\right] |E_l\rangle \langle E_l| \end{aligned}$$

The principal value part will cancel off when their difference is taken. The leftover terms are

$$\begin{aligned} G^<(E) &= (2\pi i) f(E) \sum_l \delta(E-E_l) |E_l\rangle \langle E_l| \\ G^>(E) &= -(2\pi i)[1-f(E)] \sum_l \delta(E-E_l) |E_l\rangle \langle E_l| \end{aligned}$$

Appendix B

Peierls substitution for other lattice geometries

The modification of the code from the square lattice to the triangular lattice is based on the following isomorphism.

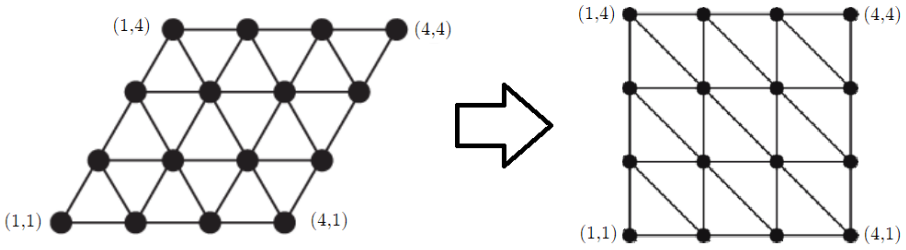

Figure B.1: Correspondence between triangular lattice and square lattice.

Thus, a triangular lattice can be viewed as a square lattice with six nearest-neighbours. Only a few lines of code needs to be modified to change the definition of the Hamiltonian. However, the Peierls phases have to be worked out analytically for all the edges. We label the lattice sites with an integer tuple coordinates (as in Fig. B.1). The relation between the coordinates and the physical position is

$$\begin{pmatrix} x \\ y \end{pmatrix} = a \begin{pmatrix} m + \frac{1}{2}n \\ \frac{\sqrt{3}}{2}n \end{pmatrix}$$

Using Landau gauge $\boldsymbol{A} = xB\hat{\boldsymbol{y}}$, the following Peierls phases are obtained.

$$\begin{aligned} \theta_{(m,n)\to(m+1,n)} &= 0 \\ \theta_{(m,n)\to(m,n+1)} &= \frac{\sqrt{3}}{2}\frac{qa^2B}{\hbar}\left(m + \frac{1}{4}\right) \\ \theta_{(m,n)\to(m-1,n+1)} &= \frac{\sqrt{3}}{2}\frac{qa^2B}{\hbar}\left(m - \frac{1}{4}\right) \end{aligned}$$

Next, we consider the hexagonal (or honeycomb) lattice. The hexagonal lattice is not a Bravais lattice, so it would appear to be harder to implement the Peierls

substitutionn in code. However, the result turns out to be quite simple if we choose the Landau gauge. Again, we have an isomorphism to convert the hexagonal lattice into a square lattice.

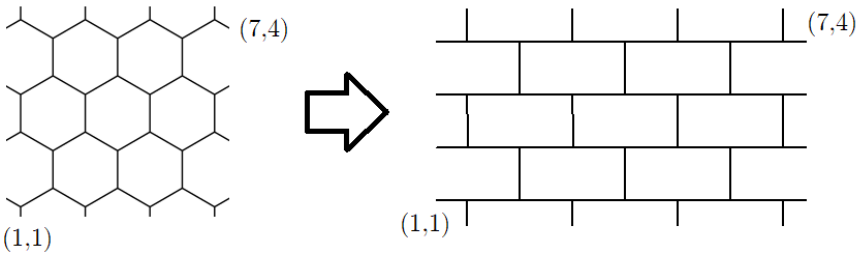

Figure B.2: Correspondence between hexagon lattice and square lattice.

The hexagonal lattice can be considered as a superposition of two triangular Bravais lattice. This means that in calculating the Peierls phase, we need to specify the sublattice which we are refering to. However, if we choose the gauge $\boldsymbol{A} = -yB\hat{\boldsymbol{x}}$, then the "horizontal" edges will all have the same Peierl phase.

$$\theta_{(m,n)\to(m+1,n)} = -\frac{3\sqrt{3}}{4}\frac{qa^2B}{\hbar}n$$

For the vertical edges, the associated Peierls phase is zero. The other only modification required is to set half of the vertical hopping to zero.

Appendix C

Proof for third order trace

Here we investigate the trace $\mathrm{Tr}(H^3 I)$ in more detail. We will show that it is zero when I is an interior edge, and non-zero when I is a boundary edge. But before that, some properties of adjacency matrices in graph theory are discussed. As a simple example, consider the following path graph of length 6.

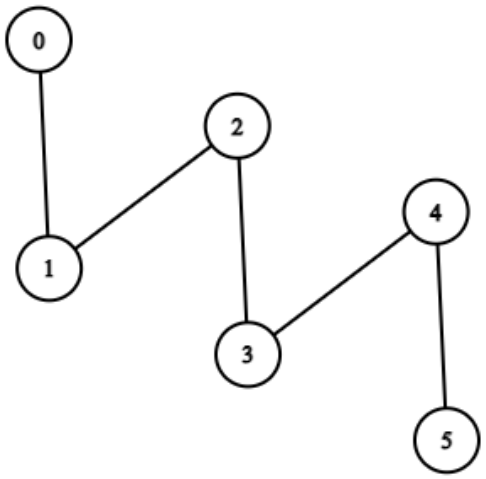

Figure C.1: Path graph with 6 vertices.

Its adjacency matrix is

$$A = \begin{pmatrix} 0 & 1 & 0 & 0 & 0 & 0 \\ 1 & 0 & 1 & 0 & 0 & 0 \\ 0 & 1 & 0 & 1 & 0 & 0 \\ 0 & 0 & 1 & 0 & 1 & 0 \\ 0 & 0 & 0 & 1 & 0 & 1 \\ 0 & 0 & 0 & 0 & 1 & 0 \end{pmatrix}$$

The adjacency matrix provides information about the neighbours of every vertex. In particular, the number of ways to travel from site j to site k in 1 step is given by

the matrix element A_{ij}. Next, we compute the higher powers of A.

$$A^2 = \begin{pmatrix} 1 & 0 & 1 & 0 & 0 & 0 \\ 0 & 2 & 0 & 1 & 0 & 0 \\ 1 & 0 & 2 & 0 & 1 & 0 \\ 0 & 1 & 0 & 2 & 0 & 1 \\ 0 & 0 & 1 & 0 & 2 & 0 \\ 0 & 0 & 0 & 1 & 0 & 1 \end{pmatrix} \qquad A^3 = \begin{pmatrix} 0 & 2 & 0 & 1 & 0 & 0 \\ 2 & 0 & 3 & 0 & 1 & 0 \\ 0 & 3 & 0 & 3 & 0 & 1 \\ 1 & 0 & 3 & 0 & 3 & 0 \\ 0 & 1 & 0 & 3 & 0 & 2 \\ 0 & 0 & 1 & 0 & 2 & 0 \end{pmatrix}$$

The matrix elements of A^2 tells us the number of ways to travel from site j to site k in exactly two steps. This can be seen from the definition of matrix multiplication. However, the Hamiltonian has complex entries, due to Peierls substitution.

$$H_{jk} = (-t)e^{i\theta_{k\to j}}$$

Thus, the higher powers of H will have matrix elements

$$\begin{aligned}(H^2)_{jl} &= (-t)^2 \sum_k H_{jk}H_{kl} \\ &= (-t)^2 \sum_k e^{i(\theta_{l\to k}+\theta_{k\to j})}\end{aligned}$$

The Peirels phases tend to add up in the complex exponential, which can also be understood as the total phase accumulated when travelling along a certain path. Thus, the matrix elements of H^3 involves count the number of ways to travel from site j to site k in exactly three steps, while also taking into account the Peierls phases. Below, the possible type of edges in a square lattice are enumerated.

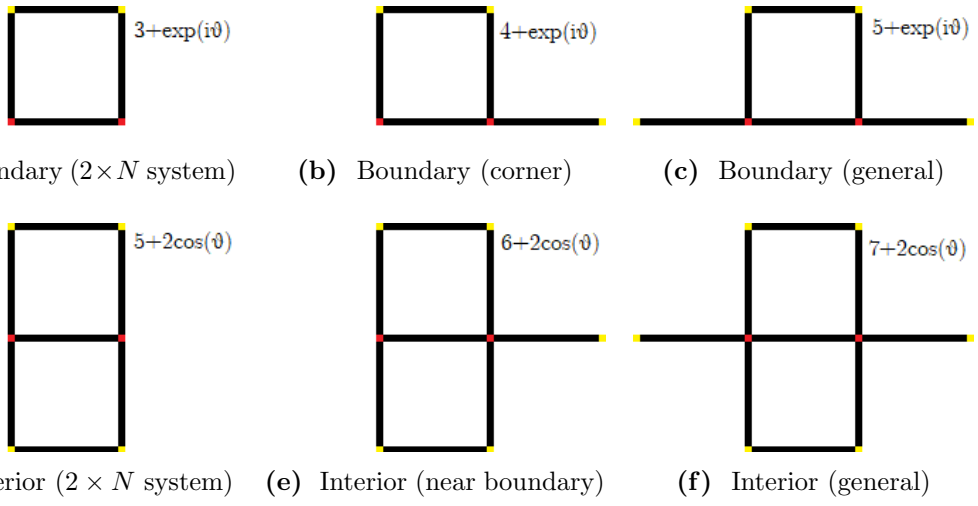

(a) Boundary ($2\times N$ system) **(b)** Boundary (corner) **(c)** Boundary (general)

(d) Interior ($2 \times N$ system) **(e)** Interior (near boundary) **(f)** Interior (general)

Figure C.2: All possible types of edges in a square lattice system.

If we consider the edge in Fig. C.2a, there are 4 ways to go from the left red site to the right red site in exactly 3 steps. They are: 1) $\uparrow\downarrow\rightarrow$, 2) $\rightarrow\leftarrow\rightarrow$, 3) $\rightarrow\uparrow\downarrow$, 4) $\uparrow\rightarrow\downarrow$. In the first three ways, there is always an edge that is traversed twice and in opposite direction. That edge does not contribute any phase to the total Peierls phase. So for those three ways, the total Peierls phase is simply the phase of the edge joining the two red sites, which we denote as $\Omega \equiv \theta_{l\to j}$.

However, for the fourth way, the total Peierls phase is not the same as the previous three. The total phase can be computed by the following trick. Extend the path to a 5-step walk, $\uparrow\rightarrow\downarrow\leftarrow\rightarrow$. This does not introduce any additional phase as the last two steps cancel each other. The total phase is then $\theta_0 + \Omega$, where Ω is as defined earlier and comes from the last step, and θ_0 is the Aharonov-Bohm phase (Eqn. 3.5) for traversing around a square plaquette (which is gauge invariant).

Therefore, the matrix element of H^3 is the sum over all these possible walks, similar to the path integral formalism of quantum mechanics. They are

$$\begin{aligned}(H^3)_{lj} &= e^{i\Omega} + e^{i\Omega} + e^{i\Omega} + e^{i\Omega}e^{i\theta_0} \\ &= (3 + e^{i\theta_0})e^{i\Omega}\end{aligned}$$

It is the relative phase $(3 + e^{i\theta_0})$ that is important, as we will see subsequently. The counting is done for each of the scenario in Fig. C.2 and the relative phase is written in the upper-right corner of each figure. The key observation is that for the interior edges, the relative phase is real, while for the boundary edges, the relative phase is complex. This arises because in the cases of the interior edges, there are always two paths that give phases which are complex conjugate of each other (going upwards versus going downwards). The imaginary part of the phase cancels when the contributions from the two paths are added. For boundary edges, there is no such path to go downwards and so the total phase still has an imaginary component.

Now, we are ready to give a proof on why the third-order trace vanishes in the interior. Suppose the matrix H^3 is written as

$$H^3 = \begin{pmatrix} z_{11} & z_{12} & z_{13} & \cdots & z_{1N} \\ z_{21} & z_{22} & z_{23} & & \\ z_{31} & z_{31} & z_{33} & & \\ \vdots & & & \ddots & \\ z_{N1} & & & & z_{NN} \end{pmatrix}$$

The current operator can also be written as a matrix

$$I_{j\rightarrow l} = = \frac{q}{i\hbar}\begin{pmatrix} & & H_{lj} & \\ & & & \\ & -H_{jl} & & \\ & & & \end{pmatrix}$$

Their matrix product is

$$H^3 I_{j\rightarrow l} = = \frac{q}{i\hbar}\begin{pmatrix} -H_{jl}z_{1j} & H_{lj}z_{1l} \\ -H_{jl}z_{2j} & H_{lj}z_{2l} \\ -H_{jl}z_{3j} & H_{lj}z_{3l} \\ \vdots & \vdots \\ -H_{jl}z_{Nj} & H_{lj}z_{Nl} \end{pmatrix}$$

Therefore, the trace is given by

$$\begin{aligned}\mathrm{Tr}(H^3 I_{j\to l}) &= \frac{q}{i\hbar}(-H_{jl}z_{lj} + H_{lj}z_{jl}) \\ &= -\frac{2q}{i\hbar}\Im H_{jl}z_{lj}\end{aligned}$$

However, since only the current between nearest neighbours are considered (otherwise $H_{lj} = 0$), the matrix element is actually

$$H_{jl} = (-t)e^{-i\Omega}$$

Hence, whether the trace is zero or not depends on whether the relative phase is real or complex.

This manner of reasoning has many other implications. For example, we can immediately conclude that $\mathrm{Tr}(H^2 I) = 0$ for square lattice as it is a bipartite graph and there is no way to reach a nearest-neighbour in exactly two steps. For a hexagonal lattice, the current decays as T^{-5} at the boundary in the high temperature limit. This is because the minimum number of steps to reach a nearest neighbour while having a non-trivial phase (going around a hexagonal plaquette) is 5. This argument is also useful when interactions between next-nearest neighbours are allowed.

Appendix D

Derivation of current-current correlation function

D.1 Time evolution of fermionic operators

We start by stating that the anti-commmutation relations hold whenever the operators are taken to be at the same time.

$$\begin{aligned}
\{c_m^\dagger(t), c_n(t)\} &= \{U(t)c_m^\dagger U(t)^\dagger, U(t)c_n U(t)^\dagger\} \\
&= U(t)c_m^\dagger U(t)^\dagger U(t)c_n U(t)^\dagger + U(t)c_n U(t)^\dagger U(t)c_m^\dagger U(t)^\dagger \\
&= U(t)c_m^\dagger c_n U(t)^\dagger + U(t)c_n c_m^\dagger U(t)^\dagger \\
&= U(t)\{c_m^\dagger, c_n\}U(t)^\dagger \\
&= U(t)\delta_{mn}U(t)^\dagger \\
&= \delta_{mn}
\end{aligned}$$

In the context of the non-interacting Hamiltonian, as given in Eqn, 2.3, we can solve for the equations of motion for the fermion annihilation operators.

$$\begin{aligned}
i\hbar\frac{\mathrm{d}}{\mathrm{d}t}c_j(t) &= [c_j(t), \mathcal{H}] \\
&= \sum_{mn} H_{mn}[c_j(t), c_m^\dagger(t)c_n(t)] \\
&= \sum_{mn} H_{mn}(c_j(t)c_m^\dagger(t)c_n(t) - c_m^\dagger(t)c_n(t)c_j(t)) \\
&= \sum_{mn} H_{mn}((-c_m^\dagger(t)c_j(t) + \delta_{mj})c_n(t) + c_m^\dagger(t)c_j(t)c_n(t)) \\
&= \sum_{mn} H_{mn}\delta_{mj}c_n(t) \\
&= \sum_{n} H_{jn}c_n(t)
\end{aligned}$$

If we put the annihilation operator into a column vector, $\boldsymbol{c}$, the system of differential equations can be written in a Schrödinger-like form

$$i\hbar\frac{\mathrm{d}}{\mathrm{d}t}\boldsymbol{c}(t) = H\boldsymbol{c}(t)$$

The solution is

$$\boldsymbol{c}(t) = e^{-\frac{i}{\hbar}Ht}\boldsymbol{c}(0) \equiv U(t)\boldsymbol{c}(0)$$

where $U(t) \equiv e^{-\frac{i}{\hbar}Ht}$ is a unitary matrix. In component form,

$$c_l(t) = \sum_q U_{lq}(t)c_q$$

The time evolution of the creation operator is obtained simply by taking the Hermitian conjugate.

$$c_k^\dagger(t) = \sum_p U_{kp}^*(t)c_p^\dagger$$

D.2 Wick's theorem

Wick's theorem states that the average of the following 4 fermionic operators at equal time is

$$\langle c_i^\dagger c_j c_p^\dagger c_q\rangle = \langle c_i^\dagger c_q\rangle\langle c_j c_p^\dagger\rangle + \langle c_i^\dagger c_j\rangle\langle c_p^\dagger c_q\rangle$$

Using the results above, the generalization to operators at different time is as follows.

$$\begin{aligned}
\langle c_i^\dagger c_j c_k^\dagger(t)c_l(t)\rangle &= \sum_{pq} U_{lq}(t)U_{kp}^*(t)\langle c_i^\dagger c_j c_p^\dagger c_q\rangle \\
&= \sum_{pq} U_{lq}(t)U_{kp}^*(t)(\langle c_i^\dagger c_q\rangle\langle c_j c_p^\dagger\rangle + \langle c_i^\dagger c_j\rangle\langle c_p^\dagger c_q\rangle) \\
&= \underbrace{\langle c_i^\dagger c_l(t)\rangle}_{-i\hbar G_{li}^<(t)}\underbrace{\langle c_j c_k^\dagger(t)\rangle}_{i\hbar G_{jk}^>(-t)} + \underbrace{\langle c_i^\dagger c_j\rangle}_{-i\hbar G_{lk}^<(0)}\underbrace{\langle c_k^\dagger(t)c_l(t)\rangle}_{-i\hbar G_{ji}^<(0)}
\end{aligned}$$

Subsequently, we will see that the second term contributes nothing in the expression of the current-current correlation function.

D.3 Current-current correlation

Here, we define one variant of the current-current correlation function. It is also proportional to the velocity-velocity correlation function due to Eqn. 4.4.

$$\Pi_{\mu\nu}^<(t) = \frac{1}{i\hbar}\langle I^\nu(0)I^\mu(t)\rangle$$

$$
\begin{aligned}
&= \frac{q^2}{i\hbar}\langle V^\nu(0)V^\mu(t)\rangle \\
&= \frac{q^2}{i\hbar}\sum_{ijkl} V^\nu_{ij}V^\mu_{kl}\langle c_i^\dagger c_j c_k^\dagger(t)c_l(t)\rangle
\end{aligned}
$$

Using Wick's theorem,

$$
\begin{aligned}
\Pi^<_{\mu\nu}(t) &= \frac{q^2}{i\hbar}\sum_{ijkl} V^\nu_{ij}\langle c_j c_k^\dagger(t)\rangle V^\mu_{kl}\langle c_l(t)c_i^\dagger\rangle + \frac{q^2}{i\hbar}\sum_{ij} V^\nu_{ij}\langle c_i^\dagger c_j\rangle \sum_{kl} V^\mu_{kl}\langle c_k^\dagger c_l\rangle \\
&= -i\hbar q^2 \sum_{ijkl} V^\mu_{kl}G^<_{li}(t)V^\nu_{ij}G^>_{jk}(-t) + \frac{q^2}{i\hbar}\sum_{ij}(-i\hbar V^\nu_{ij}G^<_{ji}(0))\sum_{kl}(-i\hbar V^\mu_{kl}G^<_{lk}(0)) \\
&= -i\hbar q^2 \mathrm{Tr}[V^\mu G^<(t)V^\nu G^>(-t)] + \frac{q^2}{i\hbar}\underbrace{\langle V^\nu\rangle}_{=0}\underbrace{\langle V^\mu\rangle}_{=0} \\
&= -i\hbar q^2 \mathrm{Tr}[V^\mu G^<(t)V^\nu G^>(-t)]
\end{aligned}
$$

This is Eqn. 5.1 in the main text.

Appendix E

Derivation of radiation formulae

In classical electromagnetism, the Poynting vector represents the flow of electromagnetic (EM) energy and momentum. It can be expressed in terms of the electric and magnetic fields [30].

$$\boldsymbol{S} = \frac{1}{\mu_0}\boldsymbol{E} \times \boldsymbol{B}$$

In QM, it is more favorable to express everything in terms of the EM potentials. We adopt the temporal gauge, where there is no scalar potential, $\phi = 0$. The EM fields can then be expressed in terms of the vector potential $\boldsymbol{A}$ alone.

$$\begin{aligned}\boldsymbol{E} &= -\frac{\partial \boldsymbol{A}}{\partial t} \\ \boldsymbol{B} &= \nabla \times \boldsymbol{A}\end{aligned}$$

Or in terms of indices (with implied summation over repeated indices)

$$\begin{aligned}E_\mu &= -\partial_t A_\mu \\ B_\nu &= \epsilon_{\nu\gamma\delta}\partial_\gamma A_\delta\end{aligned}$$

The components of the Poynting vector are thus

$$\begin{aligned}S_\alpha &= \frac{1}{\mu_0}\epsilon_{\alpha\mu\nu}E_\mu B_\nu \\ &= -\frac{1}{\mu_0}\epsilon_{\nu\gamma\delta}\epsilon_{\alpha\mu\nu}(\partial_t A_\mu)(\partial_\gamma A_\delta)\end{aligned}$$

At this point, we introduce the definition of the photon Green functions.

$$D^<_{\mu\nu}(\boldsymbol{r}, t, \boldsymbol{r}', t') \equiv \frac{1}{i\hbar}\langle A_\nu(\boldsymbol{r}', t')A_\mu(\boldsymbol{r}, t)\rangle \tag{E.1}$$

$$D^>_{\mu\nu}(\boldsymbol{r}, t, \boldsymbol{r}', t') \equiv \frac{1}{i\hbar}\langle A_\mu(\boldsymbol{r}, t)A_\nu(\boldsymbol{r}', t')\rangle \tag{E.2}$$

Then, the expectation value of the Poynting vector is

$$\langle S_\alpha\rangle = -\frac{1}{\mu_0}\epsilon_{\nu\gamma\delta}\epsilon_{\alpha\mu\nu}\langle(\partial_t A_\mu)(\partial_\gamma A_\delta)\rangle$$

$$= -\frac{1}{\mu_0}\epsilon_{\nu\gamma\delta}\epsilon_{\alpha\mu\nu}\partial_{t'}\partial_\gamma\langle A_\mu(\boldsymbol{r}',t')A_\delta(\boldsymbol{r},t)\rangle|_{\boldsymbol{r}'=\boldsymbol{r},t'=t}$$

In the classical world, the order of the product of quantities do not matter. However, in the quantum world, there is a difference in writing $A_\mu A_\nu$ versus $A_\nu A_\mu$. Also, the product of two Hermitian operators is not necessarily Hermitian. According to Janowicz et al. [31], the correct way to proceed is to use normal ordering.

$$\langle :S_\alpha: \rangle = -\frac{1}{\mu_0}\epsilon_{\nu\gamma\delta}\epsilon_{\alpha\mu\nu}\partial_{t'}\partial_\gamma\langle :A_\mu(\boldsymbol{r}',t')A_\delta(\boldsymbol{r},t):\rangle|_{\boldsymbol{r}'=\boldsymbol{r},t'=t}$$

Normal ordering involves decomposing the operator into the sum of a "positive frequency part" and a "negative frequency part". To do this, we need to use the Fourier transform of the operator.

$$A(\omega) = \int_{-\infty}^{\infty} A(t)e^{i\omega t}\,\mathrm{d}t$$

We assume that the Fourier transform and the inverse Fourier transform both exist, and the Fourier inversion theorem holds. $A(t)$ is assumed to be a Hermitian operator, so

$$\begin{aligned} A(\omega)^\dagger &= \int_{-\infty}^{\infty} A(t)e^{-i\omega t}\,\mathrm{d}t \\ &= A(-\omega) \end{aligned}$$

We define the positive and negative frequency terms of $A(t)$ using with a slight modification of the inverse Fourier transform

$$\begin{aligned} A^{(+)}(t) &\equiv \frac{1}{2\pi}\int_0^{\infty} A(\omega)e^{-i\omega t}\,\mathrm{d}\omega \\ A^{(-)}(t) &\equiv \frac{1}{2\pi}\int_{-\infty}^{0} A(\omega)e^{-i\omega t}\,\mathrm{d}\omega \end{aligned}$$

such that $A(t) = A^{(+)}(t) + A^{(-)}(t)$. Since $A(t)^\dagger = A(t)$, we have a relation between the positive and negative frequency terms.

$$\begin{aligned} A^{(+)}(t)^\dagger &= \frac{1}{2\pi}\int_0^{\infty} A(\omega)^\dagger e^{i\omega t}\,\mathrm{d}\omega \\ &= \frac{1}{2\pi}\int_0^{\infty} A(-\omega)e^{i\omega t}\,\mathrm{d}\omega \\ &= \frac{1}{2\pi}\int_{-\infty}^{0} A(\omega)e^{-i\omega t}\,\mathrm{d}\omega \\ &= A^{(-)}(t) \end{aligned}$$

The normal ordering ensures that whenever there are product of operators, the negative frequency term is on the left and the positive frequency term is on the right. To be less cumbersome, we temporarily suppress the time dependence of A in the next few lines.

$$:A_\mu A_\nu: = :(A_\mu^{(+)} + A_\mu^{(-)})(A_\nu^{(+)} + A_\nu^{(-)}):$$

$$
\begin{aligned}
&=: A_\mu^{(+)} A_\nu^{(+)} + A_\mu^{(+)} A_\nu^{(-)} + A_\mu^{(-)} A_\nu^{(+)} + A_\mu^{(-)} A_\nu^{(-)} : \\
&= A_\mu^{(+)} A_\nu^{(+)} + A_\nu^{(-)} A_\mu^{(+)} + A_\mu^{(-)} A_\nu^{(+)} + A_\mu^{(-)} A_\nu^{(-)} \\
&= A_\mu^{(+)} A_\nu^{(+)} - A_\nu^{(+)} A_\mu^{(+)} + A_\nu^{(+)} A_\mu^{(+)} + A_\nu^{(-)} A_\mu^{(+)} + A_\mu^{(-)} A_\nu^{(+)} + A_\mu^{(-)} A_\nu^{(-)} \\
&= [A_\mu^{(+)}, A_\nu^{(+)}] + A_\nu A_\mu^{(+)} + A_\mu^{(-)} A_\nu
\end{aligned}
$$

The commutator between the positive frequency terms is zero. Therefore, the expectation value is a real quantity.

$$
\begin{aligned}
\langle : A_\mu A_\nu : \rangle &= \langle A_\nu A_\mu^{(+)} \rangle + \langle A_\mu^{(-)} A_\nu \rangle \\
&= 2\Re \langle A_\nu A_\mu^{(+)} \rangle
\end{aligned}
$$

The order of the indices μ, ν does not matter here. One can show using the same approach that

$$
: A_\nu A_\mu : = A_\nu A_\mu^{(+)} + A_\mu^{(-)} A_\nu + [A_\nu^{(-)}, A_\mu^{(-)}]
$$

and

$$
\langle : A_\mu A_\nu : \rangle = 2\Re \langle A_\nu A_\mu^{(+)} \rangle = \langle : A_\nu A_\mu : \rangle
$$

Now, we are interested to evaluate the expectation $\langle A_\nu A_\mu^{(+)} \rangle$. We aim to write this in terms of the photon Green function defined in Eqn. E.1.

$$
\begin{aligned}
\frac{1}{i\hbar} \langle A_\nu(t') A_\mu^{(+)}(t) \rangle &= \frac{1}{i\hbar} \langle A_\nu(0) A_\mu^{(+)}(t - t') \rangle \\
&= \frac{1}{2\pi} \int_0^\infty \frac{1}{i\hbar} \langle A_\nu(0) A_\mu(\omega) \rangle e^{-i\omega(t-t')} \mathrm{d}\omega \\
&= \frac{1}{2\pi} \int_0^\infty D_{\mu\nu}^<(\omega) e^{-i\omega(t-t')} \, \mathrm{d}\omega
\end{aligned}
$$

Where we have introduce the photon Green function in frequency domain.

$$
\begin{aligned}
D_{\mu\nu}^<(\boldsymbol{r}, \boldsymbol{r}', \omega) &\equiv \int_{-\infty}^\infty D_{\mu\nu}^<(\boldsymbol{r}, t, \boldsymbol{r}', t') e^{i\omega(t-t')} \mathrm{d}t \\
&= \int_{-\infty}^\infty D_{\mu\nu}^<(\boldsymbol{r}, t, \boldsymbol{r}', t' = 0) e^{i\omega t} \mathrm{d}t \\
&= \frac{1}{i\hbar} \langle A_\nu(\boldsymbol{r}', t' = 0) \int_{-\infty}^\infty A_\mu(\boldsymbol{r}, t) e^{i\omega t} \mathrm{d}t \rangle \\
&= \frac{1}{i\hbar} \langle A_\nu(\boldsymbol{r}', t' = 0) A_\mu(\boldsymbol{r}, \omega) \rangle
\end{aligned}
$$

Therefore, the average value of the normal-ordered operators is

$$
\langle : A_\mu(\boldsymbol{r}', t') A_\delta(\boldsymbol{r}, t) : \rangle = -\frac{\hbar}{\pi} \Im \int_0^\infty D_{\mu\delta}^<(\boldsymbol{r}, \boldsymbol{r}', \omega) e^{-i\omega(t-t')} \, \mathrm{d}\omega
$$

The expression for the Poynting vector involves differentiation in time and space. The temporal derivative becomes the factor $i\omega$ under the Fourier transform.

$$
\partial_{t'} \partial_\gamma \langle : A_\mu(\boldsymbol{r}', t') A_\delta(\boldsymbol{r}, t) : \rangle = -\frac{\hbar}{\pi} \Im \int_0^\infty i\omega \partial_\gamma D_{\mu\delta}^<(\boldsymbol{r}, \boldsymbol{r}', \omega) e^{-i\omega(t-t')} \, \mathrm{d}\omega
$$

$$= -\frac{\hbar}{\pi}\Re\int_0^\infty \omega\partial_\gamma D^<_{\mu\delta}(\boldsymbol{r},\boldsymbol{r}',\omega)e^{-i\omega(t-t')}\,\mathrm{d}\omega$$

Finally, the expression for the average Poynting vector is

$$\begin{aligned}\langle :S_\alpha(\boldsymbol{r},t): \rangle &= -\frac{1}{\mu_0}\epsilon_{\nu\gamma\delta}\epsilon_{\alpha\mu\nu}\partial_{t'}\partial_\gamma\langle :A_\mu(\boldsymbol{r}',t')A_\delta(\boldsymbol{r},t): \rangle|_{\boldsymbol{r}'=\boldsymbol{r},t'=t}\\ &= \frac{\hbar}{\pi\mu_0}\epsilon_{\nu\gamma\delta}\epsilon_{\alpha\mu\nu}\Re\int_0^\infty \omega\partial_\gamma D^<_{\mu\delta}(\boldsymbol{r},\boldsymbol{r}',\omega)e^{-i\omega(t-t')}\,\mathrm{d}\omega|_{\boldsymbol{r}'=\boldsymbol{r},t'=t}\\ &= \frac{\hbar}{\pi\mu_0}\epsilon_{\nu\gamma\delta}\epsilon_{\alpha\mu\nu}\Re\int_0^\infty \omega\partial_\gamma D^<_{\mu\delta}(\boldsymbol{r},\boldsymbol{r}',\omega)\,\mathrm{d}\omega|_{\boldsymbol{r}'=\boldsymbol{r}}\end{aligned}$$

Using the identity $\epsilon_{\nu\gamma\delta}\epsilon_{\alpha\mu\nu} = \delta_{\alpha\gamma}\delta_{\mu\delta} - \delta_{\alpha\delta}\delta_{\mu\gamma}$, the expression can be simplified to

$$\langle :S_\alpha(\boldsymbol{r},t): \rangle = \frac{\hbar}{\pi\mu_0}(\delta_{\alpha\gamma}\delta_{\mu\delta} - \delta_{\alpha\delta}\delta_{\mu\gamma})\Re\int_0^\infty \omega\partial_\gamma D^<_{\mu\delta}(\boldsymbol{r},\boldsymbol{r}',\omega)\,\mathrm{d}\omega|_{\boldsymbol{r}'=\boldsymbol{r}} \tag{E.3}$$

Next, write $D^<_{\mu\nu}(\boldsymbol{r},\boldsymbol{r}',\omega)$ as a matrix and use the Keldysh equation.

$$D^<(\omega) = D^r(\omega)\Pi^<(\omega)D^a(\omega) \approx d^r(\omega)\Pi^<(\omega)d^a(\omega) \tag{E.4}$$

D^r and D^a are the retarded and advanced photon Green functions, with $(D^r)^\dagger = D^a$, and Π is the current-current correlation function. D^r can be approximated with the free photon Green functions, d^r, by truncating the Dyson series at the zeroth order

$$\begin{aligned}D^r &= d^r + d^r\Pi^r D^r\\ &= d^r + d^r\Pi^r d^r + d^r\Pi^r d^r\Pi^r d^r + \ldots\\ &\approx d^r\end{aligned}$$

Eqn. E.4 in component form is

$$D^<_{\mu\delta}(\boldsymbol{r},\boldsymbol{r}',\omega) = \sum_{\sigma\beta jl} d^r_{\mu\sigma}(\boldsymbol{r},\boldsymbol{r}_j,\omega)\Pi^<_{\sigma\beta}(\boldsymbol{r}_j,\boldsymbol{r}_l,\omega)d^a_{\beta\delta}(\boldsymbol{r}_l,\boldsymbol{r}',\omega)$$

Since we are later going to integrate over a large spherical surface, we make the following monopole approximation.

$$d^r_{\mu\sigma}(\boldsymbol{r},\boldsymbol{r}_j,\omega) = d^r_{\mu\sigma}(\boldsymbol{r}-\boldsymbol{r}_j,\omega) \approx d^r_{\mu\sigma}(\boldsymbol{r},\omega)$$

The expressions for the free photon Green functions are [32]

$$d^r_{\mu\sigma}(\boldsymbol{r},\omega) = -\frac{e^{i\frac{\omega}{c}r}}{4\pi\epsilon_0 c^2 r}\left(\delta_{\mu\sigma} - \frac{x_\mu x_\sigma}{r^2}\right) + \mathcal{O}(1/r^2) \tag{E.5}$$

$$d^a_{\beta\delta}(\boldsymbol{r},\omega) = -\frac{e^{-i\frac{\omega}{c}r}}{4\pi\epsilon_0 c^2 r}\left(\delta_{\beta\delta} - \frac{x_\beta x_\delta}{r^2}\right) + \mathcal{O}(1/r^2) \tag{E.6}$$

The higher order terms can be neglected as there will be a surface integral later, and we will take r to be large. The next step is to work out the derivative ∂_γ.

$$\partial_\gamma D^<_{\mu\delta}(\boldsymbol{r},\boldsymbol{r}',\omega) = (\partial_\gamma d^r_{\mu\sigma}(\boldsymbol{r},\omega))\left(\sum_{jl}\Pi^<_{\sigma\beta}(\boldsymbol{r}_j,\boldsymbol{r}_l,\omega)\right)d^a_{\beta\delta}(\boldsymbol{r}',\omega)$$

We try to perform the derivatives term by term.

$$\partial_\gamma \left(\frac{e^{ikr}}{r} \right) = ik \frac{x_\gamma}{r^2} e^{ikr} + \mathcal{O}(1/r^2)$$
$$\partial_\gamma \left(\frac{e^{ikr} x_\mu x_\sigma}{r^3} \right) = ik \frac{x_\mu x_\sigma x_\gamma}{r^4} e^{ikr} + \mathcal{O}(1/r^2)$$

so that

$$\begin{aligned} \partial_\gamma d^r_{\mu\sigma}(\boldsymbol{r}, \omega) &= -i\omega x_\gamma \frac{e^{i\frac{\omega}{c}r}}{4\pi\epsilon_0 c^3 r^2} \left(\delta_{\mu\sigma} - \frac{x_\mu x_\sigma}{r^2} \right) \\ &= i\frac{\omega x_\gamma}{cr} d^r_{\mu\sigma}(\boldsymbol{r}, \omega) \end{aligned}$$

and

$$\partial_\gamma D^<_{\mu\delta}(\boldsymbol{r}, \boldsymbol{r}', \omega) = i\frac{\omega x_\gamma}{cr} d^r_{\mu\sigma}(\boldsymbol{r}, \omega) \left(\sum_{jl} \Pi^<_{\sigma\beta}(\boldsymbol{r}_j, \boldsymbol{r}_l, \omega) \right) d^a_{\beta\delta}(\boldsymbol{r}', \omega)$$

The current-current correlation function is obtained using the random phase approximation.

$$\begin{aligned} \sum_{jl} \Pi^<_{\sigma\beta}(\boldsymbol{r}_j, \boldsymbol{r}_l, \omega) &= \Pi^<_{\sigma\beta}(\omega) \\ &= \int_{-\infty}^{\infty} \Pi^<_{\sigma\beta}(t) e^{i\omega t} \, \mathrm{d}t \end{aligned}$$

where the current-current correlation in the time-domain is given in the main text in Eqn. 5.1. Therefore, continuing from Eqn. E.3, the Poynting vector is

$$\begin{aligned} \langle : S_\alpha(\boldsymbol{r}, t) : \rangle &= \frac{\hbar}{\pi\mu_0} (\delta_{\alpha\gamma}\delta_{\mu\delta} - \delta_{\alpha\delta}\delta_{\mu\gamma}) \Re \int_0^\infty i\frac{\omega^2 x_\gamma}{cr} d^r_{\mu\sigma}(\boldsymbol{r}, \omega) \Pi^<_{\sigma\beta}(\omega) d^a_{\beta\delta}(\boldsymbol{r}, \omega) \mathrm{d}\omega \\ &= -\frac{\hbar x_\gamma}{\pi\mu_0 cr} (\delta_{\alpha\gamma}\delta_{\mu\delta} - \delta_{\alpha\delta}\delta_{\mu\gamma}) \Im \int_0^\infty \omega^2 d^r_{\mu\sigma}(\boldsymbol{r}, \omega) \Pi^<_{\sigma\beta}(\omega) d^a_{\beta\delta}(\boldsymbol{r}, \omega) \mathrm{d}\omega \end{aligned}$$

Using Eqn. E.5 and Eqn. E.6, the free photon Green functions can be eliminated.

$$\begin{aligned} \langle : S_\alpha(\boldsymbol{r}, t) : \rangle &= -\frac{\hbar x_\gamma}{\pi\mu_0 cr} (\delta_{\alpha\gamma}\delta_{\mu\delta} - \delta_{\alpha\delta}\delta_{\mu\gamma}) \Im \int_0^\infty \mathrm{d}\omega \, \omega^2 \\ &\qquad \frac{e^{i\frac{\omega}{c}r}}{4\pi\epsilon_0 c^2 r} \left(\delta_{\mu\sigma} - \frac{x_\mu x_\sigma}{r^2} \right) \Pi^<_{\sigma\beta}(\omega) \frac{e^{-i\frac{\omega}{c}r}}{4\pi\epsilon_0 c^2 r} \left(\delta_{\beta\delta} - \frac{x_\beta x_\delta}{r^2} \right) \\ &= \frac{-\hbar x_\gamma}{16\pi^3 \epsilon_0^2 \mu_0 c^5 r^3} (\delta_{\alpha\gamma}\delta_{\mu\delta} - \delta_{\alpha\delta}\delta_{\mu\gamma}) \left(\delta_{\mu\sigma} - \frac{x_\mu x_\sigma}{r^2} \right) \left(\delta_{\beta\delta} - \frac{x_\beta x_\delta}{r^2} \right) \Im \int_0^\infty \mathrm{d}\omega \, \omega^2 \Pi^<_{\sigma\beta}(\omega) \end{aligned}$$

With some contractions of the Kronecker delta's, it can be shown that

$$x_\gamma (\delta_{\alpha\gamma}\delta_{\mu\delta} - \delta_{\alpha\delta}\delta_{\mu\gamma}) \left(\delta_{\mu\sigma} - \frac{x_\mu x_\sigma}{r^2} \right) \left(\delta_{\beta\delta} - \frac{x_\beta x_\delta}{r^2} \right) = x_\alpha \left(\delta_{\beta\sigma} - \frac{x_\beta x_\sigma}{r^2} \right)$$

so the expression of the Poynting vector simplifies to

$$\langle : S_\alpha(\boldsymbol{r}, t) : \rangle = \frac{-\hbar x_\alpha}{16\pi^3 \epsilon_0 c^3 r^3} \left(\delta_{\beta\sigma} - \frac{x_\beta x_\sigma}{r^2} \right) \Im \int_0^\infty \mathrm{d}\omega \, \omega^2 \Pi^<_{\sigma\beta}(\omega)$$

Since S_α is proportional to x_α, the average Poynting vector is radial. To find the total power emitted, we integrate the flux over a large sphere. This is also the reason we only keep the Poynting vectors to term of order $1/r^2$. Instead of having the terms which sums over β, σ, we can write it as a matrix product instead.

$$\left(\delta_{\beta\sigma} - \frac{x_\beta x_\sigma}{r^2}\right) \Pi^<_{\sigma\beta}(\omega) = \mathrm{Tr}\left(\mathbb{I} - \hat{\boldsymbol{r}}\hat{\boldsymbol{r}}^T\right) \Pi^<$$

where $\mathbb{I}$ is the 3x3 identity matrix and $\hat{\boldsymbol{r}}$ is the unit position vector as a column vector. The trace is summing over the diagonal elements. When calculating the surface integral over the sphere, we need to know the angular average of the quantity $\boldsymbol{S}\cdot\hat{\boldsymbol{r}}$, which is proportional to $\mathrm{Tr}\left(\mathbb{I} - \hat{\boldsymbol{r}}\hat{\boldsymbol{r}}^T\right)\Pi^<$. The matrix $\left(\mathbb{I} - \hat{\boldsymbol{r}}\hat{\boldsymbol{r}}^T\right)$ is a projector and it turns out that the angular average is

$$\langle \mathrm{Tr}\left(\mathbb{I} - \hat{\boldsymbol{r}}\hat{\boldsymbol{r}}^T\right)\Pi^< \rangle_{\hat{\boldsymbol{r}}} = \frac{2}{3}\mathrm{Tr}\Pi^<$$

The notation $\langle \ldots \rangle_{\hat{\boldsymbol{r}}}$ is to average over all unit vectors $\hat{\boldsymbol{r}}$ (angular average over a unit sphere). We are now finally in a position to calculate the total power. First, the angular average of $\boldsymbol{S}\cdot\hat{\boldsymbol{r}}$ is

$$\begin{aligned}
\langle \boldsymbol{S}\cdot\hat{\boldsymbol{r}}\rangle_{\hat{\boldsymbol{r}}} &= \left\langle \frac{x_\alpha}{r} \langle : S_\alpha(\boldsymbol{r},t) : \rangle \right\rangle_{\hat{\boldsymbol{r}}} \\
&= \frac{-\hbar}{16\pi^3\epsilon_0 c^3 r^2} \Im \int_0^\infty \mathrm{d}\omega\, \omega^2 \left\langle \left(\delta_{\beta\sigma} - \frac{x_\beta x_\sigma}{r^2}\right) \Pi^<_{\sigma\beta}(\omega) \right\rangle_{\hat{\boldsymbol{r}}} \\
&= \frac{-\hbar}{24\pi^3\epsilon_0 c^3 r^2} \Im \int_0^\infty \mathrm{d}\omega\, \omega^2 \mathrm{Tr}\Pi^<
\end{aligned}$$

For the last step, multiply by the area of the sphere.

$$\begin{aligned}
P_\infty &= \lim_{r\to\infty} 4\pi r^2 \langle \boldsymbol{S}\cdot\hat{\boldsymbol{r}}\rangle_{\hat{\boldsymbol{r}}} \\
&= \frac{-\hbar}{6\pi^2\epsilon_0 c^3} \Im \int_0^\infty \mathrm{d}\omega\, \omega^2 \mathrm{Tr}\Pi^<
\end{aligned}$$

This is Eqn. 5.3 in the main text.

Appendix F

Energy spectra for small systems

This section is meant to be a mini database collecting the exact spectrum for small systems. We have managed to find the eigenvalues for the cases 2×2, 2×3, 2×4 and 3×3. For convenience, set $t = -1$ in this appendix.

F.1 2x2 square lattice

The 2×2 square lattice Hamiltonian can be written as

$$H = \begin{pmatrix} 0 & 1 & 1 & 0 \\ 1 & 0 & 0 & e^{i\theta} \\ 1 & 0 & 0 & e^{-i\theta} \\ 0 & e^{-i\theta} & e^{i\theta} & 0 \end{pmatrix}$$

The symmetric gauge is used here, and $\theta = \frac{Ba^2q}{2\hbar}$ is the associated Peierls phase. The eigenvalues are very simple.

$$\epsilon_0 = -2\sin\frac{\theta}{2}, \quad \epsilon_1 = 2\cos\frac{\theta}{2}, \quad \epsilon_2 = 2\sin\frac{\theta}{2}, \quad \epsilon_3 = -2\cos\frac{\theta}{2}$$

A plot of the eigenvalues against the magnetic field is shown below

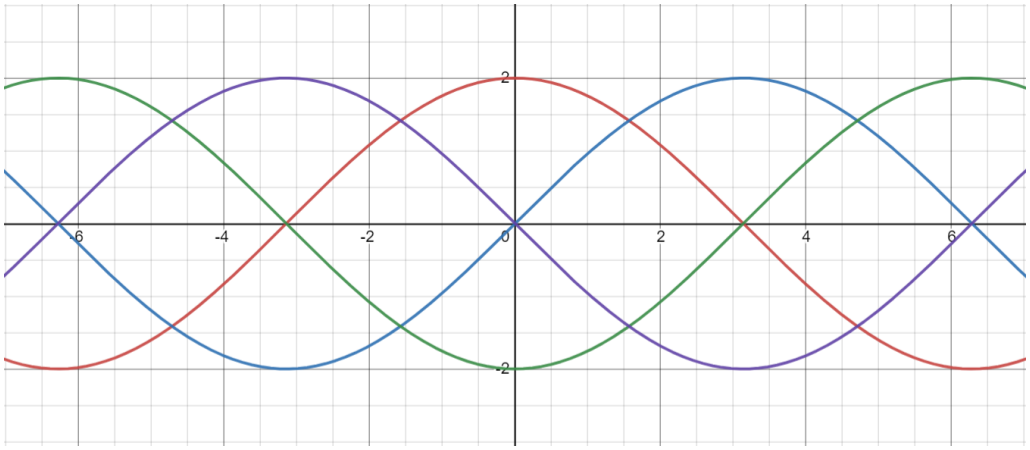

Figure F.1: Eigenvalues for 2×2 square lattice.

The (right) eigenvectors are

$$
\begin{aligned}
|\epsilon_0\rangle &= \frac{1}{2}(1, -ie^{i\frac{\theta}{2}}, ie^{-i\frac{\theta}{2}}, -1)^T \\
|\epsilon_1\rangle &= \frac{1}{2}(1, -e^{i\frac{\theta}{2}}, -e^{-i\frac{\theta}{2}}, 1)^T \\
|\epsilon_2\rangle &= \frac{1}{2}(1, ie^{i\frac{\theta}{2}}, -ie^{-i\frac{\theta}{2}}, -1)^T \\
|\epsilon_3\rangle &= \frac{1}{2}(1, e^{i\frac{\theta}{2}}, e^{-i\frac{\theta}{2}}, 1)^T
\end{aligned}
$$

F.2 3x2 square lattice

We look at the next-simplest square lattice, the 3×2 lattice. The Hamiltonian is of the following form.

$$
H = \begin{pmatrix}
0 & 1 & 0 & 1 & 0 & 0 \\
1 & 0 & 1 & 0 & e^{i\theta} & 0 \\
0 & 1 & 0 & 0 & 0 & e^{2i\theta} \\
1 & 0 & 0 & 0 & e^{-i\theta} & 0 \\
0 & e^{-i\theta} & 0 & e^{i\theta} & 0 & e^{-i\theta} \\
0 & 0 & e^{-2i\theta} & 0 & e^{i\theta} & 0
\end{pmatrix}
$$

Its eigenvalues can be solved exactly. For convenience, define the quantity

$$
\phi = \cos^{-1}\left[\sqrt{\frac{729}{1000}}\left(\cos 2\theta + \frac{1}{27}\right)\right]
$$

Note that $\cos^{-1}\sqrt{\frac{98}{125}} \leq \phi \leq \pi - \cos^{-1}\sqrt{\frac{169}{250}}$. The eigenvalues can then be written as

$$
\begin{aligned}
\epsilon_0 &= 2\sqrt{\frac{10}{9}}\cos\left(\frac{\phi}{3}\right) + \frac{1}{3} \\
\epsilon_1 &= 2\sqrt{\frac{10}{9}}\cos\left(\frac{\phi - \pi}{3}\right) - \frac{1}{3} \\
\epsilon_2 &= 2\sqrt{\frac{10}{9}}\cos\left(\frac{\phi - 2\pi}{3}\right) + \frac{1}{3} \\
\epsilon_3 &= 2\sqrt{\frac{10}{9}}\cos\left(\frac{\phi - 3\pi}{3}\right) - \frac{1}{3} \\
\epsilon_4 &= 2\sqrt{\frac{10}{9}}\cos\left(\frac{\phi - 4\pi}{3}\right) + \frac{1}{3} \\
\epsilon_5 &= 2\sqrt{\frac{10}{9}}\cos\left(\frac{\phi - 5\pi}{3}\right) - \frac{1}{3}
\end{aligned}
$$

A plot of the spectrum is provided below. Note the appearance of "higher harmonics" as compared to the 2x2 case.

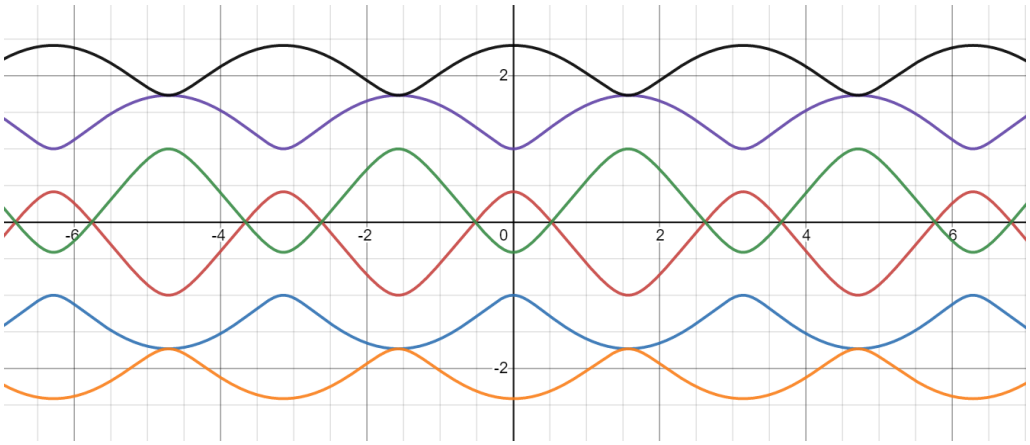

Figure F.2: Eigenvalues for 3×2 square lattice.

F.3 4x2 square lattice

For the family of $2 \times N$ systems, the next one is 4×2 lattice. The Hamiltonian is of the following form.

$$H = \begin{pmatrix} 0 & 1 & 0 & 0 & 1 & 0 & 0 & 0 \\ 1 & 0 & 1 & 0 & 0 & e^{i\theta} & 0 & 0 \\ 0 & 1 & 0 & 1 & 0 & 0 & e^{2i\theta} & 0 \\ 0 & 0 & 1 & 0 & 0 & 0 & 0 & e^{3i\theta} \\ 1 & 0 & 0 & 0 & 0 & e^{-i\theta} & 0 & 0 \\ 0 & e^{-i\theta} & 0 & 0 & e^{i\theta} & 0 & e^{-i\theta} & 0 \\ 0 & 0 & e^{-2i\theta} & 0 & 0 & e^{i\theta} & 0 & e^{-i\theta} \\ 0 & 0 & 0 & e^{-3i\theta} & 0 & 0 & e^{i\theta} & 0 \end{pmatrix}$$

The eigenvalues are

$$\epsilon_0 = \sqrt{\frac{\sqrt{8\cos 3\theta + 10\cos 2\theta + 12\cos\theta + 15}}{2} + \cos\theta + \frac{5}{2}}$$

$$\epsilon_1 = \sqrt{\frac{\sqrt{-8\cos 3\theta + 10\cos 2\theta - 12\cos\theta + 15}}{2} - \cos\theta + \frac{5}{2}}$$

$$\epsilon_2 = \sqrt{-\frac{\sqrt{8\cos 3\theta + 10\cos 2\theta + 12\cos\theta + 15}}{2} + \cos\theta + \frac{5}{2}}$$

$$\epsilon_3 = \sqrt{-\frac{\sqrt{-8\cos 3\theta + 10\cos 2\theta - 12\cos\theta + 15}}{2} - \cos\theta + \frac{5}{2}}$$

$$\epsilon_4 = -\sqrt{\frac{\sqrt{8\cos 3\theta + 10\cos 2\theta + 12\cos\theta + 15}}{2} + \cos\theta + \frac{5}{2}}$$

$$\epsilon_5 = -\sqrt{\frac{\sqrt{-8\cos 3\theta + 10\cos 2\theta - 12\cos\theta + 15}}{2} - \cos\theta + \frac{5}{2}}$$

$$\epsilon_6 = -\sqrt{-\frac{\sqrt{8\cos 3\theta + 10\cos 2\theta + 12\cos\theta + 15}}{2} + \cos\theta + \frac{5}{2}}$$

$$\epsilon_7 = -\sqrt{-\frac{\sqrt{-8\cos 3\theta + 10\cos 2\theta - 12\cos\theta + 15}}{2} - \cos\theta + \frac{5}{2}}$$

The energy spectrum is shown below.

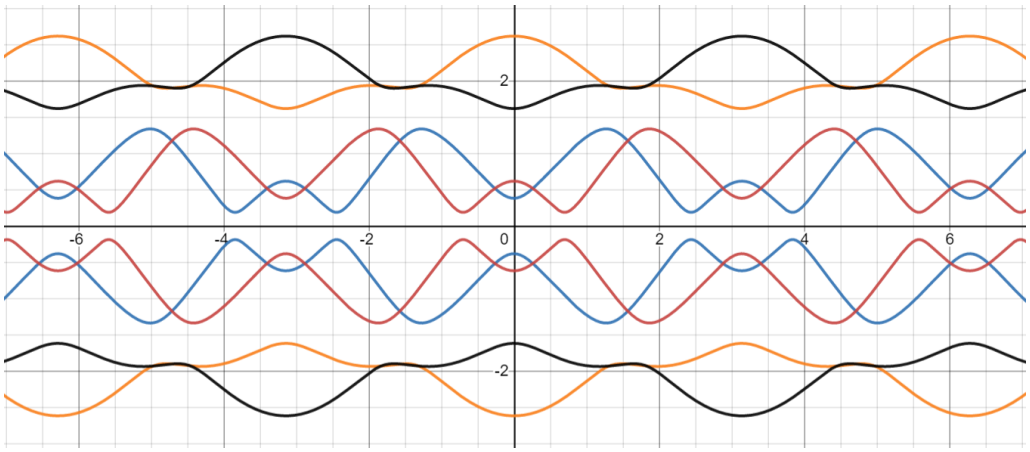

Figure F.3: Eigenvalues for 4×2 square lattice.

F.4 3x3 square lattice

Lastly, we examine the 3 $\times$3 lattice, which the energy eigenvalues can be solved analytically too. The Hamiltonian is

$$H = \begin{pmatrix}
0 & 1 & 0 & 1 & 0 & 0 & 0 & 0 & 0 \\
1 & 0 & 1 & 0 & e^{i\theta} & 0 & 0 & 0 & 0 \\
0 & 1 & 0 & 0 & 0 & e^{2i\theta} & 0 & 0 & 0 \\
1 & 0 & 0 & 0 & e^{-i\theta} & 0 & 1 & 0 & 0 \\
0 & e^{-i\theta} & 0 & e^{i\theta} & 0 & e^{-i\theta} & 0 & e^{i\theta} & 0 \\
0 & 0 & e^{-2i\theta} & 0 & e^{i\theta} & 0 & 0 & 0 & e^{2i\theta} \\
0 & 0 & 0 & 1 & 0 & 0 & 0 & e^{-2i\theta} & 0 \\
0 & 0 & 0 & 0 & e^{-i\theta} & 0 & e^{2i\theta} & 0 & e^{-2i\theta} \\
0 & 0 & 0 & 0 & 0 & e^{-2i\theta} & 0 & e^{2i\theta} & 0
\end{pmatrix}$$

The eigenvalues are

$$\epsilon = 0, \pm 2\sin\theta, \pm 2\sqrt{1+\cos^2\theta}, \pm 2\sin\left(\theta + \frac{\pi}{4}\right), \pm 2\sin\left(\theta - \frac{\pi}{4}\right)$$

Graphs of the energy spectrum is shown below.

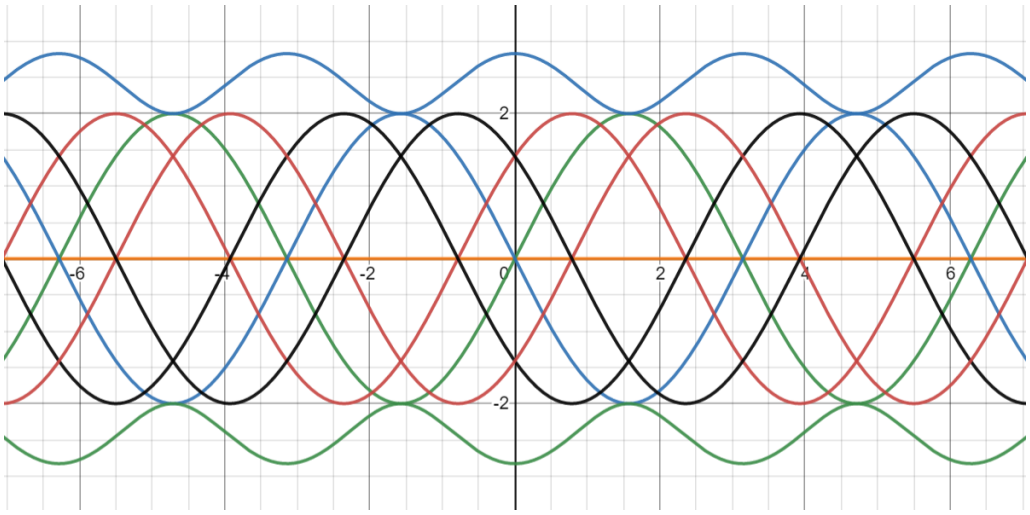

Figure F.4: Eigenvalues for 3×3 square lattice.

As the system grow larger, it becomes almost impossible to solve the characteristic polynomial when the degree is larger than 5. Thus, we do not pursue further in this direction.

Appendix G

Matlab code

Code for Hamiltonian on square lattice with Peierls substitution

```
% r = B * q * a^2 / hbar is dimensionless B field
% Landau gauge: (Ax, Ay, Az) = B (-y, 0, 0)
function H = Hamiltonian(t, Nx, Ny, r)
    N = Nx * Ny;
    H = zeros([N, N]);

    for index1 = 1:Nx % creation index
        for index2 = 1:Ny % creation index
            for x = 1:Nx % annihilation index
                for y = 1:Ny % annihilation index
                    % flattened indices
                    C = flatten(index1,index2,Nx);
                    Z = flatten(x,y,Nx);

                    if index1==x+1 && index2==y % right
                        H(C,Z) = exp(-1i*y*r);
                    elseif index1==x-1 && index2==y % left
                        H(C,Z) = exp(+1i*y*r);
                    elseif index1==x && index2==y+1 % top
                        H(C,Z) = 1;
                    elseif index1==x && index2==y-1 % bottom
                        H(C,Z) = 1;
                    % else not nearest neighbours, remains 0
                    end
                end
            end
        end
    end

    H = -t * H; % hopping
end
```

```
function flattened = flatten(x,y,Nx)
    flattened = (y-1)*Nx + x;
end
```

Appendix H

Units

Below are the units used in the calculations. We define the following 5 units and derive the rest from them.

Table H.1: Defined units

Physical quantity	Defined unit
Angular momentum	$\hbar$
Energy/torque	$1\,\mathrm{eV}$
Mass	m_e
Charge	e
Temperature	$1\,\mathrm{K}$

These units are chosen such that the numerical values for our physical quantities are in a reasonable range. The other units derived from them are

Table H.2: Derived units

Physical quantity	Derived unit
Time	$\frac{\hbar}{1\,\mathrm{eV}} = 6.582 \times 10^{-16}\,\mathrm{s}$
Length	$\frac{\hbar}{\sqrt{m_e(1\,\mathrm{eV})}} = 2.760 \times 10^{-10}\,\mathrm{m}$
Velocity	$\sqrt{\frac{1\,\mathrm{eV}}{m_e}} = 4.194 \times 10^{5}\,\mathrm{m/s}$
Magnetic field	$\frac{m_e(1\,\mathrm{eV})}{e\hbar} = 8636\,\mathrm{T}$
Voltage	$1\,\mathrm{V}$
Current	$\frac{e(1\,\mathrm{eV})}{\hbar} = 2.434 \times 10^{-4}\,\mathrm{A}$
Power	$\frac{(1\,\mathrm{eV})^2}{\hbar} = 2.434 \times 10^{-4}\,\mathrm{W}$
Force	$\frac{\sqrt{m_e(1\,\mathrm{eV})^3}}{\hbar} = 5.804 \times 10^{-10}\,\mathrm{N}$

Only four significant figures are written down in the table above due to aesthetics. However, we try to be as precise as possible when implementing them in the code.